AD_____

Award Number: W81XWH-09-1-0004

TITLE: A Novel Hand-Held Optical Imager with Real-Time Co-Registration Facilities Towards Diagnostic Mammography

PRINCIPAL INVESTIGATOR: Sarah Erickson, Ph.D.
Anuradha Godavarty, Ph.D.

CONTRACTING ORGANIZATION: Florida International University
Miami, FL 33199

REPORT DATE: January 2012

TYPE OF REPORT: Annual Summary

PREPARED FOR: U.S. Army Medical Research and Materiel Command
Fort Detrick, Maryland 21702-5012

DISTRIBUTION STATEMENT: Approved for Public Release;
Distribution Unlimited

The views, opinions and/or findings contained in this report are those of the author(s) and should not be construed as an official Department of the Army position, policy or decision unless so designated by other documentation.

REPORT DOCUMENTATION PAGE

Form Approved
OMB No. 0704-0188

Public reporting burden for this collection of information is estimated to average 1 hour per response, including the time for reviewing instructions, searching existing data sources, gathering and maintaining the data needed, and completing and reviewing this collection of information. Send comments regarding this burden estimate or any other aspect of this collection of information, including suggestions for reducing this burden to Department of Defense, Washington Headquarters Services, Directorate for Information Operations and Reports (0704-0188), 1215 Jefferson Davis Highway, Suite 1204, Arlington, VA 22202-4302. Respondents should be aware that notwithstanding any other provision of law, no person shall be subject to any penalty for failing to comply with a collection of information if it does not display a currently valid OMB control number. **PLEASE DO NOT RETURN YOUR FORM TO THE ABOVE ADDRESS.**

1. REPORT DATE	2. REPORT TYPE	3. DATES COVERED
January 2012	Annual Summary	1 January 2009 – 31 December 2011

4. TITLE AND SUBTITLE

A Novel Hand-Held Optical Imager with Real-Time Co-Registration Facilities Towards Diagnostic Mammography

5a. CONTRACT NUMBER

5b. GRANT NUMBER
W81XWH-09-1-0004

5c. PROGRAM ELEMENT NUMBER

6. AUTHOR(S)

Sarah J. Erickson
Anuradha Godavarty

E-Mail: sarah.erickson@fiu.edu

5d. PROJECT NUMBER

5e. TASK NUMBER

5f. WORK UNIT NUMBER

7. PERFORMING ORGANIZATION NAME(S) AND ADDRESS(ES)

Florida International University
Miami, FL 33199

8. PERFORMING ORGANIZATION REPORT NUMBER

9. SPONSORING / MONITORING AGENCY NAME(S) AND ADDRESS(ES)
U.S. Army Medical Research and Materiel Command
Fort Detrick, Maryland 21702-5012

10. SPONSOR/MONITOR'S ACRONYM(S)

11. SPONSOR/MONITOR'S REPORT NUMBER(S)

12. DISTRIBUTION / AVAILABILITY STATEMENT
Approved for Public Release; Distribution Unlimited

13. SUPPLEMENTARY NOTES

14. ABSTRACT

Hand-held optical imaging devices using near-infrared (NIR) light are currently developed toward clinical translation of the technology. However, none of the devices developed to date have been used toward 3D tomography since they are not able to coregister the image to the tissue geometry. The objective for the work described herein is the clinical translation of a hand-held optical imager with automated coregistration facilities toward 3D tomography. Studies were performed in phantoms, in vitro, and in vivo with healthy female volunteers. A spherical target filled with a fluorescent contrast agent was placed superficially underneath the breast tissue to represent a tumor. Images were collected and coregistered using the hand-held imager. The data from the coregistered image was used to generate a 3D image of the target within the breast tissue. Preliminary studies were carried out to demonstrate 2D diffuse optical imaging with actual breast cancer subjects. The results show for the first time the feasibility of performing 3D tomography in human breast tissue and imaging of human breast cancer in vivo using a hand-held optical imager.

15. SUBJECT TERMS
Diffuse optical imaging, near-infrared, breast cancer, hand-held device, fluorescence, coregistration, in-vivo, 3D tomography

16. SECURITY CLASSIFICATION OF:			17. LIMITATION OF ABSTRACT	18. NUMBER OF PAGES	19a. NAME OF RESPONSIBLE PERSON
a. REPORT	b. ABSTRACT	c. THIS PAGE			USAMRMC
U	U	U	UU	55	19b. TELEPHONE NUMBER *(include area code)*

Table of Contents

A Novel Hand-Held Optical Imager with real-Time Coregistration Facilities toward Diagnostic Mammography

Annual Report (Year 1, Jan 2009-Dec 2009)

PI: Sarah J. Erickson (seric001@fiu.edu)
Contact Details: Postdoctoral Fellow, Department of Biomedical Engineering
College of Engineering and Computing, Florida International University, Miami, FL
Grant No. BC083282
Mentor: Dr. Anuradha Godavarty (godavart@fiu.edu)

INTRODUCTION

Optical imaging using near-infrared (NIR) light is an emerging technique toward non-invasive breast cancer diagnosis. Hand-held based optical imaging devices are currently developed toward clinical translation of the technology.[1] However, the NIR devices developed to date have not attempted three-dimensional (3D) tomography since they are not able to accurately coregister the image to the geometry of the object. ***The overall goal of the research is to implement and test a novel hand-held based optical imager with capabilities of automated coregistration on any tissue curvature for real-time surface imaging and 3D tomographic analysis, on tissue phantoms and in vivo with human subjects.*** The purpose for this research is to translate the device to the clinical setting for breast cancer imaging. The scope of the research involves experimental studies on tissue phantoms and *in vitro*, and *in vivo* studies with normal human subjects prior to clinical studies with breast cancer patients.

BODY

The tasks that were completed in Year-1 of the proposed projects are described herein. The tasks were categorized according to three specific aims as outlined in the statement of work:

Specific Aim# 1:

Demonstrate imaging and 3-D tomography using hand-held probe on different curved tissue phantoms.

Work Completed to Date (Reported in 2009 Annual Report):

Proposed Task A: *Modify probe design to achieve uniform source intensity.*

The current design of the hand-held device (shown in Figure 1) utilizes a single laser diode source and a custom built collimator package which divides the laser light among six optical fibers attached to the probe face. The limitation of this design is that the output intensity of the laser light is not divided equally among the six fibers. The goal of this task was to modify the

collimator package in order to achieve the desired uniform source intensity distribution. However, during the course of this task, it was found that achieving uniform intensity distribution is difficult using a single laser diode. Hence, a new design was developed to use six laser diodes individually attached to the six optical fibers which can be adjusted individually to the desired intensity. This design is currently carried out in a parallel project by a team of graduate and undergraduate students in our lab and will be implemented with the second generation of the optical imaging system.

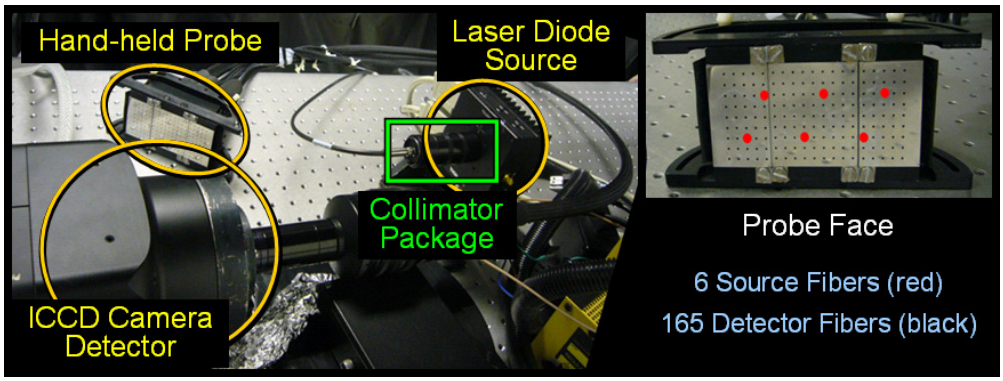

Figure 1. The three major components of the hand-held device (left) are the hand-held probe, the intensified charge-coupled device (ICCD) camera detector, and the laser diode source. The light from the single laser diode source is divided via a collimator package into six source fibers at the probe face (right).

Proposed Task B: *Perform experiments using the hand-held probe in the curved position on curved tissue phantoms.*

Experiments were carried out using the probe in the maximum curved position (45° curvature of each wing) on octagonal phantoms designed to fit the curvature of the probe with full contact. During these studies, it was found that there was interference in the collected signal due to the sharp edges of the octagonal phantom. These studies were discontinued. Further studies focused directly on human breast tissues to demonstrate imaging of curved geometries in the realistic case. *In vivo* studies were performed on normal human subjects to demonstrate the feasibility of using the hand-held device to perform fast 2D imaging toward target detection prior to 3D tomography studies. The device was used to collect images of a fluorescent target with a background of real human breast tissue. Fast imaging was performed in near real time (~5 sec). All human subject studies were approved by the Florida International University Institutional Review Board. Healthy female volunteers age 21 and above were recruited for the studies. A fluorescent target (acrylic sphere filled with 1 μM indocyanine green) was used to simulate a tumor and was placed underneath the flap of the breast tissue (i.e. between breast tissue and chest wall, underneath the tissue). Table 1 gives a summary of the *in vivo* experimental cases performed.

Table 1 Summary of experimental cases performed for *in vivo* fast 2D imaging studies.

Experimental Case #		Number of Targets	Target Depth (cm)	Target Volume (cc)	T:B Contrast Ratio
In vivo with normal human subject	1	1	2.5	0.23	1:0
	2	1	2.5	0.45	1:0
	3	2	2.5	0.23 & 0.45	1:0

Figure 2 shows the results of images (i.e. 2D surface contour plots of fluorescence intensity) collected with the probe in both the flat (Figure 2A) and curved (Figure 2B) position. When the probe was in the flat position, it was placed with gentle compression against the tissue surface to allow full contact with the probe face, whereas in the curved position it was able to contour around the tissue in its natural shape.

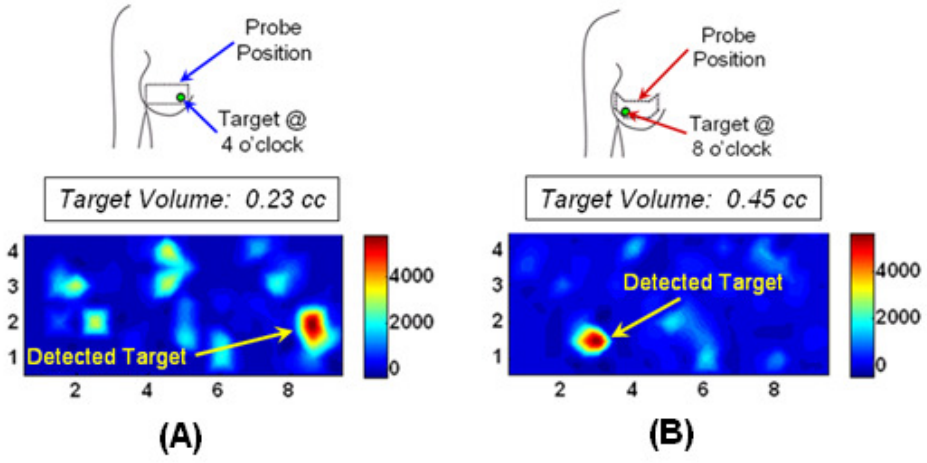

Figure 2. Results for *in vivo* studies with normal human subjects. (A) 0.23 cc target was placed at the 4 o'clock position and imaged with the probe in the flat position. (B) 0.45 cc target was placed at the 8 o'clock position and imaged with the probe in the curved position.

The results show that a fluorescent target was detectable through ~2.5 cm of actual human breast tissue using the probe in both the flat and curved positions. The results for these studies were published in *Translational Oncology*[2] and the article in press is attached in Appendix A.

Specific Aim # 2:

Implement 3-D automated co-registration using acoustic-based tracking system in order to perform real-time in-vivo optical imaging.

Work Completed to Date:

Proposed Task A (Reported in 2009 Annual Report): *Implement a 3D motion tracking device in order to randomly track the movement of the hand-held probe.*

Coregistered imaging is required in order to perform 3D tomography since the 2D image must be located in the exact position of the hand-held probe on the tissue surface. A 3D tracking system was implemented on the probe in order to perform coregistered imaging using MATLAB/LabView software developed by a master's student in house. Experimental studies using an exogenous fluorescent contrast agent Indocyanine Green (ICG) were performed to demonstrate the feasibility of coregistered imaging using the hand-held probe based optical imager. The contrast agent is placed in a small spherical target and embedded within the phantom to represent a tumor within a tissue background. Successful implementation of the coregistered tracking method would be indicated by the ability to track the actual location of the target as the probe is moved to different positions with respect to the phantom surface. Coregistered imaging was demonstrated in slab tissue phantoms (composed of 1% Liposyn) and the results published in *Review of Scientific Instruments*[3] (article in press is attached in Appendix B). Additional experiments were performed in phantoms composed of minced chicken breast combined with 1% Liposyn to demonstrate coregistered imaging *in vitro*, and the results were published in *Review of Scientific Instruments* (Appendix B).[3] ***The results showed that the 3D tracking system was able to track the position of the probe in real-time and accurately coregister the image to the geometry of the object in tissue phantoms and in vitro.*** During these coregistered imaging studies, it was found that by collecting multiple coregistered images and applying a post-processing summation technique, a target can be detected at greater depths than with a single image alone. A 0.45 cm^3 target was detected at a depth of 3.0 cm in the slab tissue phantom, and a 0.45 cm^3 target was detected at a depth of 2.5 cm in the *in vitro* phantom.[3] ***These results show that by summating multiple coregistered images, deeper targets can be detected.*** Ongoing studies are currently performed to determine the deepest and smallest size target that can be detected using this technique.

Proposed Task B (Reported in 2010 Annual Report): *Adapt and improve 3D reconstruction tools for optical tomography studies.*

The procedure developed herein for performing 3D tomography *in vivo* in order to reconstruct a target within the breast tissue geometry of a human subject involves ten major steps. Step 1: Acquire the coregistered image of optical intensity data from the breast tissue. Step 2: Use the 3D surface geometry from the 3D scanner to generate a 3D volume. Step 3: Generate a 3D tetrahedral volume mesh and corresponding triangular surface (or boundary) mesh for the volume breast geometry. Step 4: Determine the nodes and coordinates of the breast mesh that correspond to the source and detector positions in the coregistered probe location. The positional information of the coregistered probe location was used to find the closest nodes in the unstructured breast mesh to each source and detector in the probe, and the coordinates of those nodes were assigned as the coordinates of the sources and detectors. The procedure developed

for performing this step ensures that the source and detector positions assigned to the mesh correspond to the data collected with the probe and coregistered to the tissue during live imaging. Step 5: Convert text files and source/detector positional information into data files that will be used in the reconstruction code. Step 6: Acquire the optical intensity data for each detector position in the 3D breast mesh from the coregistered image data. A code was written in MATLAB to extract the optical intensity data from the coregistered mesh at the detector nodes and generate a data file containing the coordinates of the detector nodes and the corresponding intensity values from the breast data. Step 7: Use the intensity data acquired from Step 6 to generate the data files used in the AEKF algorithm. These data files contain the AC, DC, phase, and modulation depth information (or DC only for CW data) along with the optical properties of the background tissue. In this case, average optical property values of human breast tissue acquired from the literature[4] were used in the reconstruction. Step 8: Perform 3D reconstruction using a computationally efficient version of the AEKF based algorithm to reconstruct the absorption coefficient due to the fluorophore (μ_{axf}) within the 3D discretized geometry of the breast tissue. Given the estimation of measurement error covariance *R*, model error covariance *Q*, and parameter error covariance *P*, the AEKF algorithm recursively minimizes the variance of the parameter error, in this case the $\mu_{axf.}$ The variances of the means of five repeated experimental measurements from each detector point were used to estimate the measurement error covariance *R*. The model error covariance *Q* was empirically chosen to be one fourth of the measurement error covariance *R*.[5] The *R* and *Q* were used in the reconstruction to weight the updates at each iteration. The parameter error covariance *P* (the error in the unknown spatially distributed parameter values μ_{axf}) was used to damp into the inversion for better convergence. When the root mean square output error (RMSE) was less than 1% or the total number of iterations exceeded 50, the reconstruction was assumed to have converged. The reconstruction parameter μ_{axf} was set at an arbitrary initial guess of 0.003 cm^{-1}. The resulting 3D μ_{axf} distribution was plotted in Tecplot.

Figure 3 shows the experimental result of the image reconstructions plotted in Tecplot. Figure 3A shows the 3D tetrahedral unstructured mesh of the scanned breast tissue geometry and Figure 3B shows the reconstructed optical property (i.e. recovered absorption coefficient due to the fluorophore as a series of contour slices in the x-plane. The slices are plotted in profile view to show their location within the tissue geometry (in the breast tissue region only). Individual detailed slices are shown in frontal view in Figure 4.

The coronal slices in Figure 4 begin at the tissue surface close to the central (nipple) region and progress depth-wise toward the chest wall. The initial slices at depths less than 1.0 cm from the tissue surface at the nipple region (slices 1-3) show signal (the recovered absorption coefficient due to the fluorophore, μ_{axf}) from the 2D target location. At a depth of 1.0 cm and greater (slices 4-12), additional signal appears to the left side of the breast tissue away from the true target location at 6 o'clock position.

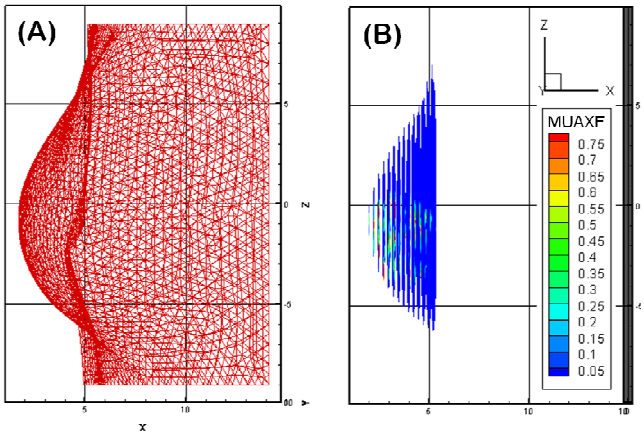

Figure 3. 3D reconstruction result using the coregistered experimental data from case #1 (section 3.1). (A) Plot of the 3D tetrahedral unstructured mesh used in the reconstruction. (B) The reconstructed parameter, absorption coefficient due to the fluorophore, μ_{axf} as a series of contour slices in the x-plane for the in vivo experimental CW-imaging. The slices are plotted in profile view to show their location within the tissue geometry (in the breast tissue region only). Individual detailed slices are shown in frontal view in Figure 4.

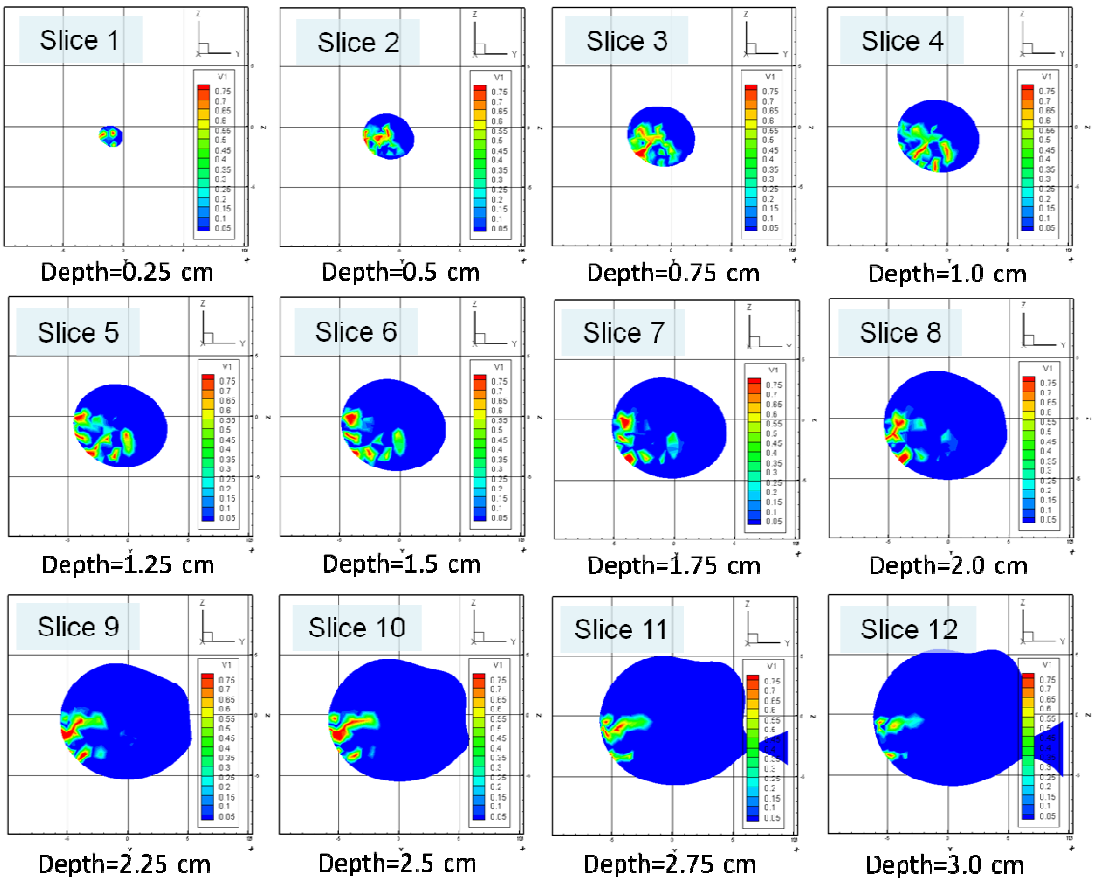

Figure 4. Contour slices of the reconstructed parameter, μaxf in the x-plane at 0.25 cm intervals, for the same reconstruction case shown in Figure 1. The contour slices begin at

the tissue surface at the nipple region and slice depth is indicated as depth from the tissue surface at the center (nipple) region.

Figure 5 shows slices of the reconstructed parameter in y-plane representing the sagittal view. Slice 4 in the center gives the sagittal slice at the y=0 location which is the central part of the tissue (the slice at the nipple region). The other slices represent the locations in 0.25 cm increments to the left or towards the 9 o'clock direction (slices 1-3) and right or towards the 3 o' clock direction (slices 5-7) of the center. The images show that within this central region, there is a maximum signal intensity at the central location of the tissue which corresponds to the 6 o'clock position of the fluorescent target, and the signal diminishes in either direction away from the center.

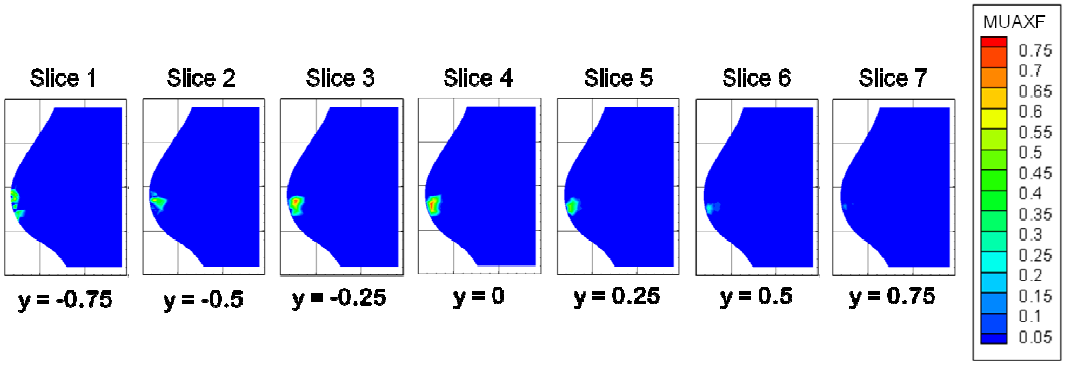

Figure 5. Contour slices of the reconstructed parameter, μaxf in the y-plane at 0.25 cm intervals, for the same reconstruction case shown in Figure 6. Slice 4 shows the central (nipple) region of the tissue which contains the true target location. The signal in highest in slice 4 and then lessens as the slices move away from center in both directions.

Specific Aim # 3:

Perform feasibility in-vivo studies using diffuse optical imaging on normal subjects to demonstrate real-time co-registered imaging.

Proposed Task A (Reported in 2010 Annual Report): *Perform in-vivo studies with ~5 normal human subjects at Florida International University.*

Healthy female human subjects were recruited for the study which was approved by the FIU Institutional Review Board. After the 3D scan of the tissue geometry was acquired, the subject was seated an upright position in the imaging room. Spherical target(s) of 0.23-0.45 cm^3 volume filled with 1 μM indocyanine green were superficially placed underneath the flap of the breast tissue at different locations (the 6 o'clock position is shown in Figure 6). The probe was placed in full contact with the breast tissue and CW images of fluorescence intensity were collected and automatically coregistered to the tissue geometry. A subtraction-based post-processing technique was used to eliminate excitation leakage for each image.

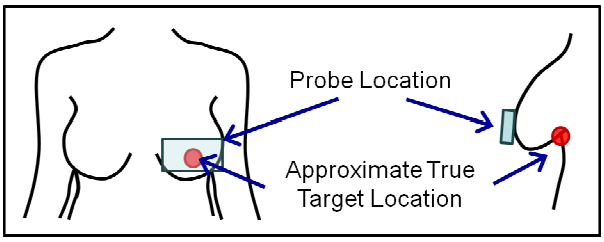

Figure 6. Schematic showing location of target placed superficially at the 6 o'clock position underneath the breast tissue and location of probe during imaging.

A commercially available handheld 3D scanner was employed to acquire the breast tissue geometry. Use of the scanner on human subjects was approved by the FIU Institutional Review Board. A motorized system was implemented with the scanner to automatically acquire the scan without requiring an operator to hold the scanner. This method was designed to enable the scanning procedure to be independent of the operator as well as to allow more privacy for the subject since the scanner would be operated by computer from outside a curtained room. Each scan was composed of a series of four sweeps of the scanner which covered both sides of the breast tissue as well as part of the chest wall and ribcage area. The acquired geometry was displayed by the scanner software (Figure 7A) and then exported as a .MAT file. The geometry was then discretized using MATLAB software developed in house, and loaded into the coregistration software (Figure 7B).

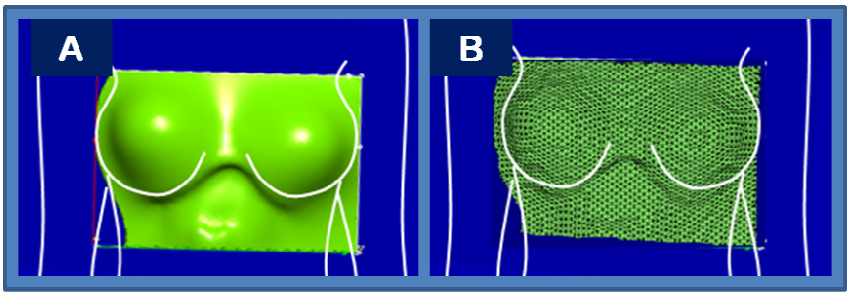

Figure 7. (A) Scanned surface breast tissue geometry. (B) Discretized mesh of breast tissue surface geometry.

Coregistered imaging is required in order to perform 3D tomography since the 2D images (contour plots of fluorescent intensity data acquired using the hand-held optical imager) must be coregistered to the appropriate probe location on the tissue surface. In coregistered imaging, the position and orientation of the probe is tracked with respect to the tissue or phantom surface being imaged. This tracked 3D positional information is then used to accurately position the acquired optical images onto the tissue geometry.

Coregistration was carried out as a three-step process using MATLAB/LabVIEW software developed in house[3]: (1) a real-time tracking system was used to find the probe location in 3D with respect to the tissue; (2) a real-time 2D surface contour optical image was acquired at the probe location; (3) the 3D probe location and 2D optical image were coregistered onto a discretized phantom mesh. The 3-step process is automated to enable fast 2D coregistered imaging (~35 seconds per image).

The automated coregistered imaging process was previously validated in human subjects. The probe was placed at reference points of known coordinates and the distance off between the true and measured position was calculated for each probe location. The average distance off was ~ 1cm. The error can be attributed to instrumentation error such as fluctuation in the tracked position of the probe, and human error such as hand movement of the operator. Currently the tracking system and imaging set-up is being modified to improve the accuracy of the tracked probe location.

Figure 8 shows results for coregistered imaging studies with a normal subject. A spherical target filled with 1 µM ICG was placed underneath the flap of the breast tissue and fluorescence intensity images were collected and automatically coregistered using the positional tracking system. Figure 8A shows the position of the probe and the discretized geometry relative to the subject.

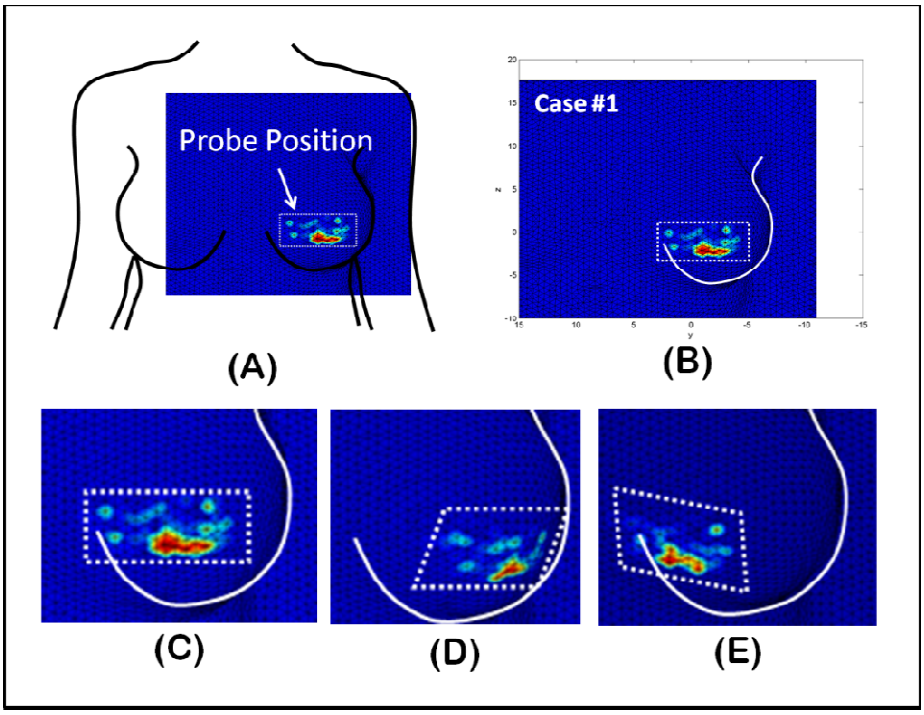

Figure 8. Coregistered images of fluorescence intensity data collected form a normal subject with an ICG-filled target using the initial set-up (subject seated in upright position). (A) Location of probe and image relative to the subject. (B) Case#1 image: 0.45 cm3 target at the 6 o'clock position. (C) Zoomed image of Case #1. (D) Case #2 image: 0.45 cm3 target at the 4 o'clock position. (E) Case #3 image: 0.23 cm3 target at the 8 o'clock position. All targets contain 1 µM indocyanine green.

Figure 8B shows the resulting coregistered image for case #1 where a 0.45 cm^3 target was placed at the 6 o'clock position. A zoomed image of the same result is shown in Figure 3C. Figures 3D and 3E show zoomed images of the results for cases #2 (0.45 cm^3 target at the 8 o'clock position) and #3 (0.23 cm^3 target at the 4 o'clock position) respectively. The results show that a 0.23-0.45 cm^3 fluorescent target was detected through ~2.5 cm of human breast tissue and coregistered to the appropriate location on the tissue geometry.

Proposed Task B (Reported in 2010 Annual Report): *Implement the tracking system to obtain real-time surface images of the human breast tissues using the hand-held optical imager.*

In order to minimize the movement of the subject and the breast tissue, the imaging set-up was modified such that the subject lay in a reclined position. A massage chair capable of reclining 45-90º with arm rests was acquired for the imaging studies (Figure 9). The subjects rested in supine position on the chair with the back reclined at 45º and arms resting at the sides or on the armrests. This position was chosen such that it would be reclined enough to minimize movement of the subject (as opposed to the upright position with no armrests in the initial set-up which allowed movement of the subject) as well as maintain line-of-sight between the probe and the tracker which would be inhibited if the chair was reclined to greater angles. In order to acquire the 3D geometry with the subject in the reclined position, the Fastscan was taken back as a hand-held scanner and used to scan the tissue by hand (the motorized system will be used in future applications described in the last chapter).

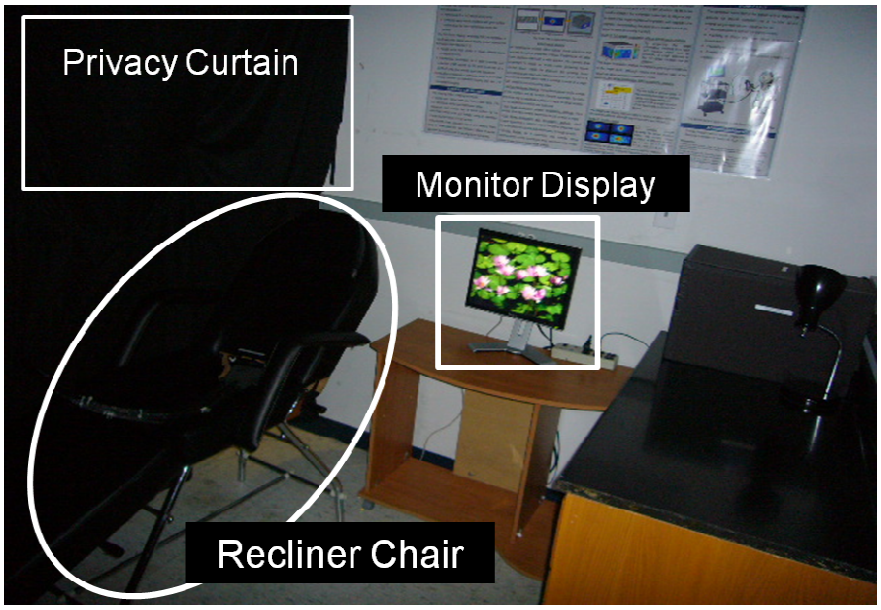

Figure 9. Modified human subject imaging set-up. Subject lies supine in recliner chair (45º) during acquisition of tissue geometry with 3D scanner and imaging using handheld imager.

Figure 10 shows the 3D scanned geometry of a normal human subject using the modified set-up where the subject was lying in supine position in a recliner chair at a 45º angle. The reclined position caused the tissue to flatten against the ribcage in order to minimize deformation of the tissue during imaging.

The imaging process using the modified set-up is shown in Figure 11, where the imaging room is closed off from the instrumentation room by a curtain and only the probe is visible in the room. The probe was placed against the breast tissue while the location was recorded by the acoustic tracker and the images were automatically coregistered at the probe location relative to the tissue

geometry. The resulting images were immediately displayed on a monitor in the imaging room that was linked to the computer operated from the instrumentation room.

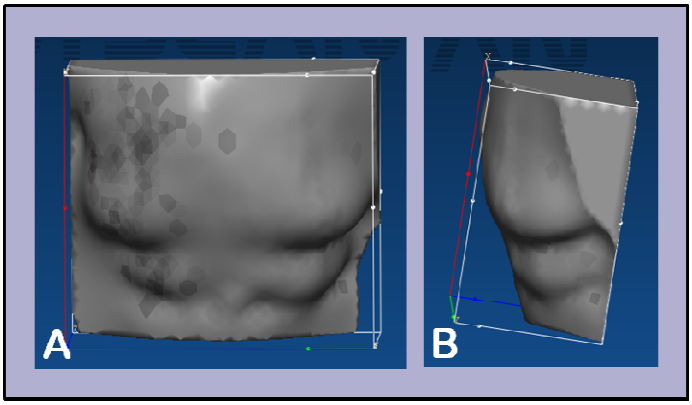

Figure 10. Geometry acquired using the modified imaging set-up with normal subject lying supine in recliner chair with 45º angle. (A) Frontal view. (B) Side view.

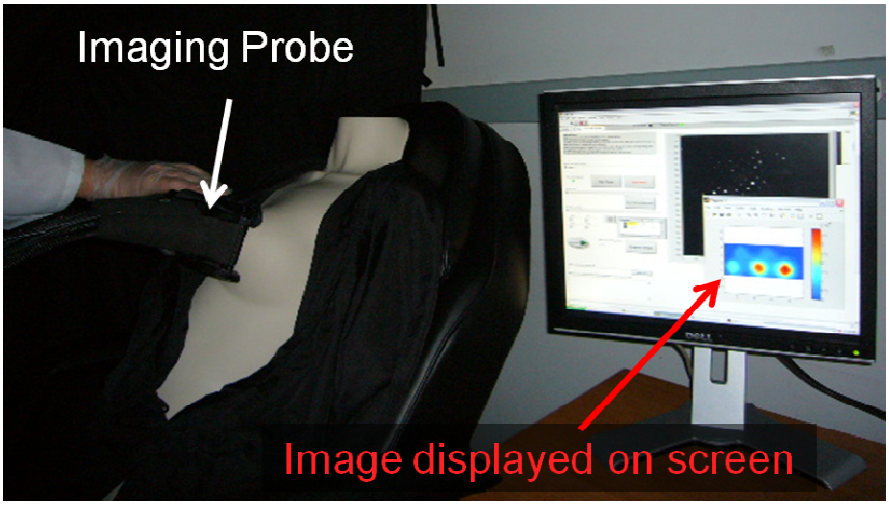

Figure 11. Modified imaging set-up. The subject lies in supine position in recliner chair while breast tissue is imaged using hand-held optical imager. Mannequin shown for demonstration only.

Figure 12 shows automated coregistered images from a normal human subject using the modified imaging set-up with the acoustic tracker. The geometry was rotated to a 45º angle over the y-axis in the coregistration software to correspond to the 45º reclined position of the subject. A default image was used in this study since the purpose of the study was to demonstrate coregistered imaging using the modified approach and not to detect a target. The probe location was coregistered to the tissue at two different locations: the first location was centered over the breast tissue with the bottom of the probe positioned 2 cm beneath the nipple region (Figure

12A-C) and the second location was above the breast in the chest wall region with the bottom of the probe positioned 3 cm above the nipple region (Figure 12D-E).

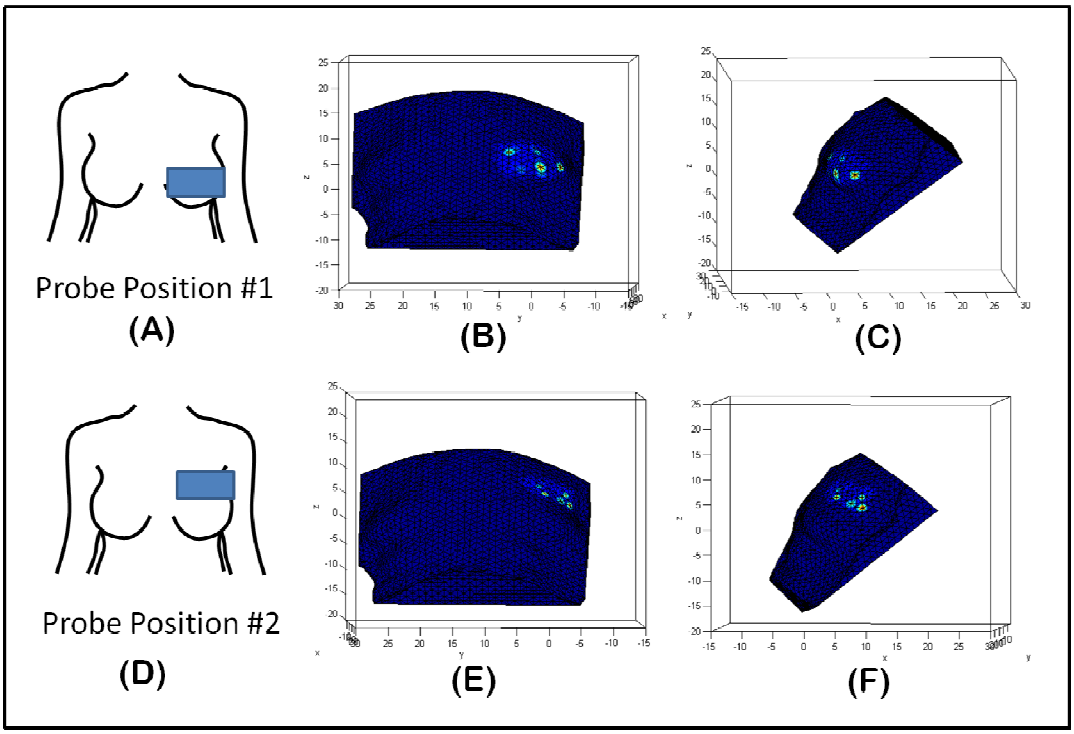

Figure 12. Automated coregistered images in normal subject (no target) using modified imaging set-up. (A) Probe position #1. (B) Frontal view of coregistered image at probe position #1. (C) Side view of coregistered image at probe position #1. (D) Probe position #2. (E) Frontal view of coregistered image at probe position #2. (F) Side view of coregistered image at probe position #2.

Problems were encountered with the acoustic based tracking system and it was determined that an alternative tracking system would need to be incorporated. A master's student in the lab took over the task of testing different tracking systems to use in place of the acoustic based tracker. In the meantime, manual coregistered imaging was performed in human subjects by measuring and marking the probe locations on the tissue.

Figure 13 shows results from absorption-based studies in a normal subject with a 0.45 cm^3 target filled with 0.08% India ink (absorbing contrast agent) placed underneath the flap of the breast tissue at the 6 o' clock position. For this study, the probe position was measured on the breast tissue and marked using surgical tape. The image was then manually coregistered at the measured position using post-processing coregistration software. Figure 13A shows the location of the probe relative to the subject. Figure 13B shows the probe location placed manually in the post-process coregistration software, and Figure 13C shows the resulting coregistered image. It can be seen that the target is detected as a lower intensity (blue) signal indicating higher absorption at the location of the target. A background image was also collected (without target) and subtracted to eliminate background noise.

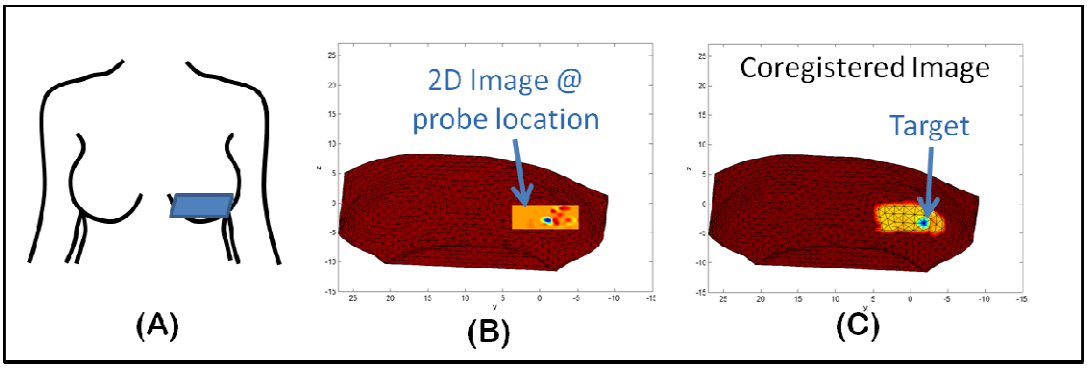

Figure 13. Manually coregistered images from normal subject with 0.45 cm3 target with 0.08% India ink placed under the breast tissue at the 6 o'clock position.

Figure 14 shows the results from a similar study where a target of lower concentration (0.02% India ink) was placed underneath the breast tissue at the 6 o' clock position. Figure 14A shows the location of the probe relative to the subject. Figure 14B shows the probe location placed manually in the post-process coregistration software, and Figure 14C shows the resulting coregistered image. The resulting contrast is lower due to the lower concentration of the absorbing agent, but the lower signal (blue) from the target can be seen at the target location in the 2D image (Figure 14B) and the coregistered image (Figure 14C).

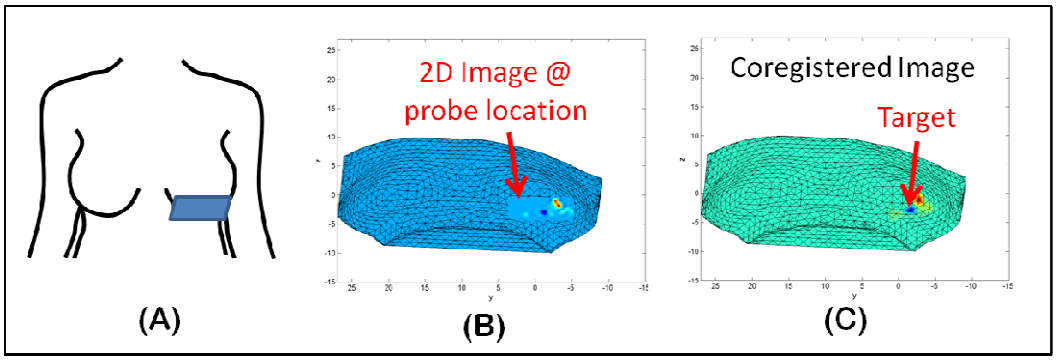

Figure 14. Manually coregistered images from normal subject with 0.45 cm3 target with 0.02% India ink placed under the breast tissue at the 6 o'clock position.

Additional Results:

Clinical imaging of breast cancer *in vivo* human subject studies.

Diffuse optical imaging studies were performed with a female subject (age 51) with breast cancer masses confirmed by prior image modalities (i.e. x-ray mammography, ultrasound). The studies were approved by the FIU Institutional Review Board and the subjects signed a consent form prior to the study and a HIPAA authorization form (for release of the medical records). The studies were performed using the modified imaging set-up described in Specific Aim #3, Proposed Task B, where the subject lay in the supine position in a recliner chair at a 45º angle. The probe was placed at different locations on the ipsilateral (tumor-containing) and contralateral (non-tumor-containing) breast and images of continuous-wave absorption-based measurements were collected. The probe positions were determined visually to cover the entire breast tissue. Initially the probe was centered over the 12 o'clock position covering the upper region of the breast tissue and part of the chest wall (probe location #1 in Figure 15), then moved vertically down toward the 6 o'clock position (probe location #4 in Figure 15). The four imaging locations relative to the subject are shown in Figure 15 (not to scale).

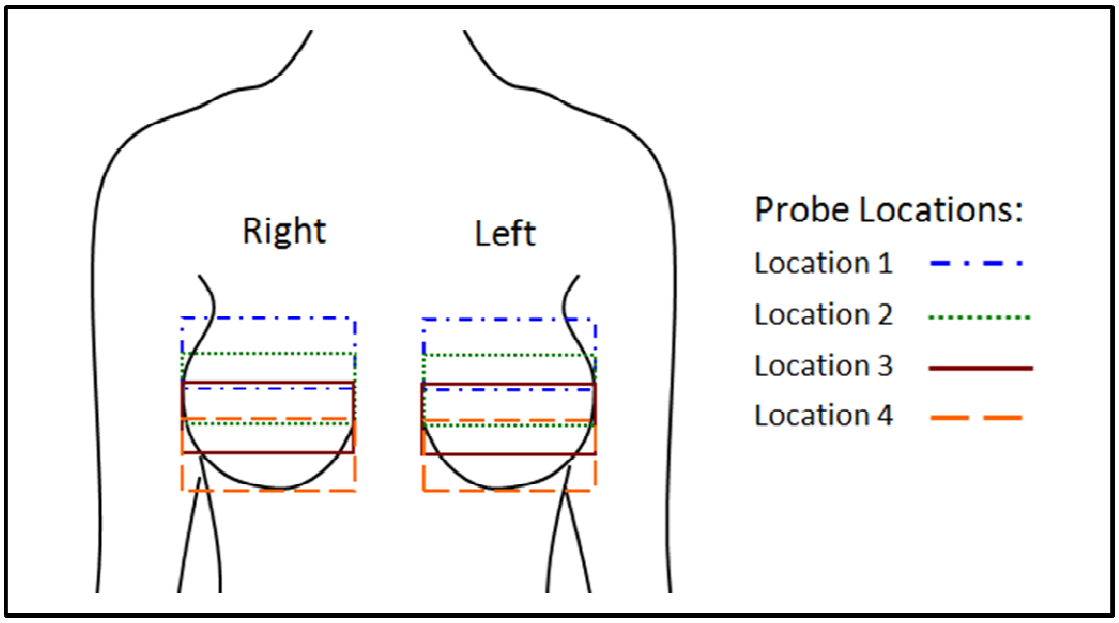

Figure 15. Schematic showing the probe locations during the imaging studies. The probe was placed at four different locations on the left breast tissue followed by the same four locations on the right breast tissue. All probe positions were estimated with reference to the nipple location and are not drawn to scale in the schematic.

Figure 16 shows x-ray mammography images from the left breast of a 51 year-old breast cancer patient (subject #2). Figure 16A is the axial view where the top of the image is toward the left side of the breast and the bottom of the image is toward the right side of the breast. Figure 16B is the oblique view where the top of the image is toward the patient's head and left side and the bottom of the image is toward the patient's feet and right side. The images show the presence of 3 masses in the outer quadrant of the tissue (indicated by the yellow arrows). The

medical reports indicated that two of the masses were cancerous with regions of abnormal tissue between the three masses.

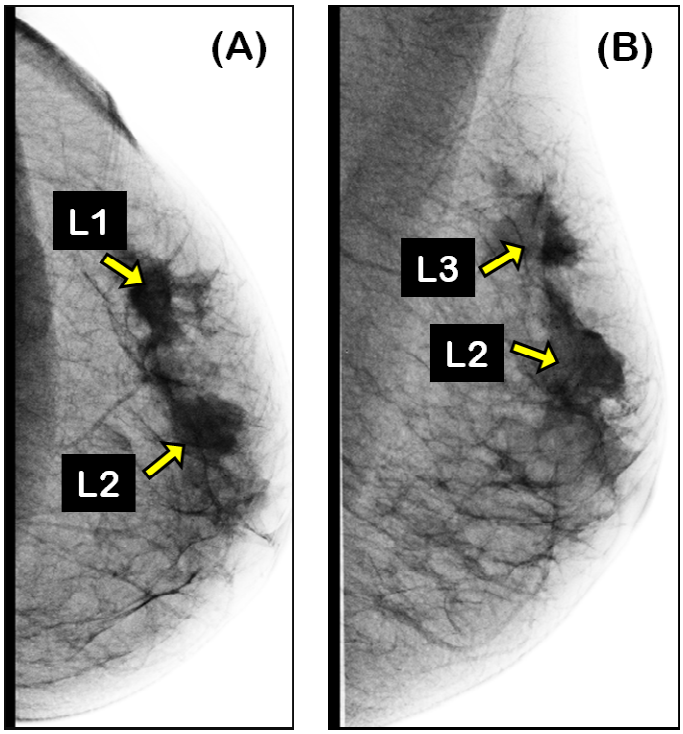

Figure 16. X-ray mammography images of the left breast from a 51 year-old breast cancer patient. (A) The top of the image is the left side and the bottom of the image is the right side of the breast tissue. (B) Oblique image where the top of the image is toward the patient's head and left side and the bottom of the image is toward the patient's feet and right side. The yellow arrows indicate 3 lesions (labeled as L1, L2, and L3) located in the 1 o'clock to 2 o'clock region of the breast.

Figure 17 shows ultrasound images from the left breast of the same subject. The image in Figure 17A was collected from the 1 to 2 o'clock position at 2-3 cm from the nipple and the image in Figure 17B was collected from the 1 to 2 o'clock position at 6 cm from the nipple. The three tumor masses in the outer quadrant of the tissue are indicated by the yellow arrows.

Figure 18 shows the continuous-wave absorption-based images collected using the hand-held optical imager. The images on the left were collected from the ipsilateral breast and the images in the center were collected from the contralateral breast. The images on the left were subtracted from the images in the center to yield the resulting postprocessed images on the right. In the post-processed images, the area of higher absorption shows as a higher (or more red) signal. The post-processed images from locations 1-3 show high intensity signal (greater absorption) in the outer quadrant of the left breast tissue which corresponds to the location of the 3 tumor masses indicated in the x-ray mammogram and ultrasound images. The image from location 4 which is from the lowest part of the tissue does not show higher absorption.

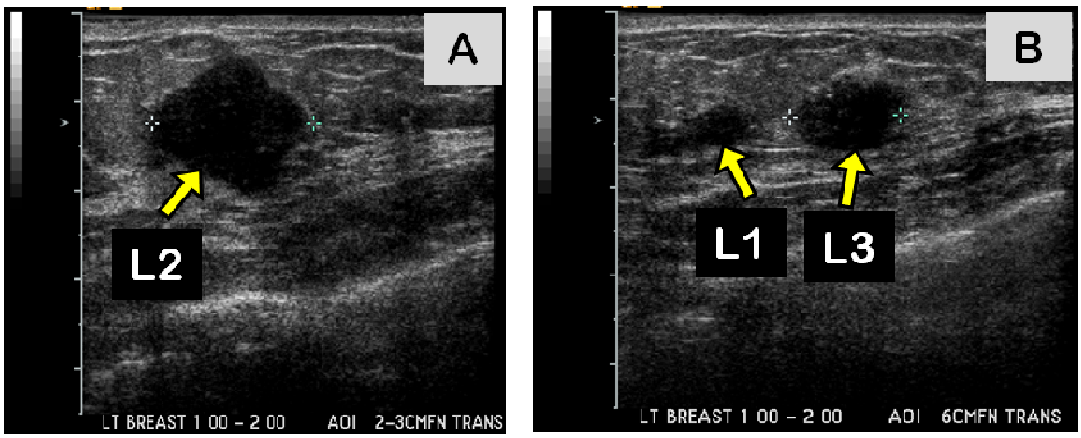

Figure 17. Ultrasound images of the left breast from a 51 year-old breast cancer patient. Both images were collected in the 1 to 2 o'clock location where image (A) was 2-3 cm from the nipple and image (B) was 6 cm from the nipple. The yellow arrows indicate 3 lesions (labeled as L1, L2, ans L3 corresponding to Figure 14.7) located in the 1 o'clock to 2 o'clock region of the breast.

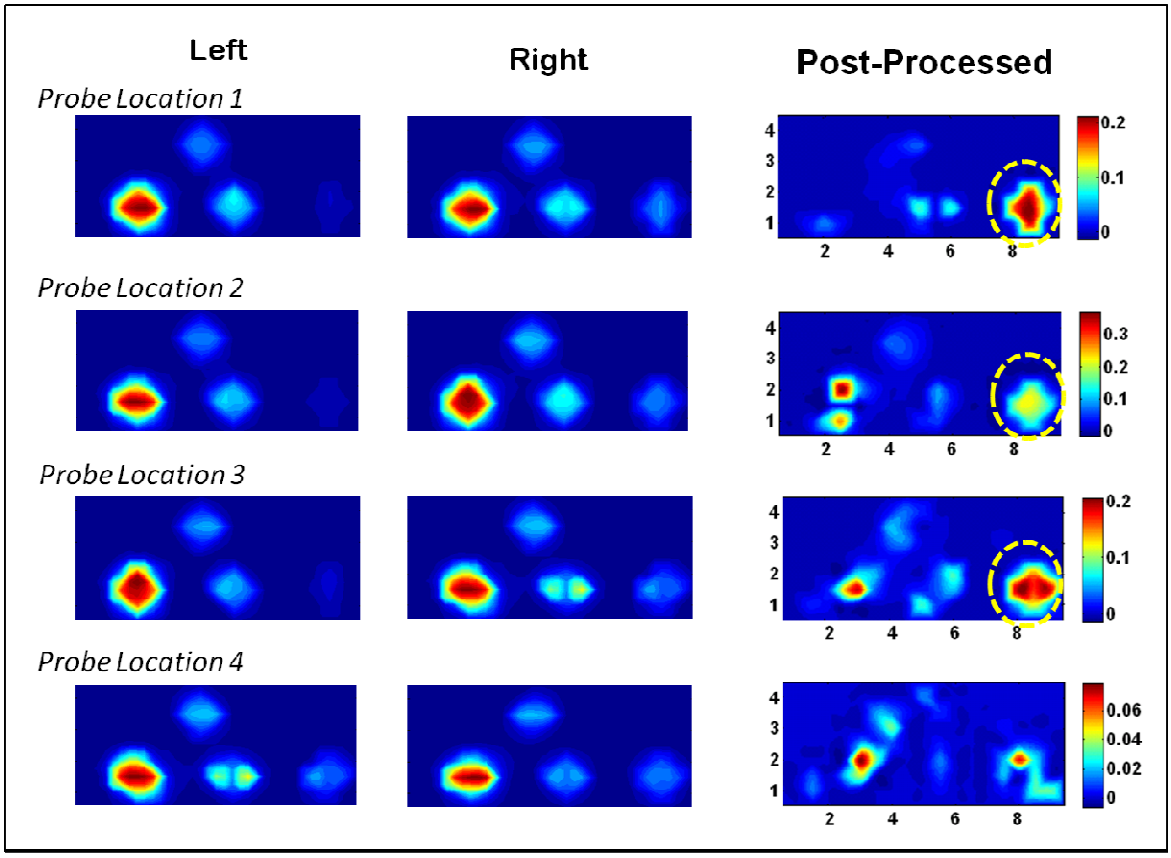

Figure 18. Optical images collected from the breast tissue of a 51 year-old breast cancer patient. The images in Set #1 were collected from the ipsilateral breast and the images in Set #2 were collected from the contralateral breast. The images from Set #1 were subtracted from Set #2 so that the area of higher absorption shows as a higher (or more red) signal in the post-processed images. The yellow dotted circle was hand-drawn to indicate the region of interest.

The performance of our hand-held based optical imager was tested in the clinical setting for the first time on actual breast cancer patients. These preliminary results indicate the ability of the device to detect tumors via continuous-wave absorption-based imaging. Extensive studies will be performed in the future to demonstrate coregistered imaging and 3D tomography in cancer subjects as well as determine the sensitivity and specificity of the device.

Training Plan:

Instrumentation and Phantom Studies:

The P.I. trained under a previous doctoral student to learn how to operate the imaging system and carry out experiments using tissue phantoms.

In Vivo Studies

The P.I. received training from Sylvester Cancer Center under Dr. Richard Kiszonas. The training involved observing breast imaging (i.e. x-ray mammography and breast ultrasound) and interacting with doctors and technicians in the clinical setting.

Mentoring

During Year-1 the P.I. mentored two undergraduate students in performing *in vivo* studies, a third undergraduate student in instrumentation, and a master's student in coregistered imaging and instrumentation.
During Year 2, the P.I. mentored two undergraduate students in experimental studies with phantoms and human subjects, and one masters student in human subject studies.
The P.I. mentored two masters students in human subject studies and image processing.

Clinical Studies

The P.I. continued meetings with Dr. Richard Kiszonas (clinical mentor) to discuss breast imaging with human subjects and challenges that are encountered.

Doctoral Dissertation

The P.I. completed all the experimental studies for the research as outlined in the Statement of Work. The P.I. wrote the dissertation which was defended on March 29, 2011 and successfully passed by the dissertation committee.

KEY RESEARCH ACCOMPLISHMENTS

- Demonstrated fast 2D imaging using the hand-held device on curved tissue geometries in normal human subjects.
  (Specific Aim #1)

- Detected fluorescent targets *in vivo* within actual human breast tissue. **(Specific Aim #1)**
- Implemented 3D tracking system and demonstrated coregistered imaging using the hand-held device on tissue phantoms and *in vitro*. **(Specific Aim #2)**
- Detected deeper targets by applying multi-scan summation technique using coregistered images. **(Specific Aim #2)**
- Adapted 3D reconstruction tools for 3D tomographic imaging in vivo. **(Specific Aim #2)**
- Demonstrated automated coregistered imaging in 2-3 normal human subjects. **(Specific Aim #3).**
- Performed manual coregistered imaging in human subjects using system of marking known probe locations on tissue.
- Demonstrated feasibility of performing 3D tomography using coresgistered image from a human subject.
- Performed initial diffuse optical imaging study in breast cancer patient using the hand-held optical imager.

REPORTABLE OUTCOMES

Peer-reviewed Journal Publications

(1) **S.J. Erickson**, A. Godavarty, S.L. Martinez, J. Gonzalez, A. Romero, M. Roman, A. Nunez, J. Ge, S. Regalado, R. Kiszonas, and Cristina Lopez-Penalver. "Hand-held optical devices for breast cancer: spectroscopy and 3D tomographic imaging," (invited paper) *IEEE Journal of Selected Topics in Quantum Electronics* (in press, 2011).

(2) **S.J. Erickson,** S.L. Martinez, J. Gonzalez, L. Caldera, and A. Godavarty. "Improved detection limits using a hand-held optical imager with coregistration capabilities," *Biomedical Optics Express* 1, 126-134 (2010).

(3) **S.J. Erickson**, J. Ge, A. Sanchez, and A. Godavarty. "Two-dimensional fast surface imaging using a hand-held optical device: in-vitro and in-vivo fluorescence studies," *Translational Oncology* 3(1): 16-22 (2010).

(4) J. Ge , **S.J. Erickson**, and A. Godavarty, "Multi-projection fluorescence optical tomography using a handheld-probe-based optical imager: phantom studies," *Applied Optics* 49, 4343-4354 (2010)

(5) S. Regalado, **S.J. Erickson**, B. Zhu, J. Ge, and A. Godavarty. "Automated coregistered imaging using a hand-held probe-based optical imager," *Review of Scientific Instruments* 81: 023702 (2010).

(6) J. Ge, **S.J. Erickson**, and A. Godavarty. "Fluorescence tomographic imaging using a hand-held probe based optical imager: extensive phantom studies," Applied Optics 48(33), 6408-6416 (2009).

National Conference Proceedings *(* presenter)*

(1) **S.J. Erickson**, S. Martinez, J. Gonzalez, M. Roman, A. Nunez, and A. Godavarty. "3D tomographic breast imaging using a hand-held optical imager," Optical Tomography and Spectroscopy of Tissue IX. Edited by Bruce J. Tromberg, Arjun G. Yodh, Mamoru Tamura, Eva M. Sevick-Muraca, and Robert R. Alfano. Proceedings of the SPIE, Volume 7896, pp. 78962H-78962H-8 (2011).

(2) **S.J. Erickson**, S. Martinez, J. Gonzalez, L. Caldera, and A. Godavarty. "Non-invasive Diagnostic Breast Imaging using a Hand-held Optical Imager," Proceedings of the 14th World Multi-Conference on Systems, Cybernetics and Informatics, 2010.

(3) **S.J. Erickson**, S. Martinez, L. Caldera, and A. Godavarty, "Improved Detection Limits Using a Hand-Held Optical Imager with Coregistration Capabilities," in Biomedical Optics, OSA Technical Digest (Optical Society of America, 2010), paper BTuD43.

(4) S. Martinez, J. DeCerce, J. Gonzalez, **S.J. Erickson**, and A. Godavarty, "Assessment of Tracking Devices towards Accurate Coregistration in a Hand-Held Optical Imager," in Biomedical Optics, OSA Technical Digest (Optical Society of America, 2010), paper BTuD58.

(5) **S.J. Erickson**, S. Martinez, J. DeCerce, A. Romero, L. Caldera, A. Godavarty. "Fast coregistered imaging in vivo using a hand-held optical imager," Advanced Biomedical and Clinical Diagnostic Systems VIII. Edited by Vo-Dinh, Tuan; Grundfest, Warren S.; Mahadevan-Jansen, Anita. Proceedings of the SPIE, Volume 7555, pp. 75550P-75550P-6 (2010).

(6) **S.J. Erickson***, J. Ge, and A. Godavarty. "Clinical Translation of a Novel Hand-Held Based Optical Imager: *In Vitro* and *In Vivo* Studies," IFMBE Proceedings 25th Southern Biomedical Engineering Conference 2009, 15 -- 17 May 2009, Miami, Florida, USA; 24: 3-4; A.J. McGoron, C.Z. Li, and W.C. Lin, eds. ISBN: 978-3-642-01696-7 (2009).

(7) J. Ge, **S.J. Erickson***, and A. Godavarty. "Fluorescence Tomographic Imaging Using a Hand-Held Optical Imager: Extensive Phantom Studies," IFMBE Proceedings 25th Southern Biomedical Engineering Conference 2009, 15 -- 17 May 2009, Miami, Florida, USA; 24: 1-2; A.J. McGoron, C.Z. Li, and W.C. Lin, eds. ISBN: 978-3-642-01696-7; 2009.

Awards

(1) **Best Doctoral Student Award**, College of Engineering and Computing, Florida International University, May 2011

(2) **Worlds Ahead Graduate**, Provost Recognition, Florida International University, May 2011

(3) **Research Excellence Travel Award**, SPIE Photonics West, San Francisco, CA, 2011

(4) **Session Best Paper Award**, 14th World Multi-Conference on Systems, Cybernetics and Informatics, Orlando, FL, 2010

(5) **1st Place Engineering Paper Competition Award**, Scholarly Forum, Florida International University, Miami, FL, 2010

(6) **Lydia I. Pickup Scholarship**, Society of Women Engineers, 2009

(7) **1st Place Doctoral Student Award**, SBEC 2009 Paper Competition, 25th Southern Biomedical Engineering Conference, Miami, FL

(8) **3rd Place Best Student Poster Award** 2009 NIH-SPIE Workshop, Bethesda, MD

(9) **3rd Place Paper Competition Award**, Engineering Division, 2009 Scholarly Forum, Florida International University

Funding Received

(1) Coulter Early Career Translational Award (to PI's mentor): The initial in-vivo results from the PI's work served as strong preliminary results in the proposal to Coulter Foundation, leading to the funding of a 2-year project for the PI's mentor.

(2) Post-doctoral Fellowship, American Cancer Society and Canary Foundation (July 1, 2011 – June 30, 2013) *Clinical Translation of a Hand-held Optical Imager for Breast Cancer Diagnostics*

CONCLUSION

A hand-held probe based optical imaging device has been developed in our Optical Imaging Laboratory towards breast cancer imaging. It is distinctive from other hand-held optical devices in its ability to perform 3D tomography in complex human breast tissues via unique self-coregistration capabilities. In the past, our device has demonstrated 3D tomography using manual coregistration in simple cubicle phantoms. The overall goal of this proposal was towards clinical translation of a novel hand-held optical imager with real-time coregistration facilities toward diagnostic mammography. A systematic experimental approach was designed and executed to evaluate the performance of the device at each stage of clinical translation. The major objectives of the studies were to demonstrate imaging and 3D tomography using the hand-held probe on different curved tissues (Specific Aim #1), implement 3D automated coregistration using an acoustic-based tracking system in order to perform real-time in vivo optical imaging (Specific Aim #2), and perform feasibility in vivo studies using diffuse optical imaging on normal subjects to demonstrate real-time coregistered imaging (Specific Aim #3). In addition to the proposed specific aims, an initial clinical study was performed to demonstrate diffuse optical imaging of breast cancer in a human subject using our hand-held optical imager. The results obtained as outcomes of this proposal were published in the peer-reviewed journals *Biomedical Optics Express, Translational Oncology, IEEE Journal of Selected Topics in Quantum Electronics,* and *Review of Scientific Instruments* and presented at the national meetings *SPIE Photonics West* and *Optical Society of America*.

REFERENCES

(1) **S.J. Erickson** and A. Godavarty. "Hand-Held Based Near-Infrared Optical Imaging Systems: A Review" Medical Engineering and Physics 31, 495-509 (2009).

(2) **S.J. Erickson**, J. Ge, A. Sanchez, and A. Godavarty. "Two-dimensional fast surface imaging using a hand-held optical device: in-vitro and in-vivo fluorescence studies," Translational Oncology 3(1): 16-22 (2010).

(3) S. Regalado, **S. J. Erickson**, B. Zhu, J. Ge, and A. Godavarty. "Automated coregistered imaging using a hand-held probe-based optical imager," Review of Scientific Instruments 81: 023702 (2010).

(4) Leff, D. R., Warren, O. J., Enfield, L. C., Gibson, A., Athanasiou, T., Patten, D. K., Hebden, J., Yang, G. Z., and Darzi, A. "Diffuse optical imaging of the healthy and diseased breast: A systematic review" Breast Cancer Research and Treatment 108, 9-22 (2008).

(5) Ge, J., Zhu, B., Regalado, S., and Godavarty, A. "Three-dimensional fluorescence-enhanced optical tomography using a hand-held probe based imaging system" Medical Physics 35(7), 3354-3363 (2008).

APPENDICES

The following appendices are attached:

Appendix A:

S.J. Erickson, A. Godavarty, S.L. Martinez, J. Gonzalez, A. Romero, M. Roman, A. Nunez, J. Ge, S. Regalado, R. Kiszonas, and Cristina Lopez-Penalver. "Hand-held optical devices for breast cancer: spectroscopy and 3D tomographic imaging," (invited paper) *IEEE Journal of Selected Topics in Quantum Electronics* (in press, 2011).

Appendix B:

S.J. Erickson, S.L. Martinez, J. Gonzalez, L. Caldera, and A. Godavarty. "Improved detection limits using a hand-held optical imager with coregistration capabilities," *Biomedical Optics Express* 1, 126-134 (2010).

Appendix C:

S.J. Erickson, J. Ge, A. Sanchez, and A. Godavarty. "Two-dimensional fast surface imaging using a hand-held optical device: in-vitro and in-vivo fluorescence studies," *Translational Oncology* 3(1): 16-22 (2010).

Hand-Held Optical Devices for Breast Cancer: Spectroscopy and 3-D Tomographic Imaging

Sarah J. Erickson, *Member, IEEE*, Anuradha Godavarty, Sergio L. Martinez, Jean Gonzalez, Adrian Romero, Manuela Roman, Annie Nunez, Jiajia Ge, Steven Regalado, Richard Kiszonas, and Cristina Lopez-Penalver

(Invited Paper)

***Abstract*—Diffuse optical imaging (DOI) is a promising noninvasive and nonionizing method for breast imaging. Several research groups have developed hand-held-based optical imaging devices which are portable and patient-comfortable toward clinical translation of the technology. The different hand-held optical devices developed to date are reviewed herein with a focus on the clinical applications. The hand-held device developed at Florida International University is unique in its ability to perform 3-D tomography using DOI alone via self-coregistration facilities. Results demonstrate the ability of the device to perform 2-D imaging and 3-D tomography in human breast tissue.**

***Index Terms*—Breast cancer, diffuse optical imaging (DOI), hand-held device, 3-D tomography.**

I. Introduction

CLINICAL imaging of breast tissue plays an essential role in cancer detection, staging, treatment monitoring, and surgical guidance. Current screening and diagnostic modalities used in the clinical setting include X-ray mammography, breast ultrasound (US), nuclear imaging, and magnetic resonance imaging (MRI). Combinations of these modalities are used complementarily to noninvasively detect the presence of lesions and determine if they are benign or malignant. However, these methods are neither comprehensive nor infallible leading to redundant biopsies and undetected cancers. Diffuse optical imaging (DOI) (also termed near-infrared spectroscopy, NIRS) using near-infrared (NIR) light is a promising technology which has been developed over the past three decades toward applications such as functional brain mapping and breast cancer diagnosis. The method is noninvasive, uses nonionizing radiation, requires relatively inexpensive instrumentation, and provides functional information from *in vivo* biological tissues. DOI plays a potential role in the clinical setting as a complementary diagnostic tool for breast cancer.

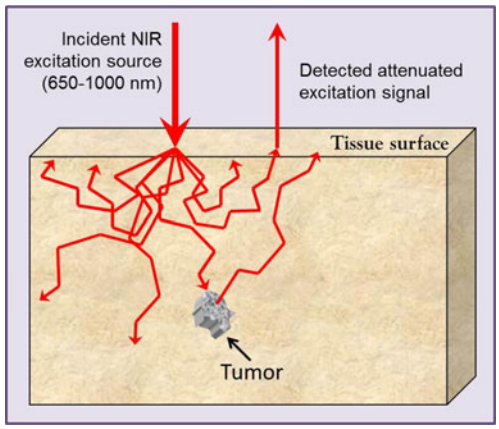

Fig. 1. Principle of DOI.

A. DOI

DOI uses NIR light between 650 and 1000 nm, which is minimally absorbed and preferentially scattered in biological tissues allowing for deep tissue penetration and imaging. The basic principle of DOI is illustrated in Fig. 1. NIR light is launched onto the tissue surface using an NIR (e.g., laser) source and collected at the tissue surface using NIR-sensitive detectors. The difference in optical properties (i.e., absorption and scattering of the light) between normal and diseased tissues is used to characterize tissues and detect abnormalities.

Manuscript received July 12, 2011; revised September 15, 2011; accepted September 19, 2011. This work was supported in part by the NIH-NCI under Grant R15CA1195253, Coulter Foundation's Translational Phase-1 Grant, Florida Department of Health's Bankhead Coley Program (08BB06, 06BB08), and the Department of Defense under Grant BC083282.

A. Godavarty, S. J. Erickson, S. L. Martinez, J. Gonzalez, and M. Roman are with the Optical Imaging Laboratory, Department of Biomedical Engineering, Florida International University, Miami, FL 33174 USA (e-mail: godavart@fiu.edu serickso@fiu.edu smart026@fiu.edu jgonz007@fiu.edu mroma014@fiu.edu)

A. Romero was with the Optical Imaging Laboratory, Department of Biomedical Engineering, Florida International University, Miami, FL 33174 USA. He is now with New York Medical College, Valhalla, NY 10595 USA (e-mail: mr.adrian.romero@gmail.com).

A. Nunez was with the Optical Imaging Laboratory, BME, Florida International University (FIU), Miami, FL 33174 USA. She is now with Bio-Tissue, Inc., Miami, FL 33173 USA (e-mail: anune019@fiu.edu)

J. Ge was with the Optical Imaging Laboratory, Department of Biomedical Engineering, Florida International University, Miami, FL 33174 USA. She is now with the Department of Radiation Oncology, University of Washington in St. Louis, St. Louis, MO 63130 USA (e-mail: gejiajia@gmail.com).

S. Regalado was with the Optical Imaging Laboratory, Department of Biomedical Engineering, Florida International University, Miami, FL 33174 USA. He is now with ENS Imaging, Pembroke Pines, FL 34236 USA (e-mail: regalado106@aol.com).

R. Kiszonas is with the Breast Imaging Division, Sylvester Comprehensive Cancer Center, Miami, FL 33442 USA, and also with the Department of Radiology, University of Miami, Coral Gables, FL 33124 USA (e-mail: rkiszonas@med.miami.edu).

C. Lopez-Penalver is with Advanced Medical Specialties, Miami, FL 33173 USA (e-mail: clopezmd@aol.com).

Color versions of one or more of the f gures in this paper are available online at http://ieeexplore.ieee.org.

Digital Object Identifie 10.1109/JSTQE.2011.2170664

1077-260X/$26.00 © 2011 IEEE

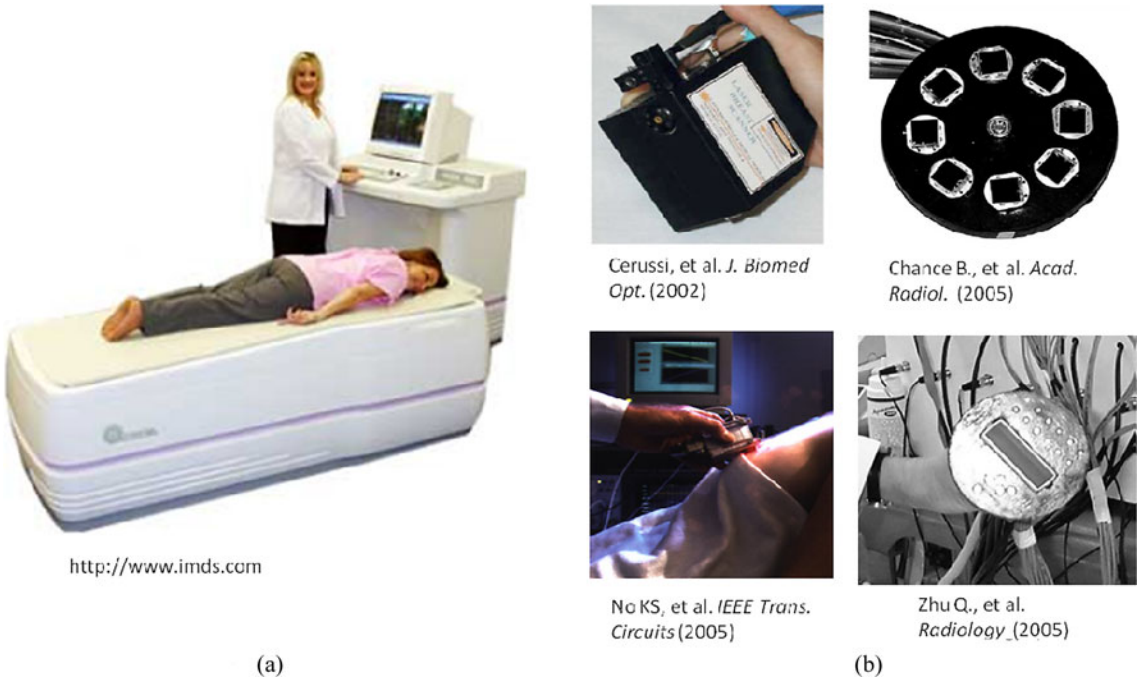

Fig. 2. Optical imaging instrumentation has been developed in the form of bed-based systems and hand-held devices. (a) Example of a bed-based imager. (b) Examples of hand-held devices developed by several research groups.

DOI uses the inherent absorption contrast in tissues. Additionally, external fluorescen contrast agents can be used to improve the contrast in order to molecularly target tumors at their early stage. In fluorescenc imaging, the incident laser causes the flu orophore to excite. Upon relaxation, light is emitted at a higher wavelength and detected at the surface using appropriate filters Example contrast agents include indocyanine green (ICG) [1], Cy5.5 [2], protoporphyrin IX [3], etc. (only sample references provided).

There are three different measurement techniques employed in optical imaging: continuous wave (CW), frequency domain (FD), and time domain (TD). In CW imaging, the source light intensity remains constant in time and attenuates as it propagates through the tissue due to absorption and (indirectly) to scattering. FD imaging uses time-dependent intensity-modulated light, which becomes attenuated and phase shifted as it propagates through the tissue. TD imaging uses time-dependent (pico- or nanosecond) pulses of light, which broaden and attenuate as it propagates through the tissue. Different types of instrumentation using one or more of these measurement techniques have been developed toward DOI of breast tissue.

B. Bed-Based Versus Hand-Held Optical Imagers

Several research groups have developed DOI instrumentation in the form of bed-based imagers [example shown in Fig. 2(a)]. Most of these imagers have a fi ed imaging geometry, which limits the volume of breast tissue that can be imaged and does not allow imaging of the chest wall and axillary regions, and/or use compression of the breast tissue which can be uncomfortable for the patient depending on the amount of compression. Hand-held devices, on the other hand, allow for fl xibility to image any tissue volume or geometry and any region of the breast, chest wall, and axillary areas. Examples of hand-held probe-based optical devices developed by several research groups are shown in Fig. 2(b). In addition to being able to image breast tissue of any size without causing discomfort to the patient, hand-held devices can also be made portable, which can facilitate rapid translation to the clinic. Clinical studies using different bed-based optical imagers have been reviewed elsewhere [4].

Herein, different hand-held probe-based optical devices (from here on, termed as hand-held optical devices for brevity) are described and categorized according to the probe design and their specifi application(s). Most of the devices are used toward spectroscopic measurements of tissue optical properties in order to detect the presence of abnormal tissue. A few hand-held devices incorporate a second imaging modality (e.g., US) in order to employ the structural information from this second modality, toward 3-D optical tomographic imaging. A hand-held optical device developed at Florida International University (FIU) is unique in its ability to perform 3-D tomographic imaging without the need for a second imaging modality, due to its self-coregistration capabilities. The details of the imager and studies demonstrating its ability to perform 2-D and 3-D imaging in human breast tissue are described in latter sections.

II. Hand-Held Optical Imagers Developed To Date Toward Breast Imaging

Hand-held optical devices have been developed by several research groups [5]–[52] with differences in the hand-held probe design, instrumentation, and their specifi goals for clinical imaging. Table I gives a summary of the different NIR hand-held devices developed to date in terms of the imaging modality (single or multimodal), measurement technique, source type and

TABLE I
SUMMARY OF DIFFERENT HAND-HELD OPTICAL DEVICES DEVELOPED TO DATE TOWARD BREAST IMAGING

Device #	Reference	Modality	Meas. Technique	Source Type	Source Wavelengths (nm)	Clinical Application(s) *(bold italics are in-vivo studies)*
1	Tromberg, 1997[5]	DOS*	FD (300 kHz – 1 GHz)	diode lasers (10-30 mW)	674, 811, 849, 956	***Compare optical properties of normal and benign lesion-containing breast tissue***
	Shah, 2004 [11]		FD (50-700 MHz)	diode lasers (5-25 mW)	674, 780, 803, 849, 894, 915, 980	***Measure optical & physiological properties of healthy breast tissue***
	Bevilacqua, 2000 [12]	DOS	CW & FD (100-700 MHz)	FD - diode lasers (<20 mW) CW – 150 W halogen lamp	672, 800, 806, 852, 896, 913, 978	***Measure the absorption spectra of normal human breast tissue***
	Cerussi, 2007 [18]	DOS	CW & FD (50-1000 MHz)	FD – diode lasers (20 mW) CW – white-light source	660, 690, 780, 808, 830, 850	***Predict postsurgical pathological response to neoadjuvant chemotherapy in 11 breast cancer subjects***
2	No, 2005 [19]	DOS	FD (10 MHz – 1 GHz)	8 laser diodes (50 mW)	783	(Phantom study)
	No, 2007 [21]	DOS	FD (50-300 MHz)	4 laser diodes (20 mW)	681, 783, 823, 850	***Detect the presence of breast cancer in a human subject***
3	Chance, 2005 [22]	DOS	CW	light emitting diodes (10-15 mA)	760, 805, 850	***Determine sensitivity and specificity of detecting breast cancer in 116 human subjects***
4	Chance, 2006 [25]	DOS	FD (3 kHz)	2 light emitting diodes (20 mA)	800	***Detection and 2D localization of brest cancer lesion in a human subject***
5	Liu, 2004 [26]	FDOI	FD (3 kHz)	4 light emitting diodes	(infrared)	(Phantom study)
6	Cheng, 2003 [27]	DOI	CW	laser diodes (0.15 W/cm^2)	690, 830	***Determine sensitivity and specificity of detecting breast cancer in 50 human subjects***
	Xu, 2007 [30]	DOI	CW	laser diodes (0.15 W/cm^2)	690, 830	Detect tissue optical, mechanical, and physiologic changes under dynamic loading
7	Durduran, 2005 [32]	DOS	CW	long coherence laser	785	***Measure blood flow contrast between tumor-containing and normal breast tissues***
8	Zhu, 1999 [35]	DOT &US	FD (200 MHz)	laser diodes	776, 834	Phantom study towards 3D tomography of breast cancer
	Chen, 2001 [38]	DOT & US	FD (140 MHz)	laser diodes	760, 830	Phantom study towards 3D tomography of breast cancer
	Zhu, 2003 [39]	DOT & US	FD (140 MHz)	laser diodes	780, 830	***Image benign and malignant breast lesions in human subjects***
	Zhu, 2010 [45]	DOT & US	FD	laser diodes	690, 780, 830	***Differentiate benign and malignant lesions at early-stage in breast tissue***
9	Ge, 2008 [46]	FDOT	FD (100 MHz)	laser diode (<5 mW)	785	Phantom towards 3D tomography of breast cancer
	Erickson, 2010 [47]	FDOI	CW	laser diode (<5 mW)	785	***Fast 2D imaging of fluorescent targets in breast tissue of healthy subjects***
10	Solomon, 2010 [48]	FDOT	CW	laser diodes (15-30 mW)	785, 830	***Phantom & small animal study towards sentinel lymph node mapping***

Selected publications are listed for each device. The applications described in the text expand beyond what is listed here.
*DOS: diffuse optical spectroscopy; DOI: diffuse optical imaging; DOT: diffuse optical tomography; FDOT: fluorescence-enhanced diffuse optical tomography.

source output power, source wavelengths, and the clinical applications. An extensive review and detailed table summarizing the different hand-held optical devices developed to date is published elsewhere [5]. The hand-held optical devices developed toward breast imaging typically use CW and/or FD measurement technique. The CW technique is simple, inexpensive, and allows rapid data acquisition. However, CW can only provide the total attenuation property of the tissue (i.e., attenuation due to both absorption and scattering is measured as a single property). The FD technique (typically in megahertz range) requires

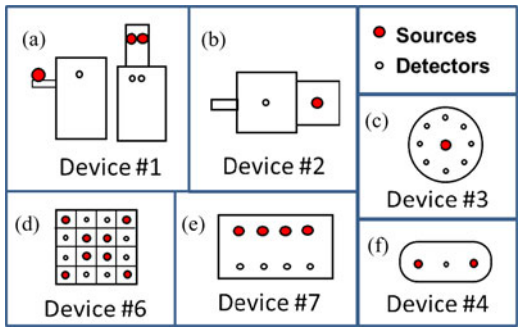

Fig. 3. Schematics of different hand-held probes with few source(s) and detector(s): (a)–(e) Spectroscopic based probes from the University of California Irvine (Device #1), the University of California Irvine (Device #2), the University of Pennsylvania (Device #3), ViOptix, Inc. (Device #6), and the University of Pennsylvania (Device #7). (f) Interference-based probe from the University of Pennsylvania (Device #4).

extensive instrumentation and relatively longer data acquisition times (over CW). However, it has the advantage of providing information about absorption and scattering properties of the tissue separately. For both the CW- and FD-based hand-held optical devices, the commonly used light sources are laser diodes amongst lasers, halogen lamps, and light emitting diodes. The maximum optical power incident on breast tissues has not exceeded 50 mW using either CW- or FD-based devices. In the following sections, the hand-held optical devices are described in terms of the differences in the probe design and clinical applications.

A. Classification of Hand-Held Optical Devices Based on Probe Design

The design of the probe for a hand-held optical device is governed by the application toward which the device will be utilized. The simplest probe design contains a single source–detector pair or a few source–detector pairs that are used to collect spectroscopic measurements of the tissue. Fig. 3(a)–(e) provides schematics of different probes designed toward spectroscopy (devices #1-3,6,7) [9]–[26], [31]–[36]. Typical measurement parameters for spectroscopic imaging are oxy- and deoxyhemoglobin concentration, water concentration, oxygen saturation, and scatter power (from absorption and scattering coefficient at multiple wavelengths). When external fluorescen contrast agents are used, the measurement parameter(s) of interest is(are) the absorption and scattering due to the fluorophor at the excitation or emission wavelength, fluorescenc lifetime, and quantum yield. These parameters provide functional information about healthy and diseased breast tissue and can be used to detect the presence of tumors. Another type of probe design incorporates the principle of interference using two or four sources and a single detector. The antiphased sources (i.e., 180° out of phase) are illuminated simultaneously in the FD, and the phase cancellation of the signal (due to destructive interference) is used to detect as well as estimate the 2-D location of a tumor within the breast tissue. A schematic of an interference-based probe design is provided in Fig. 3(f) (device #4). In addition to detection and 2-D localization of a tumor, one research group has incorporated US with optical imaging in order to perform 3-D tomography [39]–[49]. Fig. 4 shows two versions of a device which combines NIR imaging and US into a single probe. The US component is used to provide structural information to perform 3-D tomography. Fig. 5 shows a schematic of the probe developed at FIU (Optical Imaging Laboratory) which is unique in its ability to perform 3-D tomography in breast tissue without employing a second imaging modality [50], [51]. The device is described in detail in Section III.

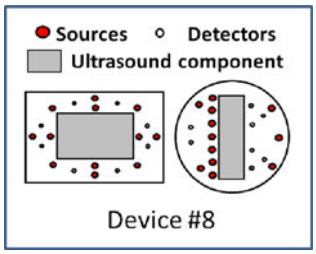

Fig. 4. Schematics of hand-held probe developed at the University of Connecticut with multiple sources and detectors which incorporate US imaging in order to perform 3-D tomography (Device #8).

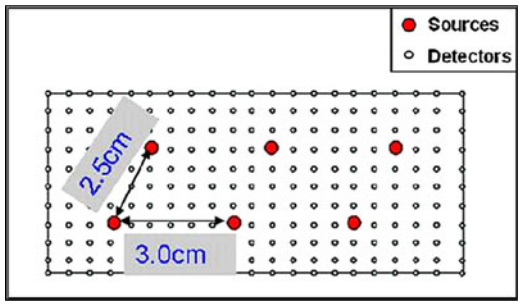

Fig. 5. Schematic of hand-held probe design from the Optical Imaging Laboratory at FIU (with 6 sources and 165 detectors) toward 3-D tomography.

B. Clinical Applications of Different Hand-Held Optical Devices

The design of any hand-held probe and the number of sources and detectors is governed by the desired clinical applications. Hand-held optical devices have been utilized toward fi e major applications of clinical breast imaging: 1) measurement of optical and physiological properties of healthy breast tissue; 2) detecting the presence of abnormal tissue (i.e., tumors); 3) distinguishing between benign and malignant tumors; 4) monitoring response to neoadjuvant chemotherapy; and 5) sentinel lymph node mapping.

Prior to imaging cancerous tissues, it is necessary to know the variations of optical properties within healthy tissue as a baseline. The multiwavelength CW and FD-based device developed at the University of California, Irvine (see device #1 in Table I) was initially used to measure the optical and physiological properties of healthy breast tissue and to compare the optical properties of healthy and benign-tumor containing tissue. The results showed the ability of the NIR device to demonstrate wavelength-dependent differences in absorption and scattering properties between pre- and postmenopausal normal breast tis-

sues as well as differences in the same breast tissue during different time periods in the menstrual cycle. It was also shown that the tissue properties vary amongst different normal subjects as well as with respect to the different locations within the same breast of a normal subject [11], [13]–[15].

Once a general baseline of variations of optical properties of healthy tissue is known, it can be used toward the second application of differentiating abnormal from healthy tissue, in order to detect the presence of disease (e.g., cancer). Device #1 (see Table I) was also used in several studies (comprised in total of about 100 subjects) to compare healthy and tumor-containing breast tissue [16], [17], [21]. The results showed differences in the optical properties of the tissue based on subject age, tumor size, and tumor pathology. Collaborating researchers at the University of California, Irvine, developed a multiwavelength full-heterodyne hand-held broadband breast scanning device (see device #2 in Table I), which was used to extract the optical properties (absorption and scattering coefficients from phantom and human tissues [23]–[25]. Based on the measured differences in the absorption coefficient between the diseased (i.e., tumor) and normal breast tissue, the device detected the presence of a lesion *in vivo* human breast tissue. A group from the University of Pennsylvania used a multiwavelength hand-held optical device (see device #3 in Table I) in an extensive study to show the differences in the biochemical and physiological properties of breast tissue containing growing cancers, compared to corresponding normal tissue in the contralateral breast [26]. They acquired data over six years from 166 patients with 44 confirme malignancies. They reported the ability to distinguish cancerous from noncancerous breast tissue with a sensitivity of 96% and specificit of 93%. Other spectroscopic-based hand-held devices (see devices #4–6 in Table I) were used similarly in phantom and human subject studies to detect the presence of tumors based on the optical property differences between healthy and diseased tissue [29]–[34]. One hand-held device (see device #7 in Table I) was designed to measure blood fl w heterogeneity in order to show that blood fl w in a breast containing a palpable tumor is different than that in a normal breast [36]. The results showed that blood fl w was greater in the tumor region than in the normal tissue.

A third clinical application is to distinguish between benign and malignant breast lesions. Studies to distinguish benign and malignant breast lesions have been reported based on diffuse optical measurements of blood volume, saturation, or both [44], [46], [49]. Several studies showed that the maximum and average total hemoglobin concentration (HbT) were significantl higher in malignant lesions than benign lesions. However, the results were from a relatively small pool of data and more extensive trials will be required to demonstrate conclusive results [4].

In addition to detecting and diagnosing lesions within breast tissue, a fourth major application of hand-held optical devices is monitoring tumor response to neoadjuvant chemotherapy. Neoadjuvant chemotherapy treatment is administered to a cancer patient prior to surgery in an attempt to decrease the size of the tumor. Optical devices have the advantage of using non-ionizing light and, therefore, can be used for multiple periodic imaging studies without causing added harm to the patient. The CW/FD-based device developed at the University of California, Irvine (see device #1 in Table I) was used in several studies conducted to monitor tumor response to neoadjuvant chemotherapy in patients [18], [19], [22]. The tumor locations were known *a priori* from mammography, US, or palpation. The device was used to measure the physiological characteristics of the tumor prior to chemotherapy. This was followed by monitoring the changes in tissue optical properties over several months, due to changes in the tumor with neoadjuvant chemotherapy treatment. The device developed at the University of Pennsylvania (see device # 7 in Table I and Fig. 3) was applied toward blood fl w measurement studies performed at the University of California, Urvine. The collaborative research group found that the information from the blood fl w changes in addition to changes in oxygenation and lipid contrast measured using the device developed at the University of California, Irvine (see device #1 in Table I and Fig. 3) enhanced the ability to monitor response to neoadjuvant chemotherapy treatment [53]. Researchers from the University of Connecticut used their multimodal hand-held device (see device #8 in Table I) to image heterogeneous hemoglobin distributions in large cancers, which are used to monitor tumor vascular responses to neoadjuvant chemotherapy [47]. The studies showed that after several cycles of neoadjuvant chemotherapy, the measured values of total hemoglobin concentration and spatial extension were much smaller in comparison to those prior to chemotherapy, as validated from US and positron emission tomography (PET) images.

A f fth application is toward imaging of sentinel lymph nodes. A hand-held optical device developed at Washington University, St. Louis (see device #10 in Table I) was developed toward the application of sentinel lymph node mapping [52]. Studies demonstrated the potential of using the device to perform video-rate fluorescenc molecular tomography in phantoms and small animals.

Hand-held optical devices have demonstrated potential of playing a significan role at various stages of clinical breast imaging. The different devices have been used toward applications of tissue characterization, lesion detection, and monitoring of neoadjuvant chemotherapy treatment. The devices mentioned previously have been primarily used to collect spectroscopic measurements (typically presented as line plots of localized points) and not toward 2-D surface imaging of large areas (e.g., 36 cm^2) from a single scan in near real-time or 3-D tomography. Only two devices (devices #8 and #10) have been used toward 3-D tomography with the addition of a second imaging modality. The device developed at FIU (device #9 in Table I) is the only one of its kind which has demonstrated 3-D tomography using optical imaging alone via its unique self-coregistration capabilities. The device is described in detail in the following section.

III. Hand-Held Optical Imager Developed at FIU

A hand-held optical device has been designed and developed in Optical Imaging Laboratory at FIU with the following unique features: 1) f exibility to image different tissue curvatures (0°–

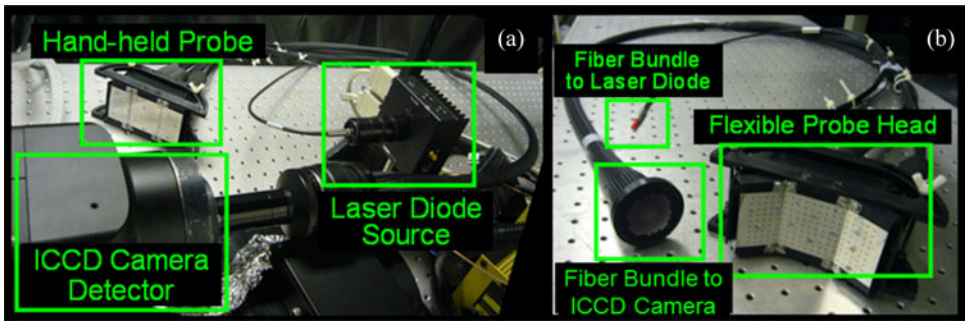

Fig. 6. (a) Hand-held probe based optical device showing the hand-held probe is fibe -optically coupled to the laser source and ICCD camera. (b) Probe face is fl xible to contour to different tissue curvatures.

45°) via a geometrically adaptive probe head; 2) ability to simultaneously illuminate (at six point locations) and collect 785-nm NIR signals (at 165 point locations) toward fast (or near real-time) 2-D imaging of a large tissue areas; and 3) coregistration facilities to enable 3-D tomographic imaging of breast tissue geometries [50], [51], [54]. The following sections describe the instrumentation of the hand-held device, the coregistered imaging approach, and various experimental (fluorescenc and absorption contrasted) studies performed in phantoms, *in vitro*, and *in vivo* human breast tissues in order to demonstrate 2-D area imaging and 3-D tomographic imaging.

A. Instrumentation and Probe Design

The three major components of the hand-held imaging device are the hand-held probe, the laser diode source, and the intensifie charge-coupled device (ICCD) detector [as shown in Fig. 6(a)]. The hand-held probe head is designed with unique features in that it is fl xible to contour to different tissue curvatures, it has a large imaging area (4 cm × 9 cm) for large volume interrogation, and it uses simultaneous illumination at six source points and detection at 165 detector points for rapid data acquisition. The hand-held probe head is shown in Fig. 6(b). The fl xible probe is divided into three sections (or plates) and each of the side sections is capable of curving up to 45°. The instrumentation is designed for collecting either CW or FD measurements as needed and based on the chosen clinical application. When operated in the FD mode, two frequency synthesizers are connected at the source and detector end to modulate the signal between 50 and 300 MHz (typically operated at 100 MHz). The FD instrumentation of the hand-held device is described in more detail elsewhere [50]. Initially, CW measurements are used for the *in vivo* studies presented here in order to demonstrate fast 2-D imaging toward tumor detection. FD measurements were demonstrated in phantoms and *in vitro* and will be used in future *in vivo* studies toward 3-D tomography.

B. Coregistered Imaging Approach

In order to perform 3-D tomography in human breast tissues of varying volumes and curvatures, it is necessary to track the probe location in real time and automatically coregister the image at its imaged location on the tissue. Coregistered imaging of tissue/phantoms is implemented as a three-stage process (see Fig. 7). Stage 1: The probe's 3-D position and orientation is tracked in real time with respect to a discretized mesh of the phantom or tissue geometry using 3-D motion tracking devices (steps 1–4 in Fig. 7). Stage 2: The hand-held device is used to acquire raw data, i.e., optical signals of intensity (or phase shift, as needed) (step 5 of Fig. 7). The raw data are postprocessed (step 6 of Fig. 7) using MATLAB software developed in house in order to generate and display the image as a 2-D surface contour plot (step 7 of Fig. 7). Stage 3: Image coregistration (where images are registered onto their true locations w.r.t. the imaged 3-D tissue geometry) is performed using tracking/coregistration interfacing software developed in house in MATLAB/LabVIEW. The optical data from the 2-D surface contour plot is coregistered onto the 3-D discretized phantom or tissue geometry at the probe location using the positional information of the entire probe head (i.e., all source and detector point locations) during each scan (i.e., at each imaged location). The entire coregistered imaging process is described in detail elsewhere [54].

Coregistered imaging was validated previously in phantoms and *in vivo*. In each case, the probe was placed at known coordinate locations that were measured and marked on the phantom or tissue. The probe was placed at each location and the tracked coordinate values were compared with the actual coordinate values of the probe. The total distance off was ∼0.19 cm in the phantom study and ∼1 cm *in vivo* [55]. The error in the phantom study can be attributed to instability of the tracking system. The greater error *in vivo* can be attributed to the additional movement of the subject and/or operator error. Efforts are being made to overcome these limitations and improve the accuracy of coregistered imaging.

C. 3-D Tomography Approach

Three-dimensional reconstruction was performed using a computationally efficien version of the approximate extended Kalman filte (AEKF)-based algorithm [50], [56], [57] in order to reconstruct the parameter of interest (in this case, the absorption coefficien due to the fluorophor at excitation wavelength, μ_{axf}) within the 3-D discretized tissue geometry. The algorithm employs 1) an initial guess of the reconstruction parameter, μ_{axf} (herein, arbitrarily set to 0.003 cm^{-1} for the entire tissue

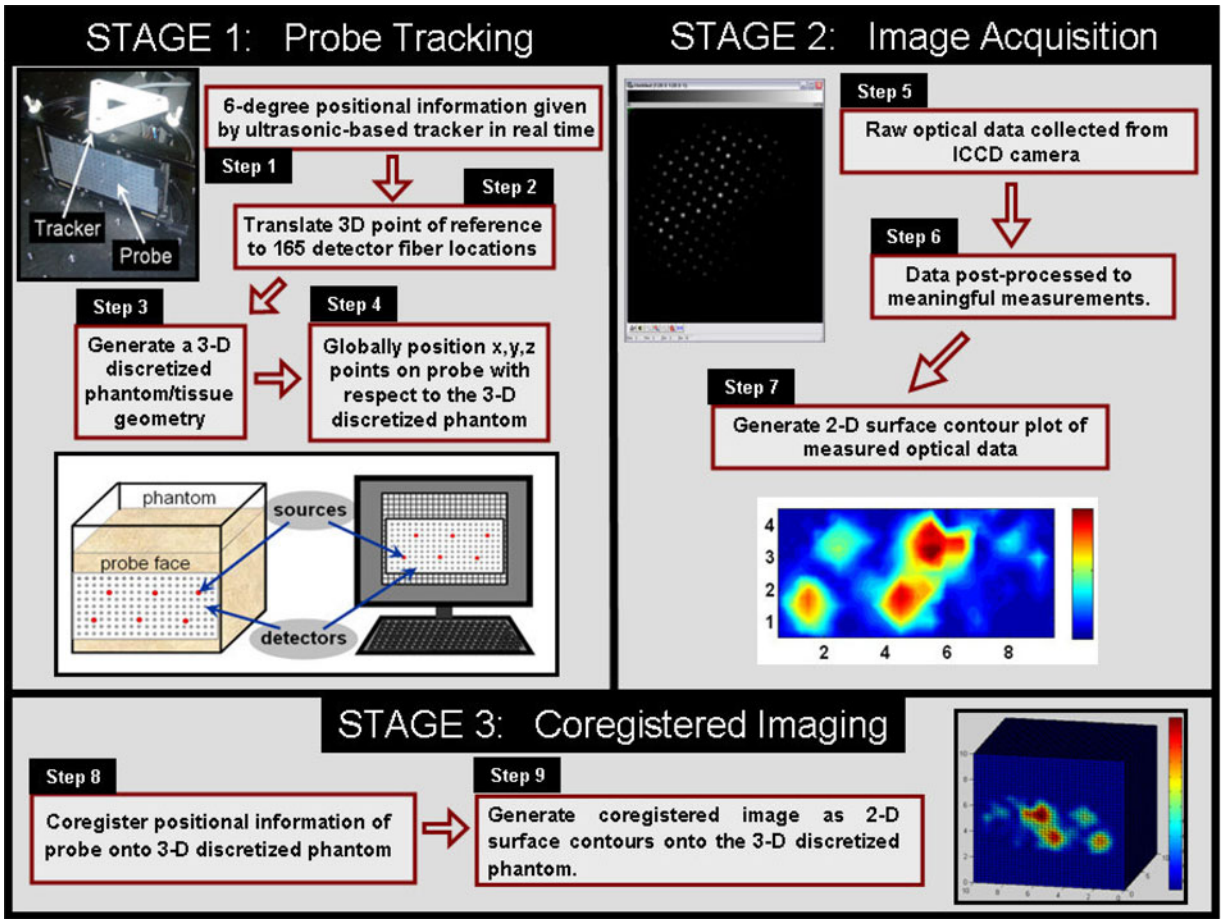

Fig. 7. Flowchart of the coregistered imaging process, implemented as automated coregistration software during optical imaging studies. (Reproduced from Regalado, *et al.*, *Rev. Sci. Inst.*, 2010 [54].)

geometry); 2) coregistered experimental data from the hand-held device; and 3) a mathematical model to represent the light propagation in tissues (here diffusion approximation to the radiative transport equation) along with the Galerkin-based finite element forward model), in order to get an updated distribution of the reconstruction parameter (μ_{axf}). The AEKF algorithm is carried out recursively, i.e., each set of measurements is used to continuously update the unknown parameter distribution and the parameter error covariance. This recursive AEKF algorithm is carried out iteratively until the reconstructions converge. The convergence criteria are met when the root-mean-square output error is less than 1%, or the total number of iterations exceeds 50. The resulting 3-D μ_{axf} distribution along the tissue geometry is plotted using Tecplot.

For phantom studies, the probe location (i.e., source and detector positions) was evaluated manually and the optical properties of the phantom were measured under different experimental conditions using a single-pixel FD homodyne system. In the case of *in vivo* tomography studies, the positional information of the probe (i.e., source detector points on the probe head) with respect to the tissue was extracted from the coregistered image. A spherical fluorescen target that was used to simulate a tumor was placed underneath the fla of the breast tissue (i.e., between breast tissue and chest wall, underneath the breast), as shown in Fig. 9. No fluorescenc was injected into the human subject. Average optical properties of normal breast tissues (i.e., endogenous absorption and scattering coefficients [5] were input into the reconstruction algorithm (with uniform distribution) as the initial guess in reconstructing the absorption coefficien due to the fluorophor (here μ_{axf}) (assuming no scattering variations).

D. Experimental Studies: Phantom and In Vitro Studies Toward 2-D Target Detection and 3-D Tomography

Studies were performed using slab tissue phantoms composed of 10 cm $\times$ 10 cm $\times$ 10 cm acrylic cubes and fille with 650 ml of 1% Liposyn solution (Liposyn II, 20%, Henry Schein, Melville, NJ) in order to mimic the optical properties of a typical breast tissue. A fluorescen target (ICG at 1 μM concentrations) was placed at different depths from the imaging surface and optical measurements were acquired. Experiments were also performed using *in vitro* phantoms, which were composed of minced chicken breast combined with 1% Liposyn solution, in order to mimic human tissue case with nonuniform scattering background. The *in vitro* mixture of minced chicken breast (480 ml) and 1% Liposyn (260 ml) was placed inside a

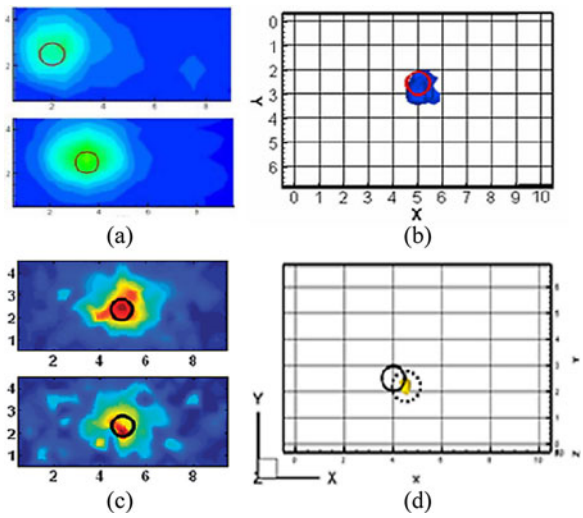

Fig. 8. (a) 2-D image of a 0.45-cm^3 fluorescen target placed at a depth of 1.5 cm from the imaging surface in a tissue phantom under perfect uptake (T:B = 1:0). The black open circle represents the true target location. (b) Isosurface contour plot of the 3-D reconstruction of a 0.45-cm^3 fluorescen target placed at a depth of 1.0 cm from the imaging surface in a tissue phantom under perfect uptake (T:B = 1:0). The red open circle represents the true target location. (c) 2-D images of a 0.45-cm^3 fluorescen target placed at a depth of 1.5 and 2.0 cm in the upper and lower images, respectively, within an *in vitro* phantom under perfect uptake (T:B = 1:0). The black open circles represent the true target location. (d) Isosurface contour plot of the 3-D reconstruction of a 0.45-cm^3 fluorescen target placed at a depth of 2.0 cm *in vitro* under perfect uptake (T:B = 1:0). The black open circle represents the true target location and the dashed open circle in (d) is used to emphasize the recovered target location.

10 cm × 10 cm × 10 cm acrylic cube and mixed thoroughly to form a gelatinous semisolid composition.

The imaging time to collect a single image is <3 s. Additionally, background images are collected and used in postprocessing to eliminate background noise in the images (i.e., subtraction technique) [50]. The total imaging time to generate one postprocessed (i.e., subtracted) image is ∼5 s. The 3–5 s image collection is termed as "fast" imaging and is described in detail in [51].

FD-based experimental studies were performed to generate 2-D area images and 3-D tomographic images of fluorescen targets within phantoms and *in vitro*. AEKF-based reconstruction algorithms were used to obtain 3-D tomographic images as described in Section III-C. Fig. 8 shows the results of 2-D imaging and 3-D tomography in tissue phantoms and *in vitro* (three example cases amongst the various experimental studies performed). Fig. 8(a) shows 2-D images of a 0.45-cm^3 fluorescen target placed at a depth of 1.5 cm from the imaging surface in a tissue phantom under perfect uptake (i.e., with target to background ratio T:B = 1:0). Fig. 8(b) shows the isosurface contour plot of the 3-D reconstruction of a 0.45-cm^3 fluorescen target placed at a depth of 1.0 cm from the imaging surface in a tissue phantom under perfect uptake ratio (T:B = 1:0). Fig. 8(c) shows 2-D images of a 0.45-cm^3 fluorescen target placed at a depth of 1.5 and 2.0 cm in the upper and lower images, respectively, within an *in vitro* phantom under perfect uptake ratio (T:B = 1:0). Fig. 8(d) shows the isosurface contour plot of the 3-D reconstruction of a 0.45-cm^3 fluorescen target placed at a depth of 2.0 cm *in vitro* under perfect uptake (T:B = 1:0). The dashed open circle is used to emphasize the recovered target location [see Fig. 8(d)]. In all figures the true target location is indicated by the solid open circle. The 2-D images show that fluorescen targets were detected close to the true location in tissue phantoms and *in vitro*. The isosurface plots show that the target was recovered close to the true location. Quantitative results from the reconstructions are provided in Table II. In the presence of a homogeneous background (i.e., Liposyn-based phantom, expt # 1), the target was reconstructed close to its true location (except depth) with similar volumes and significan T:B contrast ratio. For the heterogeneous *in vitro* case (expt #2), the target was close to its true location (except its depth), although the reconstructed target volume and T:B contrast ratio were not significan (probably from the heterogeneity of the background). In spite, a distinct target with no artifacts was reconstructed, demonstrating the capability for 3-D tomographic imaging *in vitro* heterogeneous phantoms using the hand-held device. In both the (Liposyn) phantom and *in vitro* case, the target was recovered at a shallower depth than the true target location. This is due to the physics of reflectance-base measurements and has been observed by other researchers [58]–[60]. Acquiring images from multiple projections tends to improve the depth recovery of targets in 3-D reconstructions, as observed from our parallel study [61].

These sample tissue phantom and *in vitro* experimental results demonstrate the ability of the device to perform 2-D imaging and 3-D tomography. Extensive phantom studies were performed to determine the detection limits of the device and a multiple-scan method was developed to improve the detection limits from 2.5 to 3.5 cm [62], [63]. Eventually, the effectiveness of the device is determined from its performance *in vivo* human subjects.

E. Experimental Studies: In Vivo Studies Toward 2-D Target Detection, Coregistered Imaging, and 3-D Tomography in Human Breast Tissue

Following extensive phantom studies to determine the detection limits of the hand-held device, human subject studies were performed to demonstrate the feasibility of imaging actual breast tissues. Systematic studies were performed in progression to demonstrate fast 2-D imaging, coregistered imaging, and finall 3-D tomography *in vivo*. Additionally, a preliminary study was performed in a breast cancer subject to demonstrate the ability of the device to image breast tumors in human tissue.

1) Fast Imaging Toward 2-D Target Detection in Healthy Human Subjects: Initial studies were performed in healthy human subjects to test the ability of the device to detect a fluorescen target through actual human breast tissue via fast 2-D imaging. All human subject studies were approved by the FIU Institutional Review Board (IRB). Healthy female volunteers age 21 and above were recruited for the studies. A spherical fluorescen target that was used to simulate a tumor (the same target used in phantom and *in vitro* studies) was placed underneath the fla of the breast tissue (i.e., between breast tissue and chest wall, underneath the breast) as shown in Fig. 9.

TABLE II
SUMMARY OF THE QUANTITATIVE RESULTS FOR THE TWO SAMPLE EXPERIMENTAL CASES OF 3-D TOMOGRAPHY IN TISSUE PHANTOM (EXPT #1) AND *in vitro* (EXPT #2) INCLUDING THE ACTUAL TARGET LOCATION IN CM, THE ACTUAL TARGET VOLUME, THE TARGET TO BACKGROUND RATIO (*T*:*B*), THE RECOVERED TARGET LOCATION IN CM, THE RECOVERED μ_{axf} VALUES IN CM^{-1}, AND THE RECOVERED TARGET VOLUME

Expt	Target's centroid		Distance off (in depth, z) cm	T:B ratio		Target Volume (cm^3)	
	True	Reconstructed		True	Reconstructed	True	reconstructed
# 1 (Liquid Phantom)	[5,2.5,1]	[5,2.7,0.3]	0.7	1:0	267:1	0.45	0.67
# 2 (*In-vitro)*	[4,2.5,2]	[4.6,2.3,.2]	1.8	1:0	0.14:1	0.45	0.014

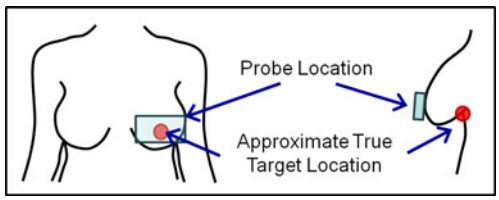

Fig. 9. Schematic showing the location of a fluorescen target (placed superficiall underneath the breast tissue) and the hand-held probe during *in-vivo* imaging.

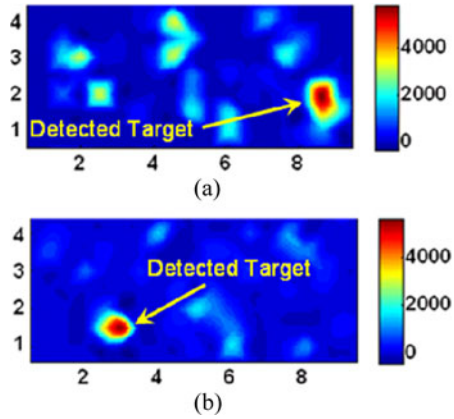

Fig. 10. Images of f uorescence intensity obtained as 2-D surface contour plots (with background subtracted), acquired *in vivo* from a human subject using a spherical fluorescen target, for two experimental cases: (a) probe was in the fla position and a 0.23-cm^3 target was placed at the 4 o'clock position, and (b) the probe was in the curved position and a 0.45-cm^3 target was placed at 8 o'clock position. The images acquired using the probe in the curved position are illustrated as projected as a f at 2-D image, in order to be consistent with the images presented in case (a) (i.e., using the probe in fla position).

In the f rst study, a 0.23-cm^3 sphere with 1-μM ICG was placed under the right breast in the 4 o'clock position. The fla probe face was placed against the breast tissue (centered at the 6 o'clock location) with gentle compression to achieve full contact with the tissue. A CW fluorescen intensity image was acquired in the target region with fi e repeated measurements at a single probe location. The depth of the target behind the tissue was approximately 2.5 cm as measured with a Vernier caliper. A second study was performed using a single target with the probe in the maximum curved position (i.e., 45° curvature of the two side plates of the three-plate based probe face). The images collected with the probe in the curved position possibly include transilluminated measurements in addition to reflectance-base measurements. This study was performed to demonstrate the feasibility of using the probe in its curved position, such that it can contour along the tissue and also provide fluorescen images that can aid in target detection. A 0.45-cm^3 fluorescen target containing 1-μM ICG was placed under the right breast in the 8 o'clock position.

Subtraction-based postprocessing was applied for each image. Fig. 10 shows the fast 2-D images of fluorescenc intensity obtained *in vivo* (from a healthy human subject using a simulated target, as described previously) with the probe in the fla position [see Fig. 10(a)] and in the curved position [see Fig. 10(b)]. The targets were clearly differentiable from the background human breast tissue at a depth of ∼2.5 cm, either with the probe in the fla position using gentle compression or with the probe in the curved position to contour around the tissue curvature. Currently work is carried out to perform multilocation imaging in order to remove the recurrently appearing artifacts in the background [63].

These subtracted image results demonstrate the feasibility of fast 2-D surface imaging (in <5 s/image) and 2-D target localization using our hand-held device in a clinical environment. The next step is to demonstrate coregistered imaging *in vivo* on human breast tissue, prior to 3-D tomographic analysis

2) Coregistered Imaging in Healthy Human Breast Tissue: In the phantom studies described in Section III-C, the simple cubical geometries were generated manually using meshing software (Gambit, Ansys Inc.). In the case of *in vivo* human subject studies, the geometry shape and volume varies for each subject and thus must be generated individually. A commercially available hand-held 3-D scanner (Polhemus, Inc.) was employed to scan the actual breast tissue and acquire the geometry. Use of the scanner on human subjects was approved by the FIU IRB. Experiments were performed using the coregistered imaging approach where the subject was seated upright at a 90° angle. A 0.23- or 0.45-cm^3 spherical target fille with 1-μM ICG was placed underneath the fla of the breast tissue as illustrated in Fig. 9. Images were collected with the target at three different locations corresponding to the 4 o'clock, 6 o'clock, and 8 o'clock positions. In each case, the fla probe was centered over the target location and placed in full contact with the breast tissue (which involved gentle compression of the tissue). CW images were acquired with the target in place and

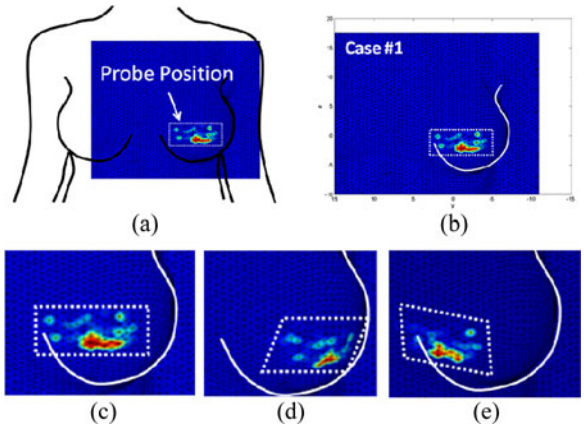

Fig. 11. Coregistered images of fluorescenc intensity data collected from a normal subject with an ICG-fille target using the initial setup (subject seated in upright position). (a) Location of probe and image relative to the subject. (b) Case #1 image: 0.45-cm^3 target at the 6 o'clock position. (c) Zoomed image of Case #1. (d) Case #2 image (zoomed): 0.45-cm^3 target at the 4 o'clock position. (e) Case #3 image (zoomed): 0.23-cm^3 target at the 8 o'clock position. All targets contain 1-μM ICG.

background images were acquired with the target removed for subtraction-based postprocessing. The subtracted images were automatically coregistered on the imaged location of the tissue, during imaging studies.

Fig. 11 shows coregistered images from a healthy breast tissue (with superficiall embedded target). Fig. 11(a) shows the position of the probe and the discretized geometry (prior to coregistration) relative to the subject. Fig. 11(b) shows the resulting coregistered image for case #1, where a 0.45-cm^3 target was placed at the 6 o'clock position. A zoomed image of the same result is shown in Fig. 11(c). Fig. 11(d) and (e) shows zoomed images of the results for cases #2 (0.45-cm^3 target at the 8 o'clock position) and #3 (0.23-cm^3 target at the 4 o'clock position), respectively. The results show that a 0.23- and 0.45-cm^3 fluorescen target(s) was detected through $\sim$2.5 cm of human breast tissue and coregistered to the appropriate location (within $\sim$1-cm error as described in Section III-B) on the tissue geometry. The fina step is to use the coregistered image to perform 3-D tomography (as described in Section III-C). Upon improving the accuracy of the coregistered images, coregistration is not only essential for 3-D tomographic imaging but can also assist in an operator-independent imaging approach, which is currently lacking in the clinical breast US.

3) 3-D Tomography of Breast Tissue in a Healthy Human Subject: The AEKF-based image reconstruction algorithm (described in Section III-C) was used along with the coregistered image(s) (from case # 1 in the previous section) in order to perform 3-D tomographic analysis. Fig. 12 shows the results of the *in vivo* 3-D reconstruction of the 3-D optical property map from a fluorescen target placed underneath the breast tissue of a healthy subject. The coronal slices in Fig. 12(a)–(d) begin at the tissue surface close to the central (nipple) region and progress depth-wise toward the chest wall. The initial slices at depths less than 1.0 cm from the tissue surface at the nipple region (a)–(c) show signal (the recovered absorption coefficien due to the fluorophore μ_{axf}) from the 2-D target location. At a depth of 1.0 cm and greater (d), additional signal (reconstructed μ_{axf}) appears to the left side of the breast tissue away from the true target location at 6 o'clock position. Any recovered signal that is not close to the true target location is assumed to be artifacts which might possibly result from improper contact of the probe with the tissue, a non uniform and unstable intensity among the six sources, and/or difference in pressure contact on the tissue when collecting the background image. The images (e)–(i) in Fig. 12 show slices of the reconstructed parameter in the y-plane representing the sagittal view. The center image shows the sagittal slice at the $y = 0$ location (g) which is the central part of the tissue (the slice at the nipple region). The other slices represent the locations in 0.25-cm increments to the left (i.e., toward the 9 o'clock direction), and right (i.e., toward the 3 o' clock direction from the center). The images show that within this central region, there is maximum signal intensity at the central location of the tissue which corresponds to the 6 o'clock position of the fluorescen target, and the signal diminishes in either direction away from the center.

From the coronal slices, significan artifacts are obvious from the reconstructed images. However, the sagittal view of the reconstructed images show a distinct target differentiable from the background breast tissue. The tomography results show the reconstructed target close to the true target location (although at a shallower depth than the $\sim$2.5-cm-deep target location) along with artifact signal away from the target location. The artifact(s) (as seen in the coronal slices) could be from the nonuniform source intensities at the six simultaneous multiple points of illumination, causing variable excitation leakage patterns and eventually impacting the image reconstructions. The recovery of the target closer to the surface can be attributed to the physics of reflectanc measurements, as observed by other research employing reflectance-base tomographic imaging [58]–[60]. This study demonstrates for the firs time the feasibility of performing 3-D tomographic imaging *in-vivo* human breast tissue using a hand-held-based optical device. Currently, various data prefilterin approaches are implemented [64] toward 3-D tomographic imaging studies, in order to account for these artifacts and remove them prior to image reconstructions.

4) 2-D Imaging of Breast Tumors in a Human Subject: DOI studies were performed on a 51-year-old woman with invasive ductal carcinoma in multiple tumor masses as confirme from prior screening (i.e., X-ray mammography and US). The optical imaging studies were approved by the FIU IRB and the subjects signed a consent form and a HIPAA authorization form (for release of their medical records) prior to the imaging study. The studies were performed where the subject lay in the supine position in a recliner chair at a 45° angle. The probe was placed at different locations on the ipsilateral (tumor-containing) and contralateral (nontumor-containing) breast and images of CW (nonfluorescent diffuse optical images were acquired. The probe positions were determined visually to cover the entire breast tissue. The four imaging locations relative to the subject are shown in Fig. 13(b) (not to the scale). Initially, the probe was centered over the 12 o'clock position covering the upper region of the breast tissue and part of the chest wall [probe location #1 in Fig. 13(b)], then moved vertically down toward

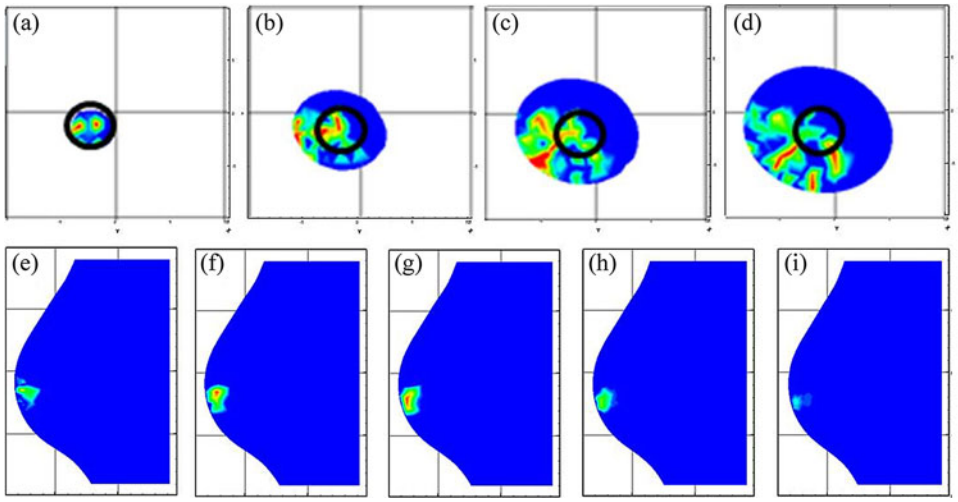

Fig. 12. *In vivo* 3-D reconstruction of a 0.45-cm^3 target (fille with 1-μM ICG) placed underneath the breast tissue of a healthy subject at ~6 o'clock location. (a)–(d) Coronal slices beginning at the nipple region and progressing back toward the chest wall in 0.25-cm increments. The black open circle represents the approximate true target location. (a)–(c) show recovered μ_{axf} as elevated (red) signal in the region of the true target location. (d) shows a slice that is deeper than the recovered target location since the signal is weaker at the center region than the background. (e)–(i) Sagittal slices in 0.25 increments centered at the nipple region, $y = 0$ (g), and moving toward the inner quadrant [(e) and (f)] and outer quadrant [(h) and (i)].

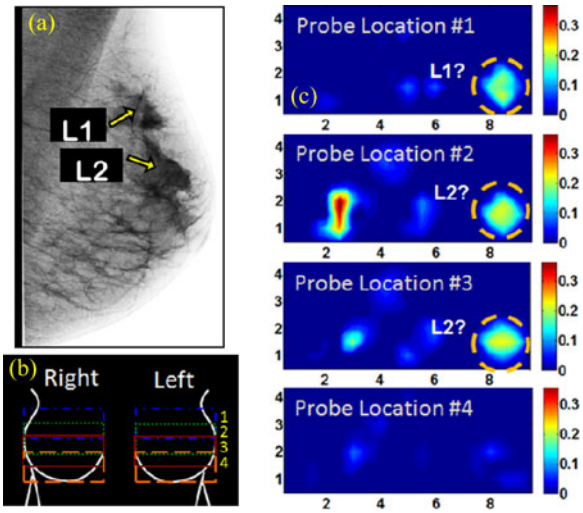

Fig. 13. (a) X-ray mammography image from a 51-year-old patient with invasive ductal carcinoma. The yellow arrows indicate two lesions labeled as L1 and L2. The lesion sizes from the medical records are 1.5- and 3.5-cm diameter for L1 and L2, respectively, along the major axis. (b) Probe locations that were imaged using DOI (not to the scale). (c) DOI images collected at four probe locations. The images represent the signal after subtraction from images collected from the contralateral breast. The images are plotted on the same scale according to the highest intensity of all the images. The yellow-dotted circle indicates signal located close to the tumor locations according to the medical records. The center of the images is closely aligned with the nipple region.

the 6 o'clock position [probe location #4 in Fig. 13(b)]. In every case (i.e., imaged location), the normalized intensity data from the ipsilateral breast were subtracted from the normalized intensity data from the contralateral breast so that the signal due to higher absorption shows as a higher intensity signal (i.e., more red) in the 2-D surface contour plot.

Fig. 13(a) shows the X-ray mammography image from the left breast of the 51-year-old breast cancer patient. The oblique view is shown where the top of the image is toward the patient's head and left side, and the bottom of the image is toward the patient's feet and right side. The images show the presence of two malignant masses in the outer quadrant of the tissue (indicated by the yellow arrows). Fig. 13(c) shows the CW absorption-based images acquired using the hand-held optical imager. All the four optical images were plotted to scale, based on the maximum intensity observed amongst those images. The images from locations 1–3 show high intensity signal (greater absorption) in the outer quadrant of the left breast tissue (indicated with the yellow-dotted circles). The image from location 4 which is from the lowest part of the tissue shows no signal. The firs image location corresponds to the location of L1 which is ~1.5-cm diameter along the major axis. The images at the second and third locations correspond to the location of L2 which is ~3.5 diameter along the major axis (although an artifact was observed in the second location of the probe). The fourth image location corresponds to the tissue beneath both the lesions. It can, therefore, be inferred that the absorption signal in the outer quadrant of images 1–3 can be attributed to the presence of the lesions (L1 and L2) at those locations. The fourth image shows no signal which corresponds to an area of the tissue that does not contain tumors.

The performance of our hand-held-based optical imager was tested in the clinical setting for the f rst time on an actual breast cancer patient. These preliminary results indicate the ability of the device to detect tumors via CW absorption-based imaging. Studies will be performed in the future to quantitatively correlate the images to their truly imaged location w.r.t the breast tissue (via coregistered imaging). This would provide a standardized approach to compare the 2-D tumor location as observed from the hand-held optical device and other imaging modalities. Additionally, coregistration can assist in an operator-independent imaging approach that is currently lacking in the standard US technique.

IV. Conclusion

Breast cancer affects one in eight women in the U.S. and is the second leading cause of death. Early detection is essential to reduce the mortality rate and improve the treatment options for women affected by the disease. X-ray mammography is the current gold standard for breast cancer screening. When a mass is detected, other imaging modalities are employed to diagnose the malignancy of the lesion. Typically, diagnostic mammography and breast US are performed, followed by MRI and finall surgical biopsy. Since 80% of biopsies turn out to be negative [65], there is a clear need for an additional method to gain more information about breast tumors noninvasively in order to reduce the amount of unnecessary physical and psychological trauma to the patient. DOI holds a potential role as a noninvasive imaging modality which can provide functional information of breast tumors prior to invasive biopsy (without the need for radiation or radioactive tracers as in other functional imaging modalities such as PET or single-photon emission computed tomography). Additionally, upon using fluorescenc contrast agents during DOI (i.e., fluorescence-enhance DOI), the technology has demonstrated to increase the tumor to background contrast in the breast [1], [66], [67] and for sentinel lymph node imaging [68] (only sample references provided).

Hand-held optical imaging devices are currently developed as a portable and patient-comfortable imaging method, which is rapidly approaching the clinical setting. Extensive human subject studies have been performed by the research groups at the University of Pennsylvania [26], the University of California, Irvine [9], [22], and the University of Connecticut [39], [49]. The devices have been applied at various stages of breast cancer imaging including tumor detection, diagnosis, and monitoring of neoadjuvant chemotherapy treatment. The applications of the devices vary from spectroscopic measuring of tissue optical properties to performing 3-D tumor localization with the guidance of a second imaging modality (i.e., US).

The hand-held optical device developed at FIU is unique in its ability to perform 3-D tomography using DOI alone via self-coregistration capabilities. Studies with human subjects demonstrate the ability of the device to perform fast 2-D imaging, coregistered imaging, and 3-D tomography in human breast tissue. A preliminary study in a cancer patient demonstrates the potential of the device to image breast cancer tumors. Extensive clinical studies are currently carried out in order to validate the performance of this device among different breast tissues within a wide variety of human subjects and also determine the sensitivity and specificit of the device.

References

[1] A. Corlu, R. Choe, T. Durduran, M. A. Rosen, M. Schweiger, S. R. Arrige, M. D. Schnall, and A. G. Yodh, "Three-dimensional *in vivo* fluorescenc diffuse optical tomography of breast cancer in humans," *Opt. Exp.*, vol. 15, no. 11, pp. 6696–6716, 2007.

[2] K. Licha, B. Riefke, V. Ntziachristis, A. Becker, B. Chance, and W. Semmler, "Hydrophilic cyanine dyes as contrast agents for near-infrared tumor imaging: Synthesis, photophysical properties and spectroscopic *in vivo* characterization," *Photochem. Photobiol.*, vol. 72, no. 3, pp. 392–398, 2000.

[3] D. Kepshire, S. C. Davis, H. Dehghani, K. D. Paulsen, and B. Pogue, "Fluorescence tomography characterization for sub-surface imaging with protoporphyrin IX," *Opt. Exp.*, vol. 16, no. 12, pp. 8581–8593, 2008.

[4] D. R. Leff, O. J. Warren, L. C. Enfield A. Gibson, T. Athanasiou, D. K. Patten, J. Hebden, G. Z. Yang, and A. Darzi, "Diffuse optical imaging of the healthy and diseased breast: A systematic review," *Breast Cancer Res. Treat.*, vol. 108, pp. 9–22, 2008.

[5] S. J. Erickson and A. Godavarty, "Hand-held based near-infrared optical imaging systems: A review," *Med. Eng. Phys.*, vol. 31, pp. 495–509, 2009.

[6] Q. Zhu, N. G. Chen, D. Q. Piao, P. Y. Guo, and X. H. Ding, "Design of near-infrared imaging probe with the assistance of ultrasound localization," *Appl. Opt.*, vol. 40, no. 19, pp. 3288–3303, 2001.

[7] B. J. Tromberg, "Optical scanning and breast cancer," *Acad. Radiol.*, vol. 12, no. 8, pp. 923–924, 2005.

[8] T. H. Pham, O. Coquoz, J. B Fishkin, E. Anderson, and B. J. Tromberg, "Broad bandwidth frequency domain instrument for quantitative tissue optical spectroscopy," *Rev. Sci. Instrum.*, vol. 71, no. 6, pp. 2500–2513, 2000.

[9] B. J. Tromberg, O. Coquoz, J. B. Fishkin, T. Pham, E. R. Anderson, J. Butler, M. Cahn, J. D. Gross, V. Venugopalan, and D. Pham, "Non-invasive measurements of breast tissue optical properties using frequency-domain photon migration," *Philos. Trans. R Soc. Lond. B Biol. Sci.*, vol. 352, pp. 661–668, 1997.

[10] R. Lanning and B. Tromberg, "Non-invasive characterization of breast cancer using near infrared optical spectroscopy," *UCI Undergraduate Res. J. II*, pp. 43–49, 1999.

[11] B. J. Tromberg, N. Shah, R. Lanning, A. Cerussi, J. Espinoza, T. Pham, L. Svaasand, and J. Butler, "Noninvasive *in vivo* characterization of breast tumors using photon migration spectroscopy," *Neoplasia*, vol. 2, no. 1–2, pp. 26–40, 2000.

[12] M. J. Holboke, A. G. Yodh, B. J. Tromberg, X. Li, N. Shah, J. Fishkin, D. Kidney, J. Butler, and B. Chance, "Three-dimensional diffuse optical mammography with ultrasound localization in a human subject," *J. Biomed. Opt.*, vol. 5, no. 2, pp. 237–247, 2000.

[13] A. E. Cerussi, A. J. Berger, F. Bevilacqua, N. Shah, D. Jakubowski, J. Butler, R. F. Holcombe, and B. J. Tromberg, "Sources of absorption and scattering contrast for near-infrared optical mammography," *Acad. Radiol.*, vol. 8, pp. 211–218, 2001.

[14] N. Shah, A. Cerussi, C. Eker, J. Espinoza, J. Butler, J. Fishkin, R. Hornung, and B. Tromberg, "Noninvasive functional optical spectroscopy of human breast tissue," in *Proc. Natl. Acad. Sci.*, USA, 2001, vol. 98, no. 8, pp. 4420–4425.

[15] N. Shah, A. E. Cerussi, D. Jakubowski, D. Hsiang, J. Butler, and B. J. Tromberg, "Spatial variations in optical and physiological properties of healthy breast tissue," *J. Biomed. Opt.*, vol. 9, no. 3, pp. 534–540, 2004.

[16] F. Bevilacqua, A. J. Berger, A. E. Cerussi, D. Jakubowski, and B. J. Tromberg, "Broadband absorption spectroscopy in turbid media by combined frequency-domain and steady-state methods," *Appl. Opt.*, vol. 39, no. 34, pp. 6498–6507, 2000.

[17] A. E. Cerussi, D. Jakubowski, N. Shah, F. Bevilacqua, R. Lanning, A. J. Berger, D. Hsiang, J. Butler, R. F. Holcombe, and B. J. Tromberg, "Spectroscopy enhances the information content of optical mammography," *J. Biomed. Opt.*, vol. 7, no. 1, pp. 60–71, 2002.

[18] D. B. Jakubowski, A. E. Cerussi, F. Bevilacqua, N. Shah, D. Hsiang, J. Butler, and B. J. Tromberg, "Monitoring neoadjuvant chemotherapy in breast cancer using quantitative diffuse optical spectroscopy: A case study," *J. Biomed. Opt.*, vol. 9, no. 1, pp. 230–238, 2004.

[19] N. Shah, J. Gibbs, D. Wolverton, A. Cerussi, N. Hylton, and B. J. Tromberg, "Combined diffuse optical spectroscopy and contrast-enhanced magnetic resonance imaging for monitoring breast cancer neoadjuvant chemotherapy: A case study," *J. Biomed. Opt.*, vol. 10, no. 5, p. 051503, 2005.

[20] D. Hsiang, N. Shah, H. Yu, M. Y. Su, A. Cerussi, J. Butler, C. Baick, R. Mehta, O. Nalcioglu, and B. Tromberg, "Coregistration of dynamic contrast enhanced MRI and broadband diffuse optical spectroscopy for characterizing breast cancer," *Technol. Cancer Res. Treat.*, vol. 4, no. 5, pp. 549–558, 2005.

[21] A. Cerussi, N. Shah, D. Hsiang, A. Durkin, J. Butler, and B. J. Tromberg, "*In vivo* absorption, scattering, and physiologic properties of 58 malignant breast tumors determined by broadband diffuse optical spectroscopy," *J. Biomed. Opt.*, vol. 11, no. 4, p. 044005, 2006.

[22] A. Cerussi, D. Hsiang, N. Shah, R. Mehta, A. Durkin, J. Butler, and B. J. Tromberg, "Predicting response to breast cancer neoadjuvant chemother-

apy using diffuse optical spectroscopy," in *Proc. Natl. Acad. Sci.*, USA, 2007, vol. 104, no. 10, pp. 4014–4019.

[23] K. S. No and P. H Chou, "Mini-FDPM and heterodyne mini-FDPM: Handheld non-invasive breast cancer detectors based on frequency-domain photon migration," *IEEE Trans. Circ. Syst.—I: Reg. Papers*, vol. 52, no. 12, pp. 2672–2685, Dec. 2005.

[24] K. S No, Q. Xie, R. Kwong, A. Cerussi, B. J Tromberg, and P Chou, "HBS: A handheld breast cancer detector based on frequency domain photon migration with full heterodyne," in *Proc. IEEE BioCAS*, Nov. 29–Dec. 1, 2006, pp. 114–117.

[25] K. S No, Q. Xie, P. H. Chou, R. Kwong, A. Cerussi, and B. J. Tromberg, "*In vivo* breast cancer measurement with a handheld laser breast scanner," in *Proc. 50th IEEE Int. Midwest Symp. Circ. Syst.*, Aug. 5–8, 2007, pp. 1–4.

[26] B. Chance, S. Nioka, E. F. Conant, E. Hwang, S. Briest, S. G. Orel, M. D. Schnall, and B. J. Czerniecki, "Breast cancer detection based on incremental biochemical and physiological properties of breast cancers: A six-year, two-site study," *Acad. Radiol.*, vol. 12, no. 8, pp. 925–933, 2005.

[27] S. Nioka and B. Chance, "NIR spectroscopic detection of breast cancer," *Technol. Cancer Res. Treat.*, vol. 4, no. 5, pp. 497–512, 2005.

[28] V. Sao, K. Pourrezaei, A. Akin, and H. Ayaz, "Breast tumor imaging using NIR LED based handheld continuous-wave imager," in *Proc. IEEE 29th Annu. NE Bioeng. Conf.*, Mar. 22–23, 2003, pp. 55–56.

[29] B. Chance, Z. Zhao, S. Wen, and Y. Chen, "Simple ac circuit for breast cancer detection and object detection," *Rev. Sci. Instr.*, vol. 77, p. 064301, 2006.

[30] Q. Liu, Q. Luo, and B. Chance, "2D phased array f uorescence wireless localizer in breast cancer detection," in *Proc. IEEE/EMBS Int. Summer School Med. Devices Biosensors*, Jun. 26–Jul. 2, 2004, pp. 71–73.

[31] X. Cheng, J. Mao, R. Bush, D. B. Kopans, R. H. Moore, and M. Chorlton, "Breast cancer detection by mapping hemoglobin concentration and oxygen saturation," *Appl. Opt.*, vol. 42, pp. 6412–6421, 2003.

[32] R. Xu, B. Qiang, and J. Mao, "Near infrared imaging of tissue heterogeneity: Probe design and sensitivity analysis," in *Proc. IEEE Eng. Med. Biol. 27th Annu. Conf.*, Shanghai, China, Sep. 1–4, 2005, pp. 278–281.

[33] R. X. Xu, J. O. Olsen, S. P. Povoski, L. D. Yee, and J. Mao, "Localization and functional parameter reconstruction of suspicious breast lesions by near infrared/ultrasound dual mode imaging," in *Proc. IEEE Eng. Med. Biol. 27th Annu. Conf.*, Shanghai, China, Sep. 1–4, 2005, pp. 4473–4476.

[34] J. R. Xu, B. Qiang, J. J. Mao, and S. P. Povoski, "Development of a handheld near infrared imager for dynamic characterization of *in vivo* biological tissue systems," *Appl. Opt.*, vol. 46, pp. 7442–7451, 2007.

[35] R. Choe, "Diffuse optical tomography and spectroscopy of breast cancer and fetal brain," Ph.D. dissertation, Univ. Pennsylvania, Philadelphia, 2005.

[36] T. Durduran, R. Choe, G. Yu, C. Zhou, J. C. Tchou, B. J. Czerniecki, and A. G. Yodh, "Diffuse optical measurement of blood fl w in breast tumors," *Opt. Lett.*, vol. 30, no. 21, pp. 2915–2917, 2005.

[37] A. Liebert, H. Wabnitz, J. Steinbrink, M. Möller, R. Macdonald, H. Rinneberg, A. Villringer, and H. Obrig, "Bed-side assessment of cerebral perfusion in stroke patients based on optical monitoring of a dye bolus by time-resolved diffuse reflectance, *NeuroImage*, vol. 24, pp. 426–435, 2005.

[38] U. Sunar, H. Quon, T. Durduran, J. Zhang, J. Du, C. Zhou, G. Yu, R. Choe, A. Kilger, R. Lustig, L. Loevner, S. Nioka, B. Chance, and A. G. Yodh, "Noninvasive diffuse optical measurement of blood fl w and blood oxygenation for monitoring radiation therapy in patients with head and neck tumors: A pilot study," *J. Biomed. Opt.*, vol. 11, no. 6, p. 064021, 2006.

[39] Q. Zhu, T. Durduran, V. Ntziachristos, M. Holboke, and A. G. Yodh, "Imager that combines near-infrared diffusive light and ultrasound," *Opt. Lett.*, vol. 24, no. 15, pp. 1050–1052, 1999.

[40] P. Guo, D. Piao, Q. Zhu, and J. Fikiet, "A combined 2-D ultrasound and NIR imaging system," in *Proc. IEEE 26th Annu. NE Bioeng. Conf.*, Apr. 8–9, 2000, pp. 77–78.

[41] Q. Zhu, N. G Chen, P. Guo, S. K. Yan, and D. Piao, "Combined ultrasound and near infrared diffusive light imaging," *IEEE Symp. Ultrason.*, vol. 2, pp. 1629–1632, Oct. 2000.

[42] N. G. Chen, P. Guo, S. Yan, D. Piao, and Q. Zhu, "Simultaneous near-infrared diffusive light and ultrasound imaging," *Appl. Opt.*, vol. 40, no. 34, pp. 6367–6380, 2001.

[43] Q. Zhu, N. G. Chen, and S. H. Kurtzman, "Imaging tumor angiogenesis by use of combined near-infrared diffusive light and ultrasound," *Opt. Lett.*, vol. 28, no. 5, pp. 337–339, 2003.

[44] Q. Zhu, M. Huang, N. Chen, K. Zarfos, B. Jagjivan, M. Kane, P. Hegde, and H. S. Kurtzman, "Ultrasound-guided optical tomographic imaging of malignant and benign breast lesions: Initial clinical results of 19 cases," *Neoplasia*, vol. 5, no. 5, pp. 379–388, 2003.

[45] N. G. Chen, M. Huang, H. Xia, and D. Piao, "Portable near-infrared diffusive light imager for breast cancer detection," *J. Biomed. Opt.*, vol. 9, no. 3, pp. 504–510, 2004.

[46] Q. Zhu, E. B. Cronin, A. A. Currier, H. S. Vine, M. Huang, N. Chen, and C. Xu, "Benign versus malignant breast masses: Optical differentiation with US-guided optical imaging reconstruction," *Radiology*, vol. 237, pp. 57–66, 2005.

[47] Q. Zhu, S. H. Kurtzman, P. Hegde, S. Tannenbaum, M. Kane, M. Huang, N. G. Chen, B. Jagjivan, and K. Zarfos, "Utilizing optical tomography with ultrasound localization to image heterogeneous hemoglobin distribution in large breast cancers," *Neoplasia*, vol. 7, no. 3, pp. 263–270, 2005.

[48] C. Xu and Q. Zhu, "Optimal probe design for dual-modality breast imaging," in *Optical Tomography and Spectroscopy of Tissue VII (Proceedings of the SPIE)*, B. Chance, R. R. Alfano, B. J. Tromberg, M. Tamura, and E. M. Sevick-Muraca, Eds. Bellingham, WA: Int. Soc. Opt. Eng., Feb. 13, 2007, p. 64340B.

[49] Q. Zhu, P. U. Hegde, A. Ricci, Jr., M. Kane, E. B. Cronin, Y. Ardeshirpour, C. Xu, A. Aguirre, S. H. Kurtzman, P. J. Deckers, and S. H. Tannenbaum, "Early-stage invasive breast cancers: Potential role of optical tomography with US localization in assisting diagnosis," *Radiology*, vol. 256, no. 2, pp. 367–378, Aug. 2010.

[50] J. Ge, B. Zhu, S. Regalado, and A. Godavarty, "Three-dimensional fluorescence-enhance optical tomography using a hand-held probe based imaging system," *Med. Phy.*, vol. 35, no. 7, pp. 3354–3363, 2008.

[51] S. J. Erickson, J. Ge, A. Sanchez, and A. Godavarty, "Two-dimensional fast surface imaging using a hand-held optical device: In-vitro and in-vivo fluorescenc studies," *Trans. Oncol.*, vol. 3, no. 1, pp. 16–22, 2010.

[52] M. Solomon, B. R. White, A. Q. Bauer, G. Perry, and J. P. Culver, "Hand-held video rate fluorescenc diffuse optical tomography," presented at the Biomed. Opt., OSA Tech. Digest (CD), Miami, FL, 2010, Paper BTuD9.

[53] C. Zhou, R. Choe, G. Yu, A. G. Yodh, N. Shah, A. Durkin, A. Cerussi, B. J. Tromberg, T. Durduran, D. Hsiang, R. Mehta, and J. Butler, "Diffuse optical monitoring of blood fl w and oxygenation in human breast cancer during early stages of neoadjuvant chemotherapy," *J. Biomed. Opt.*, vol. 12, no. 5, p. 051903, 2007.

[54] S. Regalado, S. J. Erickson, B. Zhu, J. Ge, and A. Godavarty, "Automated coregistered imaging using a hand-held probe-based optical imager," *Rev. Sci. Inst.*, vol. 81, p. 023702, 2010.

[55] S. J. Erickson, S. Martinez, J. DeCerce, A. Romero, L. Caldera, and A. Godavarty, "Fast coregistered imaging *in vivo* using a hand-held optical imager," in *Advanced Biomedical and Clinical Diagnostic Systems VIII (Proceedings of the SPIE)*, T. Vo-Dinh, W. S. Grundfest, and A. Mahadevan-Jansen, Eds. Bellingham, WA: Int. Soc. Opt. Eng., 2010, vol. 7555, pp. 75550P-1–75550P-6.

[56] M. J. Eppstein, D. J. Hawrysz, A. Godavarty, and E. M. Sevick-Muraca, "Three-dimensional near-infrared f uorescence tomography with Bayesian methodologies for image reconstruction from sparse and noisy data sets," *Proc. Natl. Acad. Sci. USA*, vol. 99, pp. 9619–9624, 2002.

[57] A. Godavarty, M. J. Eppstein, C. Zhang, S. Theru, A. B. Thompson, M. Gurfin el, and E. M. Sevick-Muraca, "Fluorescence-enhanced optical imaging in large tissue volumes using a gain modulated ICCD camera," *Phys. Med. Biol.*, vol. 48, pp. 1701–1720, 2003.

[58] A. Godavarty, A. B. Thompson, R. Roy, M. J. Eppstein, C. Zhang, M. Gurfin el, and E. M. Sevick-Muraca, "Diagnostic imaging of breast cancer using f uorescence-enhanced optical tomography: Phantom studies," *J. Biomed. Opt.: Special Edition Biomed. Opt. Women's Health*, vol. 9, no. 3, pp. 488–496, 2004.

[59] A. Joshi, W. Bangerth, K. Hwang, J. C. Rasmussen, and E. M. Sevick-Muraca, "Fully adaptive FEM based fluorescenc optical tomography from time-dependent measurements with area illumination and detection," *Med. Phys.*, vol. 33, no. 5, pp. 1299–1310, 2006.

[60] D. S. Kepshire, S. C. Davis, H. Dehghani, K. D Paulsen, and B. W. Pogue, "Subsurface diffuse optical tomography can localize absorber and f uorescent objects but recovered image sensitivity is nonlinear with depth," *Appl. Opt.*, vol. 46, no. 10, pp. 1669–1678, 2007.

[61] J. Ge, S. J. Erickson, and A. Godavarty, "Multi-projection f uorescence optical tomography using a handheld-probe-based optical imager: Phantom studies," *Appl. Opt.*, vol. 49, pp. 4343–4354, 2010.

[62] J. Ge, S. J. Erickson, and A. Godavarty, "Fluorescence tomographic imaging using a hand-held probe based optical imager: Extensive phantom studies," *Appl. Opt.*, vol. 48, no. 33, pp. 6408–6416, 2009.

[63] S. J. Erickson, S. L. Martinez, J. Gonzalez, L. Caldera, and A. Godavarty, "Improved detection limits using a hand-held optical imager with coregistration capabilities," *Biomed. Opt. Exp.*, vol. 1, pp. 126–134, 2010.
[64] B. Zhu, M. J. Eppstein, E. M. Sevick-Muraca, and A. Godavarty, "Noise pre-filterin techniques in f uorescence-enhanced optical tomography," *Opt. Exp.*, vol. 15, no. 18, pp. 11285–11300, 2007.
[65] American Cancer Society. (2011). [Online]. Available: http://www.cancer.org/
[66] A. Hagen, D. Grosenick, R. Macdonald, H. Rinneberg, S. Burock, P. Warnick, A. Poellinger, and P. M. Schlag, "Late-fluorescenc mammography assesses tumor capillary permeability and differentiates malignant from benign lesions," *Opt. Exp.*, vol. 17, no. 19, pp. 17016–17033, 2009.
[67] A. Poellinger, S. Burock, D. Grosenick, A. Hagen, L. Ludemann, F. Diekmann, F. Engelken, R. Macdonald, H. Rinneberg, and P. M. Schlag, "Breast cancer: Early- and late-fluorescenc near-infrared imaging with indocyanine green—A preliminary study," *Radiol.*, vol. 258, pp. 409–416, 2011.
[68] E. M. Sevick-Muraca, R. Sharma, J. C. Rasmussen, M. V. Marshall, J. A. Wendt, H. Q. Pham, E. Bonefas, J. P. Houston, L. Sampath, K. E. Adams, D. K. Blanchard, R. E. Fisher, S. B. Chiang, R. Elledge, and M. E. Mawad, "Imaging of lymph f ow in breast cancer patients after microdose administration of near-infrared f uorophore: A feasibility study," *Radiology*, vol. 246, no. 3, pp. 734–741, 2008.

Sarah J. Erickson (M'10) received the B.S. degree in physics from the University of South Florida, Tampa, in 2005, and the Ph.D. degree in biomedical engineering from Florida International University, Miami, in 2011.

She was an Undergraduate Researcher in the Novel Materials Laboratory, the University of South Florida under Dr. G. Nolas in 2004–2005 and a Graduate Researcher in the Optical Imaging Laboratory (OIL), Florida International University under Dr. A. Godavarty in 2007–2011. During her doctoral research, she was funded by a presidential fellowship from the university and a predoctoral fellowship from the Department of Defense Breast Cancer Research Program. She is currently a Postdoctoral Researcher at OIL.

Dr. Erickson is a member of The International Society for Optical Engineers, the Optical Society of America, The Society of Women Engineers (SWE), and the American Association for the Advancement of Science. She received the Outstanding Doctoral Student Award from the College of Engineering and Computing at Florida International University in 2011 and the Lydia I. Pickup scholarship from the SWE in 2009. She is funded by a postdoctoral fellowship from the American Cancer Society and Canary Foundation.

Anuradha Godavarty received the Ph.D. degree in chemical engineering from Texas A&M University, College Station, in 2003.

She was a Postdoctoral Associate in the Department of Computer Science, University of Vermont, Burlington, in 2003–2004. She joined the Department of Biomedical Engineering, Florida International University, Miami, as an Assistant Professor in 2004, where she has been an Associate Professor since 2010. To date, she has published her research in 30 peer-reviewed journals, and presented her work at various national/international conferences/scientifi meetings. Her research interests include developing near-infrared optical imaging technologies and applying them toward breast cancer imaging and functional brain mapping.

Dr. Godavarty has been recognized twice by the Miami Chamber of Commerce as a finalis for the Health Care Heroes Award (2010 and 2011) in the biomedical category.

Sergio L. Martinez received the B.S. and M.S. degrees in biomedical engineering from Florida International University, Miami, in 2008 and 2011, respectively.

He was a Graduate Researcher in the Optical Imaging Laboratory, Florida International University under Dr. A. Godavarty in 2009–2011.

Mr. Martinez is a member of the Optical Society of America, the Biomedical Engineering Society, and Alpha Eta Mu Beta. He received the Florida Medallion Scholarship and Hispanic Scholarship Fund Scholarship both in 2004 and the South East Alliance for Graduate Education and the Professoriate Award in 2008.

Jean Gonzalez received the B.S. degree in biomedical engineering from Florida International University, Miami, in 2009, where he is currently working toward the M.S. degree in biomedical engineering.

He has been a Graduate Researcher in the Optical Imaging Laboratory, Florida International University under Dr. A. Godavarty since 2008.

Mr. Gonzalez is a member of Tau Beta Pi, Alpha Eta Mu Beta, Theta Tau, and the Biomedical Engineering Society. He has received the Outstanding Undergraduate Student Award from the Department of Biomedical Engineering, Florida International University in 2009. During his undergraduate studies, he was funded by the Norman R. Weldon Biomedical Engineering Undergraduate Student Summer Research Internship, The Florida–Georgia Louis Stokes Alliance for Minority Participation, and the Florida International University Undergraduate Excellence Award.

Adrian Romero was born in Habana, Cuba, on March 6, 1983. After serving in the U.S. Marine Corps, he received the B.S. degree in biomedical engineering and a minor in chemistry from Florida International University, Miami, in 2008. He is currently working toward the M.D. degree in the Neurosurgery Department Cancer Research Laboratory, New York Medical College, Valhalla, under Dr. Jhanwar.

During his undergraduate program, he was a Research Assistant in the Optical Imaging Laboratory on a project related to developing an automated 3-D laser scanner. His project received the Ronald E. McNair price for best research project during the summer symposium. He was a Field Service Engineer at Physio Control (a division of Medtronic).

Mr. Romero is a member of the Society of Hispanic Professional Engineers and Alpha Eta Mu Beta, the Biomedical Engineering Honor Society. He held several leadership positions ranging from social event coordinator to community service representative.

Manuela Roman received the B.S. degree in biomedical engineering from Florida International University, Miami, in 2011, where she is currently working toward the M.S. degree in biomedical engineering.

She has been a Graduate Researcher in the Optical Imaging Laboratory, Florida International University under Dr. A. Godavarty since 2010.

Ms. Roman is also a member of Tau Beta Pi, Alpha Eta Mu Beta, the Biomedical Engineering Society, and the Society of Hispanic Professional Engineers. She received the Florida Medallion Scholarship in 2005, the South East Alliance for Graduate Education and the Professoriate Award in 2010, and The National Action Council for Minorities in Engineering in 2010.

Annie Nunez received the B.S. degree in biomedical engineering from Florida International University, Miami, in 2011.

She was a Research Assistant in the Optical Imaging Laboratory, Florida International University, in 2010–2011. Her research project was focused on *in-vivo* optical imaging studies toward breast cancer.

Jiajia Ge was born in Jiangxi, China, on April 9, 1979. She received the B.S. and M.S. degrees from Southern Yangtze University, Wuxi, China, in 1999 and 2002, respectively, and the Ph.D. degree from the Florida International University, Miami, in 2008.

She is currently a Postdoctoral Research Associate in the Department of Radiation Oncology, Washington University in St. Louis, St. Louis, MO. Her current research interests include motion tracking and management of abdominal tumor during radiation therapy.

Steven Regalado was born in Chicago, IL, on October 6, 1983. He received the combined Master's and Bachelor's degree in biomedical engineering from Florida International University (FIU), Miami, in 2008.

He is currently a Senior MRI/CT Engineer for ENS Imaging, Pembroke Pines, FL. His previous experience includes working as a Research Assistant at the FIU Optical Imaging Lab and as a Biomedical Technician at ESMO Inc., Sunrise, FL.

Richard Kiszonas received the D.O. degree in osteopathy from the Philadelphia College of Osteopathy, Philadelphia, in 1958, where he completed an internship and received the M.S. degree in radiology in 1962. He completed a Mini Fellowship in angiography at the University of Minnesota, Minneapolis.

He joined the Faculty of the Philadelphia College of Osteopathic Medicine as an Assistant Professor. In 1988, he joined the Department of Radiology, University of Miami, Coral Gables, FL, where he became an Associate Professor in 1994. Subsequently, he accepted a position at Nova Southeastern University as a Professor of radiology. In 2001, he retuned to the University of Miami. He has presented and lectured extensively at national meetings on abnormalities of the breast and was a Visiting Professor for the University of Texas Houston Medical School from 2000 to 2001. His expertise has made him an authoritative source in the f eld and he has been with the State of Florida Department of Health Medical Expert Witness Program since 1994. Currently, he is the Director of the Breast Imaging Service and Director of the Breast Imaging Fellowship Program at the University of Miami/Sylvester Comprehensive Cancer Center. His research interests include X-ray mammography, ultrasound, and MRI of the breast.

Cristina Lopez-Penalver received the B.S. degree in biology and the M.D. degree in surgery from the University of Miami, Coral Gables, FL, in 1986 and 1991, respectively. She completed internship and residency training in the Department of Surgery, Jackson Memorial Hospital, Miami, FL, in 1991–1996.

She is currently a practicing General Surgeon, with specialization in the breast, and aff liated to Advanced Medical Specialties, Miami, FL. Her research interests include breast cancer diagnosis, biopsy, surgery, and treatment process.

Dr. Lopez-Penalver is Board Certifie in Surgery by the American Board of Surgery, and a member of the American College of Surgeons and the American Society of Breast Surgeons.

Improved detection limits using a hand-held optical imager with coregistration capabilities

Sarah J. Erickson, Sergio L. Martinez, Jean Gonzalez, Lizeth Caldera, and Anuradha Godavarty*

Department of Biomedical Engineering, Florida International University, 10555 West Flagler Street EC2610; Miami, FL 33174, USA

**godavart@fiu.edu*

Abstract: Optical imaging is emerging as a non-invasive and non-ionizing method for breast cancer diagnosis. A hand-held optical imager has been developed with coregistration facilities towards flexible imaging of different tissue volumes and curvatures in near real-time. Herein, fluorescence-enhanced optical imaging experiments are performed to demonstrate deeper target detection under perfect and imperfect (100:1) uptake conditions in (liquid) tissue phantoms and *in vitro*. Upon summation of multiple scans (fluorescence intensity images), fluorescent targets are detected at greater depths than from single scan alone.

©2010 Optical Society of America

OCIS codes: (170.3880) Medical and Biological Imaging; (110.2970) Image Detection Systems; (110.0113) Imaging through turbid media; (110.3080) Infrared imaging; (110.6955) (300.2530) Fluorescence, laser-induced

References and links

1. S. J. Erickson, and A. Godavarty, "Hand-held based near-infrared optical imaging devices: a review," Med. Eng. Phys. **31**(5), 495–509 (2009).
2. A. E. Cerussi, A. J. Berger, F. Bevilacqua, N. Shah, D. Jakubowski, J. Butler, R. F. Holcombe, and B. J. Tromberg, "Sources of absorption and scattering contrast for near-infrared optical mammography," Acad. Radiol. **8**(3), 211–218 (2001).
3. N. Shah, A. E. Cerussi, D. Jakubowski, D. Hsiang, J. Butler, and B. J. Tromberg, "Spatial variations in optical and physiological properties of healthy breast tissue," J. Biomed. Opt. **9**(3), 534–540 (2004).
4. A. Cerussi, N. Shah, D. Hsiang, A. Durkin, J. Butler, and B. J. Tromberg, "In vivo absorption, scattering, and physiologic properties of 58 malignant breast tumors determined by broadband diffuse optical spectroscopy," J. Biomed. Opt. **11**(4), 044005 (2006).
5. B. Chance, S. Nioka, J. Zhang, E. F. Conant, E. Hwang, S. Briest, S. G. Orel, M. D. Schnall, and B. J. Czerniecki, "Breast cancer detection based on incremental biochemical and physiological properties of breast cancers: a six-year, two-site study," Acad. Radiol. **12**(8), 925–933 (2005).
6. B. Chance, Z. Zhao, S. Wen, and Y. Chen, "Simple ac circuit for breast cancer detection and object detection," Rev. Sci. Instrum. **77**(6), 064301 (2006).
7. J. Ge, B. Zhu, S. Regalado, and A. Godavarty, "Three-dimensional fluorescence-enhanced optical tomography using a hand-held probe based imaging system," Med. Phys. **35**(7), 3354–3363 (2008).
8. J. Ge, S. J. Erickson, and A. Godavarty, "Fluorescence tomographic imaging using a handheld-probe-based optical imager: extensive phantom studies," Appl. Opt. **48**(33), 6408–6416 (2009).
9. S. J. Erickson, J. Ge, A. Sanchez, and A. Godavarty, "Two-dimensional fast surface imaging using a handheld optical device: *In vitro* and *in vivo* fluorescence studies," Transl Oncol **3**(1), 16–22 (2010).
10. S. Regalado, S. J. Erickson, B. Zhu, J. Ge, and A. Godavarty, "Automated coregistered imaging using a hand-held probe-based optical imager," Rev. Sci. Instrum. **81**(2), 023702 (2010).
11. A. Godavarty, C. Zhang, M. J. Eppstein, and E. M. Sevick-Muraca, "Fluorescence-enhanced optical imaging of large phantoms using single and simultaneous dual point illumination geometries," Med. Phys. **31**(2), 183–190 (2004).
12. A. Corlu, R. Choe, T. Durduran, M. A. Rosen, M. Schweiger, S. R. Arridge, M. D. Schnall, and A. G. Yodh, "Three-dimensional in vivo fluorescence diffuse optical tomography of breast cancer in humans," Opt. Express **15**(11), 6696–6716 (2007).

1. Introduction

Optical imaging is a growing area of research, with efforts to translate the technology to the clinic and aid in early-stage breast cancer detection, diagnosis, and/or prognosis of the disease. Optical imaging systems are developed by various research groups with differences in

#129379 - $15.00 USD Received 1 Jun 2010; revised 10 Jul 2010; accepted 12 Jul 2010; published 15 Jul 2010
(C) 2010 OSA

their imaging technique (continuous-wave, frequency-domain, or time-domain), and source-detector configuration (single or multiple sources/detectors that are either for point/area imaging). While most of these systems are bulky and yet capable of three-dimensional (3D) tomographic imaging of large tissue volumes, there are a whole class of hand-held optical imaging systems that are portable and capable of two-dimensional (2D) spectroscopic imaging [1–6].

In the past five years, our Optical Imaging Laboratory has been focused in developing a hand-held (portable) optical imaging system that is capable of 3D tomographic imaging beyond the 2D spectroscopic imaging capabilities (available to date) [7]. The recently developed hand-held optical imager is unique in its following features: (i) a probe head to image a large surface area simultaneously; (ii) a simultaneous illumination and detection geometry that enhances the overall imaging time; (iii) a flexible probe head to contour to any tissue curvature and volume; and (iv) a novel coregistration approach to acquire the positional information using a motion tracker (towards 3D tomography studies). The feasibility of 2D target detection(s) and 3D tomographic analysis using this hand-held optical imager has been demonstrated from tissue phantom and *in-vitro* fluorescence imaging studies [7–9]. During these studies, a single scan in the region of interest was acquired to detect and recover the embedded target(s) tomographically (using manually coregistered optical images). However, it was observed that as the target depth was increased and/or its volume decreased, the target was not detectable from 2D images, nor was it recovered from 3D tomography studies. An alternate imaging approach of using multiple-scans from various locations of the tissue surface was developed (using automatically coregistered optical images) and its feasibility to detect deeper targets was assessed [10].

In the current work, the recently developed multi-scan imaging approach is extensively assessed to determine the target detection limits of our hand-held optical imager. Studies were performed using the liquid tissue phantoms in order to determine the extent of improvement upon the previous studies using single-scan. Studies were also extended to *in vitro* tissue models in order to assess the performance of the device in a non-uniform (or heterogeneous) scattering background, in order to better mimic human tissue.

2. Materials and methods

2.1 Instrumentation

The instrumentation for the hand-held optical imaging system as shown in Fig. 1 is composed of a laser diode source (785 nm, 530 mW) and intensified charge-coupled device (ICCD) detector (−24 V DC detector power), which are connected to the probe face via optical fibers. The 4 x 9 cm^2 hand-held probe head contains 6 illumination points (shown as large red dots in Fig. 1) and 165 detection points (spaced 0.5 cm apart) which illuminate and collect the signal simultaneously for rapid data acquisition. A collimator-diffuser package splits the NIR light from the laser diode into 6 simultaneous sources. The laser output from each of these 6 sources at the probe end onto the tissue geometry is only 2 mW or less at each illumination point (due to >90% intensity losses from the collimator-diffuser package). The imaging system is capable of operating in both the continuous wave (CW) and frequency domain mode. The CW mode is used here as a fast measurement technique (near real-time) to enable collection of multiple scans without greatly increasing the imaging time. During imaging studies, the integration time of the ICCD camera is kept constant (0.2 sec) and only the gain settings at the intensifier end is varied. Further details of the instrumentation have been described elsewhere [7].

#129379 - $15.00 USD Received 1 Jun 2010; revised 10 Jul 2010; accepted 12 Jul 2010; published 15 Jul 2010
(C) 2010 OSA

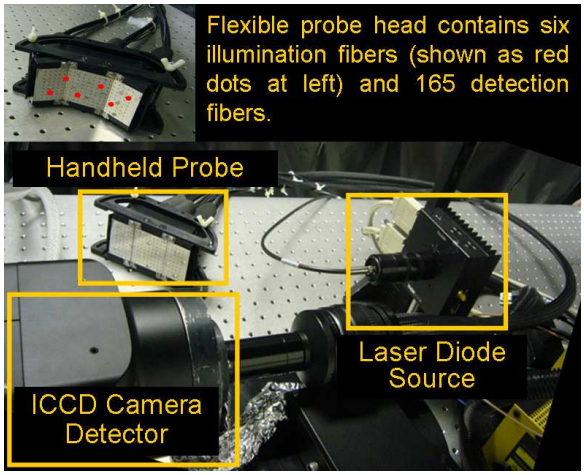

Fig. 1. Instrumentation for the hand-held probe based optical imaging system.

2.2 Coregistered imaging process

Image coregistration onto the 3D tissue geometry being scanned is necessary in order to perform 3D tomography studies. This is because the location of the image must be known with respect to the geometry of the phantom (or tissue) being imaged. Coregistered imaging involves tracking the position and orientation of the probe in real time and combining the positional information with the optical measurements to accurately position the image on the discretized phantom or tissue geometry. This is carried out as a three-step process (illustrated in Fig. 2) using MATLAB/LabVIEW software developed in house [10]. An acoustic tracker is implemented on the probe head to enable real-time tracking of the 3D position and orientation of the probe (in six degrees of freedom) with respect to the phantom surface (Step #1). The positional information is used to accurately position the 2D image of fluorescence intensity at the corresponding location on the discretized phantom geometry. The positional information is fused with the optical measurement data collected from the hand-held device (Step #2) to generate a 3D coregistered image of the phantom with the fluorescence intensity (or any other optical measurement) data at the probe's location (Step #3). The entire coregistration process is automated such that it takes ~35 seconds to acquire a single coregistered image or scan (i.e. carry out all the 3 steps described above). The actual time to acquire an optical image at a single location of the probe is ~1 sec (i.e. 0.2 sec detector integration time × 5 repetitions for each CW image), and the remaining time (~34 sec) is towards the coregistration process. The coregistration process is repeated at each probe location, during a multi-scan imaging technique (i.e. optical images are acquired from multiple locations of the probe on the tissue surface).

2.3 Validation of coregistered imaging in phantoms

In order to quantitatively determine the accuracy of the tracked location in comparison to the true location of the probe on a cubical tissue phantom, the probe was placed at five different positions of known [x,y,z] coordinates and the tracking position was recorded (5 repetitions at each location). The average and standard deviation of the tracked location, and its total distance-off from the true location at each position number were measured. The average total distance off is ~0.19 cm. For these measurements, the probe was held in place with a lab jack and the error in measurements is primarily due to error in the tracking system and possibly some movement of the phantom during positioning of the probe. Currently work is carried out to improve the accuracy of the tracking system.

#129379 - $15.00 USD Received 1 Jun 2010; revised 10 Jul 2010; accepted 12 Jul 2010; published 15 Jul 2010
(C) 2010 OSA

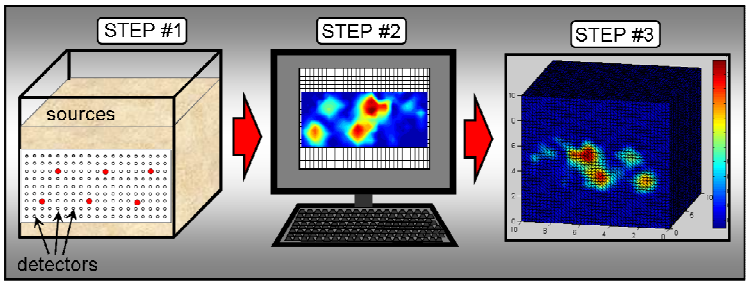

Fig. 2. Three-step coregistered imaging process. In Step #1, the source and detector locations are tracked in real-time with respect to the phantom. In Step #2, a raw image (of optical measurement) is collected and used to generate a 2D surface contour plot of the corresponding (here fluorescence intensity) data. In Step #3, the positional information is used to accurately coregister the image to the probe's location on the discretized phantom mesh.

2.4 Experimental studies

Experimental studies were performed initially using the simple case of the uniform liquid tissue phantom and were then extended to more realistic *in vitro* models. Phantom experiments were performed using tissue phantoms (as in the previous studies [7,8]) composed of 1% Liposyn (800 mL) in a 10 × 10 × 10 cm^3 acrylic cube. Acrylic sphere targets of sizes 0.23 - 0.45 cm^3 filled with 1 µM indocyanine green (ICG) were placed at different depths (2.5-4.0 cm) from the imaging surface to represent a tumor. Experiments were performed increasing the depth by 0.5 cm until the target was no longer detected. The experimental set-up is shown in Fig. 3. The probe was placed in full contact with the phantom surface and multiple scans (2D coregistered images) were collected using the method described in section 2.5 below.

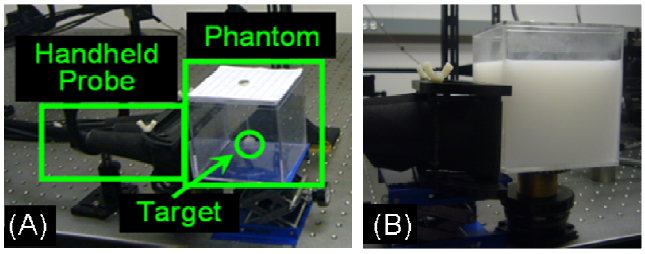

Fig. 3. Experimental set-up for phantom studies. (A) A spherical target filled with 1 µM indocyanine green is enclosed within the cubical phantom to represent a tumor. (B) The phantom is composed of a 1% Liposyn solution to mimic the optical properties of human breast tissue.

To represent the heterogeneous nature of human tissue, studies were also performed *in vitro* using minced chicken breast (480 mL) combined with 1% Liposyn (260 mL) in a 10 × 10 × 10 cm^3 acrylic cube in order to introduce a background of non-uniform scattering. The 0.45 cm^3 fluorescent target was placed at different depths between 2.0 and 4.0 cm, until the target was no longer detected. The experiments were performed for the perfect uptake case with tumor-to-background ratio (T:B) of 1:0 and imperfect uptake case with T:B of ~100:1. Table 1 summarizes the different experimental studies performed in which a target was detected. For each image collected, a subtraction-based post-processing technique was used to eliminate excitation light leakage [7].

2.5 Multiple-scan technique

The multiple scan technique involves collecting a series of scans at different probe positions and coregistering each image to its appropriate location. A scan is defined as a 2D surface contour plot of fluorescence intensity data collected from a CW image (mean of 5 repeated

#129379 - $15.00 USD Received 1 Jun 2010; revised 10 Jul 2010; accepted 12 Jul 2010; published 15 Jul 2010
(C) 2010 OSA

images at the same location) using the ICCD based detection system. Each image is immediately coregistered to the discretized phantom mesh. By scanning at multiple locations, the weak fluorescence signal from the target (that appears at the same location on the tissue geometry during each scan) can possibly dominate the strong excitation light leakage (that tends to appear at different locations on the tissue geometry during each scan).

Table 1. Summary of experimental studies in which a target was detected in tissue phantoms and *in vitro*. The cases where the deepest target was detected for phantom or *in vitro*, and perfect or imperfect uptake are highlighted in red.

Experimental Case	Experiment #	Target Volume (cm^3)	Target Depth (cm)	T:B
Tissue Phantom	1	0.45	3.0	1:0
	2	0.45	3.5	1:0
	3	0.23	2.5	1:0
	4	0.23	3.0	1:0
	5	0.23	3.5	1:0
	6	0.45	2.5	100:1
	7	0.45	3.0	100:1
	8	0.23	2.0	100:1
	9	0.23	2.5	100:1
	10	0.23	3.0	100:1
In Vitro	11	0.45	2.5	1:0
	12	0.45	3.0	1:0
	13	0.45	3.5	1:0
	14	0.45	2.0	100:1
	15	0.45	2.5	100:1

Different combinations of image positions were used to determine the optimal multi-scan method. Initially 4-5 scans were collected moving the probe 0.5 cm in the vertical direction between each scan. For the same experimental case, 9 scans were collected moving the probe in 0.25 cm increments in the vertical direction. Additionally, repeated scans were collected at each probe location. It was determined that collecting 2-3 repeated scans (i.e. 2-3 × 5 repeated images or 10-15 repeated images) at each probe location for 4-5 positions 0.5 cm apart resulted in better target detectability with fewer artifacts than collecting single scans (i.e. 1 × 5 repeated images) at each probe location for 9 positions 0.25 cm apart. This can possibly be attributed to two reasons: (i) the inaccuracy (from instability) of the positional tracking system (described in section 2.3) has greater impact at smaller positional increments (e.g. 0.25 cm), leading to increased artifacts; and (ii) the variability in the instrument's response is minimized by increasing the number of repeated scans (or images) at the same location. The number of repeated scans (or images) can be increased for the case where the probe location 0.25 cm apart. However, this further increases the overall imaging time and hence was not attempted. In the future, for an *in vivo* case, multiple images can be collected and summed from arbitrary probe positions and the number of scans can be optimized to minimize the overall imaging time and number of artifacts. The position will be known since the image is immediately coregistered at its location.

3. Results

Figure 4 shows four single images (2D contour plots of fluorescence intensity) for experimental case # 12 where a 0.45 cm^3 fluorescent target was placed 3.0 cm deep *in vitro* under perfect uptake condition (T:B = 1:0). Multiple scans were collected as described in section 2.5. In each image, the true target location is indicated by a black open circle. The images show that the target is not detected in a single scan, and only random distributions of artifacts (high intensity signals that appear in the image which do not originate from the target) are visible. Upon summation of eight scans, the fluorescent signal is detected at the target location (Fig. 5). This can be attributed to the random distribution of artifacts that appear in different locations for each single scan, while the signal from the target remains in

#129379 - $15.00 USD Received 1 Jun 2010; revised 10 Jul 2010; accepted 12 Jul 2010; published 15 Jul 2010
(C) 2010 OSA

the same location relative to its coregistered position on the phantom. Upon summation of the coregistered images, the random signals from the artifacts tend to diminish compared to the consistent signal from the target, which tends to intensify.

Figure 6 shows the result for summated multi-scan images for experimental cases 5, 10, 13, and 15 (highlighted in Table 1). Case 5 represents a 0.23 cm^3 target placed 3.5 cm deep in the tissue phantom under perfect uptake conditions (T:B = 1:0). The target was detected close to the true location and no artifacts were present. Case 10 represents a 0.23 cm^3 target placed 3.0 cm deep in the tissue phantom under imperfect uptake condition (T:B = 100:1). The target was detected at the true location with some diffused signal around it. Case 13 represents a 0.45 cm^3 target placed 3.5 cm deep *in-vitro* under perfect uptake conditions (T:B = 1:0). The target was detected at the true location with artifacts also visible far from the target location. These artifacts can be attributable to the heterogeneous nature of the *in vitro* phantom.

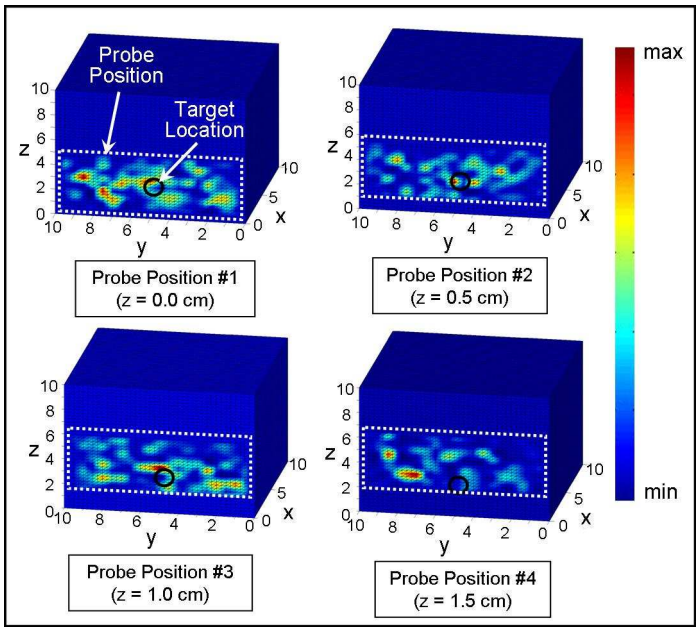

Fig. 4. Coregistered images from single scans (2D contour plots of fluorescence intensity data) at four probe positions for experimental case #12 (a 0.45 cm^3 fluorescent target placed 3.0 cm deep, x-dimension *in-vitro* phantom under T:B = 1:0). In each image, the white dotted line represents the probe position with respect to the phantom and the black open circle represents the true target location.

#129379 - $15.00 USD Received 1 Jun 2010; revised 10 Jul 2010; accepted 12 Jul 2010; published 15 Jul 2010
(C) 2010 OSA

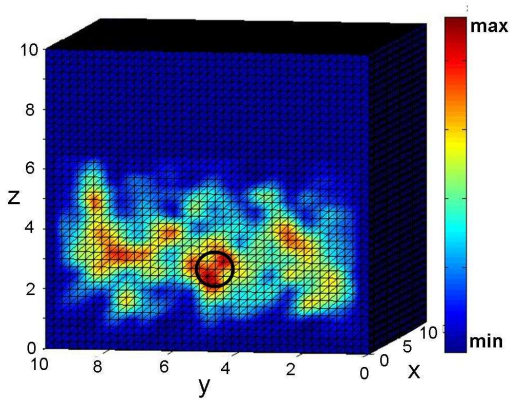

Fig. 5. Summated image of multiple scans shown in Fig. 4 (experimental case #12). The summed image represents summation of 8 single scans, where 2 scans were collected at each of the 4 probe positions shown in Fig. 4. The black open circle represents the true target location.

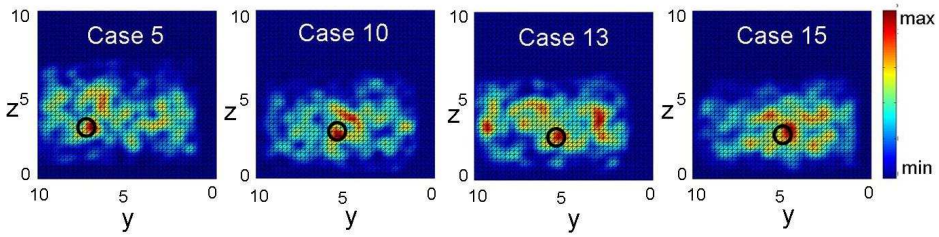

Fig. 6. Summed images of multiple coregistered scans from the four best experimental cases listed in Table 1. The black open circle indicates the true target location for each case.

Case 15 represents a 0.45 cm^3 target placed 2.5 cm deep *in-vitro* under imperfect uptake conditions (T:B = 100:1). The target was detected close to the true location along with minimal artifacts around it.

The initial experiments designed to detect deeper targets consisted of performing a single scan at 4-5 positions moving the probe 0.5 cm in the vertical (z) direction. For deeper targets (>3.0 cm), heterogeneous (*in vitro*) phantoms, and/or imperfect uptake cases, the target was not detected upon summation of four or five scans. However, it was observed that when multiple repeated scans were collected at the same location for each probe position, the targets were detectable. In other words, increasing the number of repeated scans is as important as increasing the number of scan locations towards deep target detection under heterogeneous and/or imperfect uptake conditions.

The results presented here demonstrate that deeper and smaller targets can be detected using the multiple-scan approach than using a single-scan alone. The impact of these results extend beyond target detection in 2D in that the information can be used as *a priori* information to aid 3D reconstruction using a single frequency-domain image (or scan) towards deeper target recovery (future work).

4. Discussion

The prime hypothesis for the current study is that a single scan (of a large area, 4 x 9 cm^2) can fail in detecting deeper targets during a near real-time optical imaging study. Upon scanning at multiple locations on the surface of a tissue geometry, the possibility to detect deeper targets and differentiating them from artifacts tends to improve upon summing all these

#129379 - $15.00 USD Received 1 Jun 2010; revised 10 Jul 2010; accepted 12 Jul 2010; published 15 Jul 2010
(C) 2010 OSA

multiple scans. The detection limits of our hand-held optical imager, the first of its kind that can scan large areas in near real-time, has been 2.5 cm for a 0.45 cm^3 target under T:B = 1:0 from the past studies [8] involving a single scan from the region of interest on the tissue geometry. In the current study, it was clearly observed that upon summation of the intensity signals from multiple scans of the tissue surface, targets of smaller volume and as deep as 3.5 cm were detectable. However, artifacts start appearing when the target depth is increased, the target volume is decreased, and or heterogeneity of the background increased. The reasons for these artifacts are two-fold: (i) The uneven source strength distribution of the 6 simultaneous sources affects the ability to detect the target depending on the proximity of the target to the stronger sources. As multiple scans are collected the strong source may move away from the target resulting in a more diffused signal which produces a greater number of artifacts upon subtraction of the background. (ii) The positional information of the hand-held probe is not accurately coregistered due to the instability of the motion tracking device, which can lead to misalignment of the target signal in the multiple images. As a result, some signals which originated from the target can be mistaken as artifacts due to their improper location in the image. Currently, work is carried out to homogenize the source strength distribution by altering the instrumentation set-up at the source end, and also developing alternate motion tracking approaches that are stable and more accurate in comparison to the current device.

Researchers in the past have demonstrated detection of targets as deep as 5 cm using their hand-held optical devices [6]. However, the detection was typically a point location that was spectroscopically obtained from the tissue surface. In addition, the specificity of getting a negative result (not detecting any target) in the absence of the target (i.e. in the surrounding tissues) is not described. In other words, unlike the current hand-held optical imager that can produce 2D images over large areas in near real-time, the other hand-held imagers have a limited imaging area (mostly point-based imaging) and typically produce only spectroscopic measurements from a few sources/detectors.

The advantage of the current hand-held imager's optical data is that it can be applied towards 3D tomography studies, since the positional location of the optical data with respect to the 3D tissue geometry is coregistered during imaging studies. Hence, the implementation of the multi-scan imaging approach and using the summated images towards immediate 2D deep target detection and future 3D tomographic analysis is feasible. Although the present study is focused on fluorescence-enhanced optical imaging, the multi-scan summation and imaging approach is applicable for absorption-based diffuse optical imaging studies as well.

In the area of fluorescence tomographic imaging, Sevick's research group was one of the first groups to demonstrate 3D fluorescence optical tomography in clinically relevant sized tissue phantoms, using large bulky optical imaging instrumentation [11]. Fluorescent targets of 1 cm^3 volume were recovered at depth up to 2.8 cm under perfect uptake conditions. The first *in vivo* 3D fluorescence optical tomography of breast cancer in human subjects was demonstrated by Corlu *et. al.* where tumors were recovered *in vivo* up to 2.0 cm deep in human breast tissue [12]. From our past 3D tomography studies using the hand-held imager on large tissue phantoms, 0.45 cm^3 targets as deep as 2.5 cm were recovered in uniform tissue phantoms under perfect uptake conditions [8].

In a recent *in vivo* study using a simulated fluorescent target, a single scan using our hand-held optical imager was able to detect a 0.23 cm^3 target ~2.5 cm deep in human breast tissue [9]. These past studies demonstrate the potential that upon using multiple scans and applying the summation approach, deeper and smaller targets can become detectable from the tissue surface. In addition, these summated images can also assist in tomographically recovering deeper targets beyond what is demonstrated to date in the area of fluorescence optical tomography. However, the developed hand-held optical imager is limited to reflectance based imaging, which tends to limit the recovery of the true target's depth during 3D tomography. Currently, research is carried out to develop alternate imaging approaches using the hand-held device such that trans-illumination measurements can also be acquired in an attempt to improve the target depth recovery (during 3D tomography).

#129379 - $15.00 USD Received 1 Jun 2010; revised 10 Jul 2010; accepted 12 Jul 2010; published 15 Jul 2010
(C) 2010 OSA

5. Conclusion

A hand-held optical imager has been developed with unique features of flexibility to contour to different tissue curvatures, ability to rapidly image a large area, and coregistration capabilities to enable 3D tomography. Herein we have demonstrated improved detection limits via application of a multiple-scan technique. The multi-scan imaging approach is facilitated by the use of fast 2D coregistered imaging in CW mode. Previous results using single-scan imaging showed that the greatest target depth detected was 2.5 cm and 1.5 cm for a 0.45 cm^3 target in a (liquid) tissue phantom under perfect and imperfect uptake conditions, respectively. By using the multi-scan technique, this depth was improved to 3.5 cm for a smaller target (0.23 cm^3) under the T:B = 1:0 condition. Under imperfect uptake conditions (T:B = 100:1), the detectable target depth was increased from 1.5 cm to 3.0 cm. Since these results were promising, studies were extended to *in vitro* models, which better represent the non-uniformity of human tissue. From these *in-vitro* studies the target was detected at depths of 3.5 cm and 2.5 cm for perfect (1:0) and imperfect uptake (100:1) cases, respectively. These studies demonstrate that summation of multiple coregistered images can be used towards deeper target detection than is capable from single scans alone. In a clinical setting, this technique can be used to acquire multiple images quickly in order to detect the presence of a tumor, determine its 2D location within the tissue, and also perform 3D tomography studies (as a follow-up). Thus, the hand-held optical imager has potential for fast 2D imaging and 3D tomography in the clinical setting for breast cancer diagnosis.

Acknowledgements

The current work is supported by National Institutes of Health (R15CA119253), Dept of Defense (BC083282), and Coulter Foundation.

#129379 - $15.00 USD Received 1 Jun 2010; revised 10 Jul 2010; accepted 12 Jul 2010; published 15 Jul 2010
(C) 2010 OSA

Translational Oncology
www.transonc.com

Volume 3 Number 1 February 2010 pp. 16–22 16

Two-dimensional Fast Surface Imaging Using a Handheld Optical Device: *In Vitro* and *In Vivo* Fluorescence Studies[1]

Sarah J. Erickson, Jiajia Ge, Andrea Sanchez and Anuradha Godavarty

Department of Biomedical Engineering, Florida International University, Miami, FL 33174, USA

Abstract

Near-infrared (NIR) optical imaging is a noninvasive and nonionizing modality that is emerging as a diagnostic tool for breast cancer. The handheld optical devices developed to date using the NIR technology are predominantly developed for spectroscopic applications. A novel handheld probe–based optical imaging device has been recently developed toward area imaging and tomography applications. The three-dimensional (3D) tomographic imaging capabilities of the device have been demonstrated from previous fluorescence studies on tissue phantoms. In the current work, fluorescence imaging studies are performed on tissue phantoms, *in vitro*, and *in vivo* tissue models to demonstrate the fast two-dimensional (2D) surface imaging capabilities of this flexible handheld-based optical imaging device, toward clinical breast imaging studies. Preliminary experiments were performed using target(s) of varying volume (0.23 and 0.45 cm^3) and depth (1-2 cm), using indocyanine green as the fluorescence contrast agent in liquid phantom, *in vitro*, and *in vivo* tissue models. The feasibility of fast 2D surface imaging (~5 seconds) over large surface areas of 36 cm^2 was demonstrated from various tissue models. The surface images could differentiate the target(s) from the background, allowing a rough estimate of the target's location before extensive 3D tomographic analysis (future studies).

Translational Oncology (2010) 3, 16–22

Introduction

Handheld-based optical imaging devices have been developed for breast imaging to accelerate the clinical translation of the technology toward cancer diagnosis. Several of these handheld devices have been tested *in vivo* on human subjects [1 2 3 4 5, selected publications]. However, they are unable to contour to the curvature of human breast tissue because all these devices used flat-probe faces. The predominant applications to date have been either toward spectroscopic measurement of tissue optical properties or two-dimensional (2D) localization studies of abnormal tissue within the breast. Recently, a handheld optical imaging device has been developed in our Optical Imaging Laboratory [6] toward imaging large tissue surfaces using a flexible probe face that contours to different tissue curvatures. The device is intended to augment current clinical imaging modalities for breast cancer detection and diagnosis. The three-dimensional (3D) tomographic ability of the device has been demonstrated on large tissue phantoms using a fluorescence-enhanced–based imaging technique [7]. Herein, preliminary studies are performed on tissue phantoms, *in vitro*, and *in vivo* tissue models to demonstrate the fast 2D surface imaging capabilities of this flexible handheld-based optical imaging device toward clinical breast imaging studies.

Materials and Methods

Instrumentation

The instrumentation for the handheld optical imaging device consists of a 785-nm, 500-mW laser diode source and an intensified charge-coupled device (ICCD) camera detector (with 550-850 nm bandwidth at the intensifier end) as shown in Figure 1. The source light is launched onto and collected from the tissue surface using a handheld-based probe head (4 × 9-cm^2 imaging area). The handheld probe consists of 6 points of illumination and 165 points of collection (as shown in Figure 2) of optical signals through optical fibers, which connect the probe head to the source and detector. The total

Address all correspondence to: Anuradha Godavarty, Department of Biomedical Engineering, Florida International University, Optical Imaging Laboratory, 10555 W Flagler St, EC 2675, Miami, FL 33174. E-mail: godavart@fiu.edu

[1]The authors thank the Florida Department of Health (08BB-06) and Department of Defense (BC083282) for their funding support.
Received 6 June 2009; Revised 8 September 2009; Accepted 15 September 2009

Copyright © 2010 Neoplasia Press, Inc. All rights reserved 1944-7124/10/$25.00
DOI 10.1593/tlo.09157

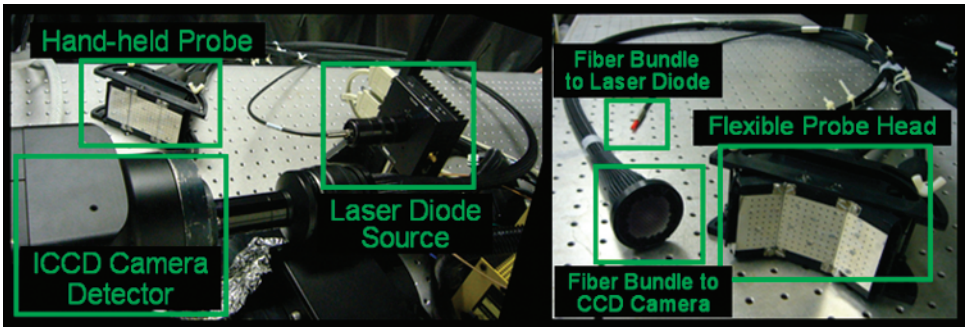

Figure 1. Handheld probe–based optical imaging system showing the handheld probe is fiber-optically coupled to the laser source and ICCD camera (left). The probe face is flexible to contour to different tissue curvatures (right).

laser power incident on the phantom or tissue is <10 mW. The device has a flexible probe head design such that it contours to different tissue curvatures during imaging. Simultaneous illumination and detection from multiple point locations is carried out to reduce the overall imaging time. Additional details of the instrumentation are provided elsewhere [7]. The instrumentation is developed such that it can acquire both continuous wave (CW)–based and frequency-domain–based optical measurements as required. To facilitate 2D imaging in real time, the device was operated in the CW mode for the current study in tissue phantoms, *in vitro*, and *in vivo*.

Data Acquisition and Analysis

Two-dimensional surface imaging was performed, using the handheld device operated in the CW mode, on tissue phantoms, *in vitro*, and *in vivo* tissue models. In all cases, fluorescence-enhanced imaging was performed using an external fluorescing agent indocyanine green (ICG) for improved contrast. Spherical acrylic targets (of different sizes) filled with 1 μM ICG were used to mimic a tumor. The target was placed at different depths from the imaging surface and different target-to-background (T:B) contrast ratios (1:0 and 100:1) were used for different experimental cases. The probe was placed in contact with the phantom or tissue surface as shown in Figure 3, and CW images of the fluorescent intensity were acquired in close to real time (~2 seconds' delay). The raw fluorescence intensity images at the ICCD camera end were acquired in 1 second (0.2-second exposure time × 5 repetitions). These images were postprocessed (~1 second) using in-house developed Matlab codes to acquire the final 2D surface contour plots of fluorescence intensity distribution of the imaged surface. The entire data acquisition and postprocessing were automated such that close to real-time (~2 seconds' delay) imaging is possible. The 2D surface contour plots of fluorescence intensity signal may or may not differentiate the target from the tissue phantom background, based on the target and background optical properties.

During fluorescence optical imaging, the output signal at the tissue surface is a mixture of fluorescence signal and the attenuated incident near-infrared (NIR) (i.e., excitation) signal. This fluorescence signal is filtered from the strong excitation signal (three to four orders of magnitude higher) using appropriate optical (band-pass) filters and imaged by the detector. However, the filters are not capable of 100% rejection of the excitation light, causing an excitation leakage and contamination of the fluorescent signal. Hence, a second level of postprocessing is carried out to subtract a background nonfluorescing image from the final fluorescence image plots for each experimental case to account for the excitation leakage. Initially, optical measurements were acquired before placing the fluorescent target in the phantom, in an attempt to represent the excitation leakage (or background noise). These (background noise) measurements were subtracted from the fluorescence optical measurements obtained from experimental cases that included fluorescent targets to effectively eliminate the signal from the excitation source light. In the clinical setting involving actual diseased tissues (unlike the simulated fluorescent targets in the current study), this could be accomplished by acquiring image(s) of the tissue before and after the contrast agent (e.g., ICG) injection. The nonfluorescent image(s) acquired before ICG injection will in turn be subtracted from the fluorescent images acquired after ICG injection to account for the background noise.

The subtracted 2D fluorescence images are generated rapidly (<5 seconds), making the entire process a fast 2D surface imaging technique. The acquisition of these subtracted fluorescence 2D surface contour plots has greater significance in 2D target localizations as well as in 3D tomographic imaging studies.

Experimental Cases

Tissue phantom studies. Studies were performed using slab tissue phantoms composed of 10 × 10 × 10-cm^3 acrylic cubes filled with 650 ml of 1% Liposyn solution (Liposyn II, 20%; Henry Schein, Melville, NJ) to mimic the optical properties of a typical breast tissue. The fluorescent target was placed at different depths (1.5-2.5 cm) from

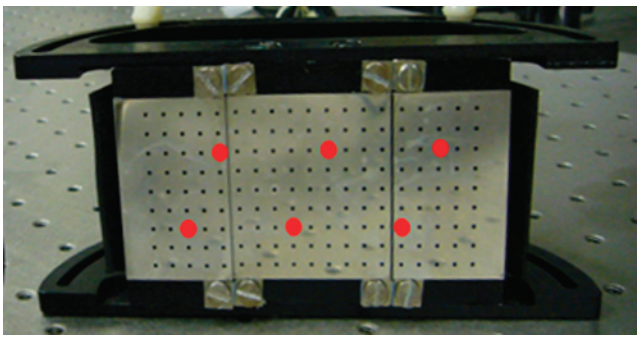

Figure 2. Picture of the handheld probe face showing the source-detector configuration. The large red dots represent the six source fiber locations, and all other small holes are the 165 detector fiber locations.

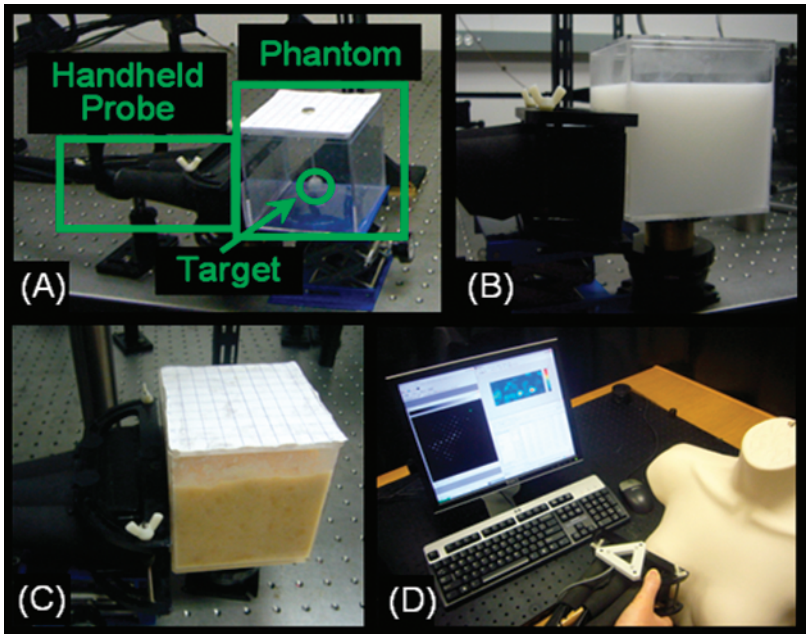

Figure 3. Experimental setup for tissue phantom, *in vitro*, and *in vivo* studies: (A) empty phantom showing target inclusion and placement of probe, (B) tissue slab phantom with 1% Liposyn solution for uniform scattering in the background, (C) *in vitro* slab phantom with heterogeneous scattering in the background, and (D) setup for *in vivo* studies using mannequin (for demonstration only) to represent human subject.

the imaging surface and real-time as well as fast (subtracted) images of fluorescence intensity were acquired. The different experimental cases are summarized in Table 1.

In vitro phantom studies. Before *in vivo* studies with human subjects, experiments were performed using *in vitro* phantoms, which were composed of minced chicken breast combined with 1% Liposyn solution, to introduce a nonuniform scattering background. The *in vitro* mixture of minced chicken breast (480 ml) and 1% Liposyn (260 ml) was placed inside a 10 × 10 × 10-cm^3 acrylic cube. Real-time as well as fast (subtracted) images of fluorescence intensity were acquired under different experimental conditions using either a 0.23-cm^3 or 0.45-cm^3 fluorescent target located at various depths between 1 and 2 cm (Table 1).

In vivo studies. *In vivo* studies were performed on healthy human subjects to demonstrate the feasibility of using the handheld device to collect images of a fluorescent target with a background of real human breast tissue. All human subject studies were approved by the Florida International University Institutional Review Board. Healthy female volunteers aged 21 and older were recruited for the studies. A fluorescent target was used to simulate a tumor (as described in Data Acquisition and Analysis) and was placed underneath the flap of the breast tissue (i.e. between breast tissue and chest wall, underneath the tissue). In the first study, a 0.23-cm^3 sphere with 1 μM ICG was placed under the right breast in the 4-o'clock position. The flat-probe face was placed against the breast tissue with gentle compression, and a real-time fluorescent intensity image was acquired (around the target region). The depth of the target within the tissue was approximately 2.5 cm as measured with a vernier caliper.

A second study was performed using a single target with the probe in the maximum curved position (i.e., 45° curvature of the two side plates of the three-plate–based probe face). The images collected with the probe in the curved position possibly include transilluminated measurements in addition to reflectance-based measurements. This study was performed to demonstrate the feasibility of using the probe

Table 1. Summary of Experimental Cases for Slab Tissue Phantom, *In Vitro*, and *In Vivo* Studies.

Subject Studied	Experiment No.	Number of Targets	Target Depth (cm)	Target Volume (cm^3)	T:B Contrast Ratio
Slab tissue phantom (uniform scattering in background)	1	1	1.5	0.45	1:0
	2	1	2.0	0.45	1:0
	3	1	2.5	0.45	1:0
In vitro phantom (nonuniform scattering in background)	4	1	1.0	0.45	1:0
	5	1	1.5	0.45	1:0
	6	1	2.0	0.45	1:0
	7	1	1.0	0.23	1:0
	8	1	1.5	0.23	1:0
	9	1	2.0	0.23	1:0
In vitro with healthy human subject	10	1	2.5	0.23	1:0
	11	1	2.5	0.45	1:0
	12	2	2.5	0.23 and 0.45	1:0

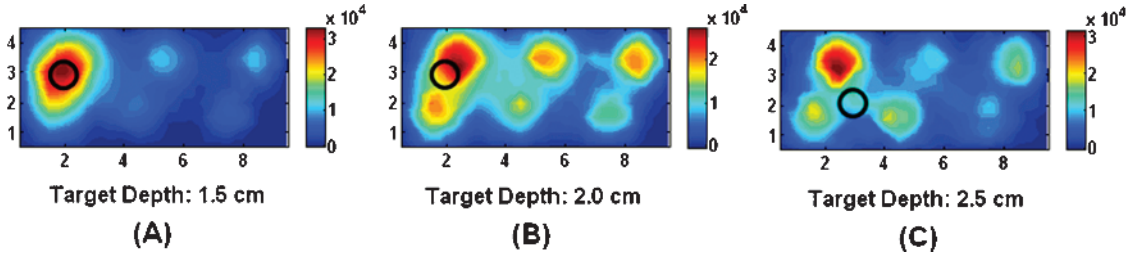

Figure 4. Near real-time images of fluorescence intensity obtained as 2D surface contour plots acquired from slab phantoms (with uniform background scattering). The fluorescent target was placed at different locations and depths: (A) target location (x,y,z) = (2.0, 2.7, 1.5), and (B) target location (x,y,z) = (2.0, 2.7, 2.0), and (C) target location (x,y,z) = (3.0, 2.2, 2.5). The black hollow circle in each subplot is the true target location.

in its curved position, such that it can contour along the tissue and also provide fluorescent images that can aid in target detection. Herein, a 0.45-cm^3 fluorescent target containing 1 μM ICG was placed under the right breast in the 8-o'clock position. A real-time as well as fast (subtracted) image of fluorescence intensity was acquired by applying gentle compression along the tissue curvature.

A third study was performed to demonstrate the feasibility of imaging multiple targets within real human breast tissue. Two targets were placed under the fold of the left breast tissue, with a 0.23-cm^3 target at the 6-o'clock position, and a 0.45-cm^3 target was placed at the 8-o'clock position of the same breast. A real-time as well as fast (subtracted) image of fluorescence intensity was acquired by applying gentle compression on the left breast tissue.

All these preliminary *in vivo* studies used micromolar concentrations of ICG in the tumor-mimicking target(s), similar to the current tissue phantom, *in vitro* phantom studies, and also that used by other researchers [7–9]. The actual *in vivo* studies on breast cancer subjects cannot estimate the concentration of ICG (after injection) at the tumor site, and the researchers typically report the injected quantities of the contrast agent [8,10].

Results

Tissue Phantom Studies

Real-time images using the slab phantom with uniform scattering in the background are shown in Figure 4 as 2D surface contour plots of the fluorescence intensity data with a target placed at different depths (1.5-2.5 cm) from the imaging surface. The nonuniform intensity distribution in Figure 4 is possibly due to the residual excitation leakage around the six source fibers (after the implementation of the subtraction technique). In addition, the input laser source signal is not evenly distributed among the six source fibers, possibly causing a variation or nonuniformity in the output fluorescence intensity distribution.

The images show the feasibility of performing (close to) real-time 2D imaging using the handheld device in tissue phantoms. The actual target location in the images is indicated in the figures by the black open circle in the *x-y* plane for different target depths in the "*z*" direction. The fast 2D image estimates the 2D target location (instantly) in the *x-y* plane. This information can then be further used toward 3D tomography (in the future) to determine the tumor volume, location, and depth [9].

From these plots, it is obvious that the real-time images are capable of differentiating the target from the background when the 0.45-cm^3 target was 1.5 cm deep. At greater tissue depths, the target was not distinctly differentiable because of the strong excitation leakage from the background. On applying the subtraction technique (as described in Data Acquisition and Analysis), the target is clearly differentiable from the background in all the experimental cases (Figure 5). These subtracted images also have potential to obtain 3D target localization through tomographic imaging, as long as the probe's location on the tissue surface is coregistered with respect to the surface fluorescence images.

In Vitro *Phantom Studies*

The results for the *in vitro* phantom experiments are shown in Figures 6 (real-time images) and 7 (fast subtracted images) for different target depths (1-2 cm) under a T:B contrast ratio of 1:0. The true

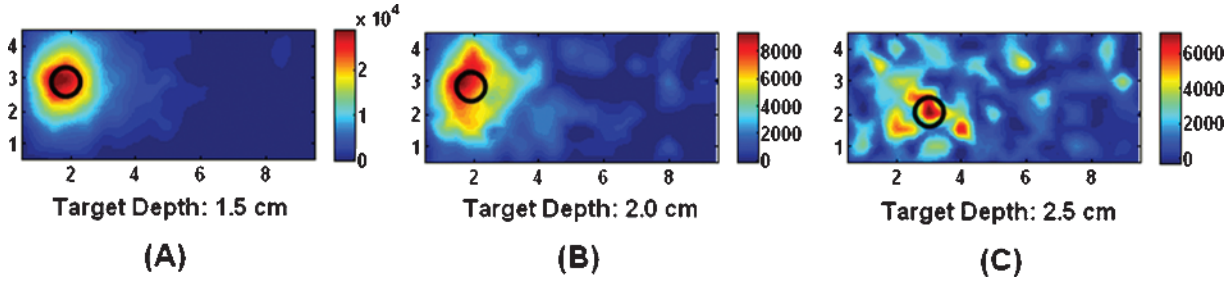

Figure 5. Fast subtracted images of fluorescence intensity obtained as 2D surface contour plots acquired from slab phantoms (with uniform background scattering). The 0.45-cm^3 fluorescent target was placed at different locations and depths: (A) target location (x,y,z) = (2.0, 2.7, 1.5), and (B) target location (x,y,z) = (2.0, 2.7, 2.0), and (C) target location (x,y,z) = (3.0, 2.2, 2.5). The black hollow circle in each subplot is the true target location.

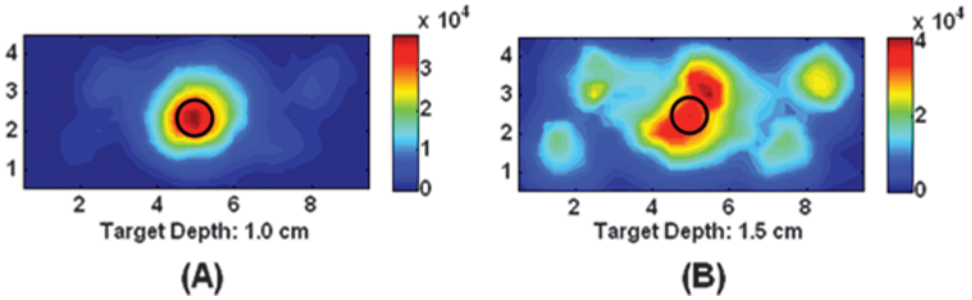

Figure 6. Near real-time images of fluorescence intensity obtained as 2D surface contour plots acquired from *in vitro* slab phantoms (with nonuniform background scattering). The 0.45-cm^3 fluorescent target was located at a depth of (A) 1.0 cm and (B) 1.5 cm from the imaging surface. The black hollow circle in each subplot is the true target location.

target location in the images is given as *x,y,z* coordinates where "*x*" is the lateral position, "*y*" is the height, and "*z*" is the depth that vary among the images. Owing to heterogeneous scattering of the background phantom, only the subtracted images were capable of clearly differentiating the target from the background for targets deeper than 1.0 cm. These studies show the ability of the handheld device to perform fast 2D surface imaging and target localization within a nonuniform scattering tissue-mimicking background.

In Vivo *Studies*

Figure 8 shows the fast 2D subtracted images of fluorescence intensity obtained *in vivo* (from a healthy human subject using a simulated target) with the probe in the flat position (Figure 8*A*) and in the curved position (Figure 8*B*). These subtracted image results demonstrate the feasibility of fast 2D surface imaging and 2D target localization in a clinical environment. The real-time (nonsubtracted) images of fluorescence intensity were unable to differentiate the target from the heterogeneous background, and hence, only the fast 2D subtracted images are shown in Figure 8.

The 2D subtracted images of fluorescent intensity from multiple simulated targets in a human subject are shown in Figure 9. The 0.23-cm^3 target is detected in the center of the image and the 0.45-cm^3 target is detected toward the left side in the image, which are very close to the true locations of these targets. This study demonstrates the potential to image and localize multiple fluorescent targets (of different sizes) within human breast tissue.

Discussion

The fluorescence imaging studies described here demonstrate for the first time the acquisition of fast 2D surface images (in <5 seconds) of a fluorescent target in uniform tissue phantoms, *in vitro*, and *in vivo* using a handheld-based optical imaging device. The subtracted images have a potential to clearly differentiate target(s) from the background (under various experimental conditions), demonstrating the potential to translate the technology toward on-site breast imaging in a clinical environment. Additional experiments were performed with the target located at greater depths in the tissue phantoms, but the target was not detected at a depth of 2.5 cm. At 2.5 cm deep, the

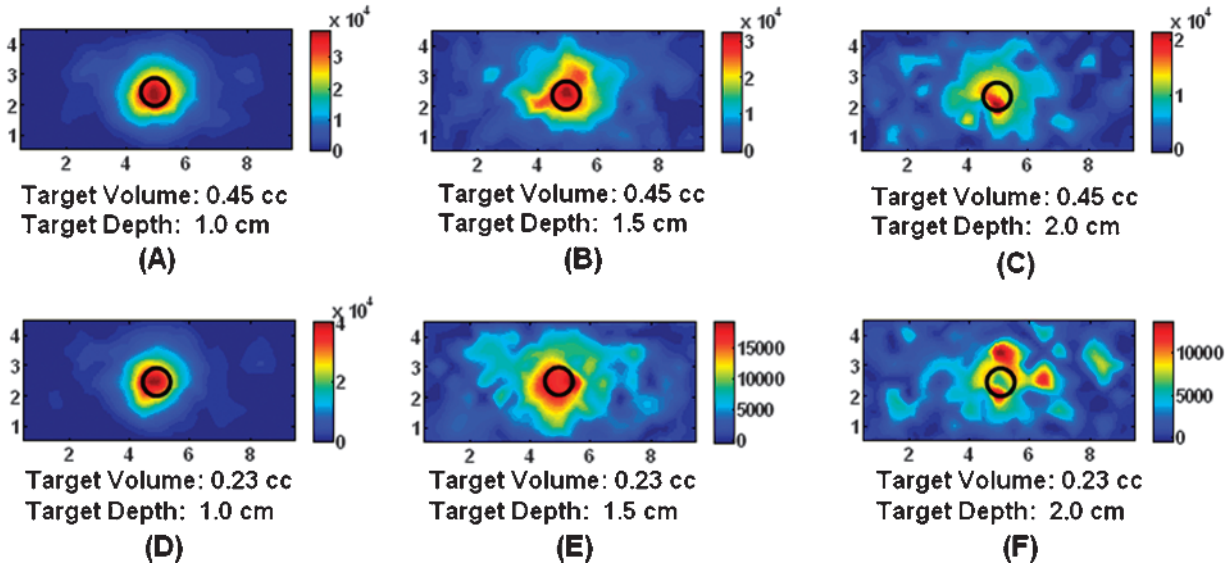

Figure 7. Fast subtracted images of fluorescence intensity obtained as 2D surface contour plots acquired from *in vitro* slab phantoms (with nonuniform background scattering). Images were collected for different target sizes and depths. Images (A) to (C) contain a target size of 0.45 cm^3 at depths of 1.0, 1.5, and 2.0 cm, respectively. Images (D) to (F) contain a target size of 0.23 cm^3 at depths of 1.0, 1.5, and 2.0 cm, respectively. The black hollow circle in each subplot is the true target location.

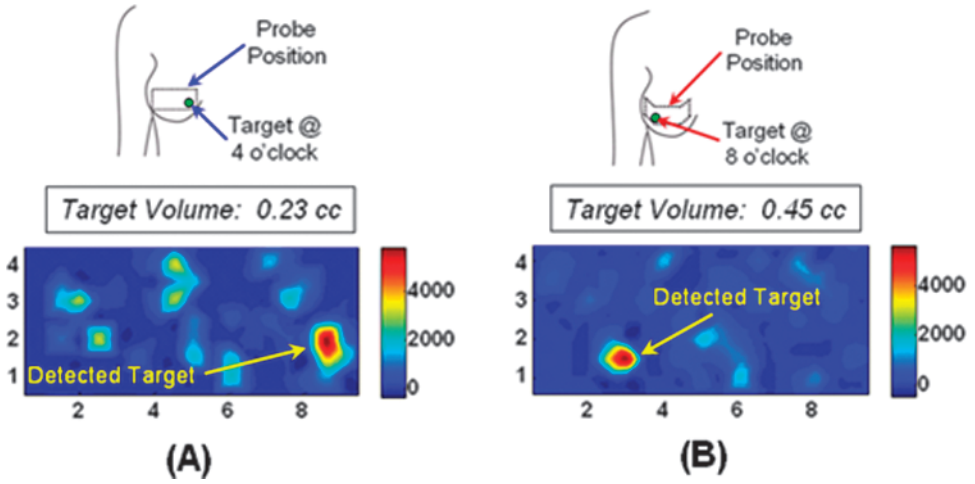

Figure 8. Fast subtracted images of fluorescence intensity obtained as 2D surface contour plots, acquired *in vivo* from a human subject using a spherical fluorescent target, for two experimental cases: (A) the probe was in the flat position and a 0.23-cm^3 target was placed at the 4-o'clock position; and (B) the probe was in the curved position and a 0.45-cm^3 target was placed at the 8-o'clock position. The images acquired using the probe in the curved position are illustrated as projected as a flat 2D image to be consistent with the images presented in case (A) (i.e., using the probe in flat position).

detected signal from the target is close to the noise floor and hence not differentiable from the background. A multilocation scanning approach is currently developed in our laboratory for differentiating deeply located or small-volume targets from homogenous or heterogeneous background [11]. In short, this approach will incorporate the use of coregistered images obtained at multiple locations on the tissue surface, such that the targets can be differentiated from artifacts as well as the background [11]. When comparing Figures 4 and 5, it can be seen that the images from the *in vitro* phantom contain more noise than those from the uniform tissue phantom. This can possibly be attributed to the heterogeneous distribution of scattering properties or shifting of the chicken breast as the target is removed (which can cause a change in the signal distribution when the background image is collected). Experiments were also performed using the *in vitro* phantoms with a T:B contrast ratio of 100:1. However, the noise from the background signal dominated the image, and a target was not detected even after subtracting the excitation background signal. On applying our multilocation scanning approach, the targets were differentiable under imperfect uptake conditions (i.e., T:B = 100:1) [11]. In addition to fast 2D imaging, the handheld device described here has demonstrated 3D tomography of fluorescent targets with tissue phantoms using frequency-domain–based measurements to estimate the 3D location and volume of the target within the tissue [9]. Our ongoing efforts will involve the implementation of fast and automated coregistration facilities to enable precise 2D target localization (instantaneously) as well as 3D tomography studies (*in vitro* as well as *in vivo*).

Conclusions

A handheld-based optical imaging device has been developed in our Optical Imaging Laboratory toward *in vivo* clinical studies on breast

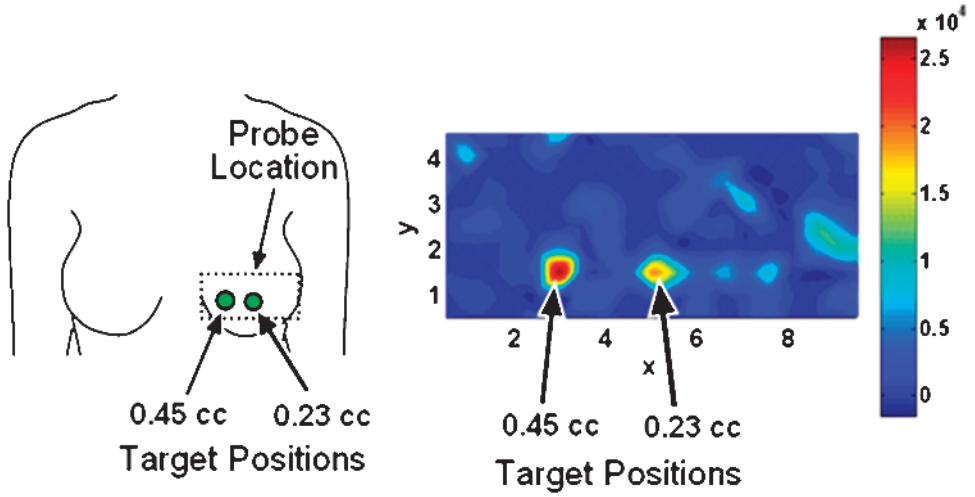

Figure 9. Fast subtracted image of fluorescence intensity obtained as 2D surface contour plot acquired *in vivo* from a human subject using two spherical fluorescent targets (0.23 and 0.45 cm^3).

tissues. The device has been tested extensively in the past on homogeneous slab phantoms (with sample results shown here). The device has been tested for CW-based fluorescence optical imaging *in vitro* as well as *in vivo*. The fluorescence studies demonstrate the ability of the handheld device to perform fast 2D imaging and also detect a fluorescent target within a heterogeneous tissue-mimicking background as well as real human breast tissue (on using subtracted images). Future work will involve fast coregistered imaging of human breast tissue to enable 3D tomography in human subjects using this novel handheld-based optical device.

References

[1] Cerussi AE, Berger AJ, Bevilacqua F, Shah N, Jakubowski D, Butler J, Holcombe RF, and Tromberg BJ (2001). Sources of absorption and scattering contrast for near-infrared optical mammography. *Acad Radiol* **8**, 211–218.

[2] Shah N, Cerussi AE, Jakubowski D, Hsiang D, Butler J, and Tromberg BJ (2004). Spatial variations in optical and physiological properties of healthy breast tissue. *J Biomed Opt* **9** (3), 534–540.

[3] Cerussi A, Shah N, Hsiang D, Durkin A, Butler J, and Tromberg BJ (2006). *In vivo* absorption, scattering, and physiologic properties of 58 malignant breast tumors determined by broadband diffuse optical spectroscopy. *J Biomed Opt* **11** (4), 044005.

[4] Chance B, Nioka S, Zhang J, Conant EF, Hwang E, Briest S, Orel SG, Schnall MD, and Czerniecki BJ (2005). Breast cancer detection based on incremental biochemical and physiological properties of breast cancers: a six-year, two-site study. *Acad Radiol* **12** (8), 925–933.

[5] Zhu Q, Cronin EB, Currier AA, Vine HS, Huang M, Chen NG, and Xu C (2005). Benign *versus* malignant breast masses: optical differentiation with US-guided optical imaging reconstruction. *Radiology* **237**, 57–66.

[6] Jayachandran B, Ge J, Regalado S, and Godavarty A (2007). Design and development of a hand-held optical probe toward fluorescence diagnostic imaging. *J Biomed Opt* **12** (5), 054014.

[7] Godavarty A, Eppstein MJ, Zhang C, Theru S, Thompson AB, Gurfinkel M, and Sevick-Muraca EM (2003). Fluorescence-enhanced optical imaging in large tissue volumes using a gain modulated ICCD camera. *Phys Med Biol* **48** (12), 1701–1720.

[8] Corlu A, Choe R, Durduran T, Rosen MA, Schweiger M, Arridge SR, Schnall MD, and Yodh AG (2007). Three-dimensional *in vivo* fluorescence diffuse optical tomography of breast cancer in humans. *Opt Express* **15** (11), 6696–6716.

[9] Ge J, Zhu B, Regalado S, and Godavarty A (2008). Three-dimensional fluorescence-enhanced optical tomography using a hand-held probe based imaging system. *Med Phys* **35** (7), 3354–3363.

[10] Sevick-Muraca EM, Sharma R, Rasmussen JC, Marshall MV, Wendt JA, Pham HQ, Bonefas E, Houston J, Sampath L, Adams KE, et al. (2008). Imaging of lymph flow in breast cancer patients after microdose administration of a near-infrared fluorophore: feasibility study. *Radiology* **246** (3), 734–741.

[11] Regalado S, Zhu B, Ge J, Erickson SJ, and Godavarty A (in press). Automated coregistered imaging using a hand-held probe-based optical imager. *Rev Sci Inst*.